

The IceCube Neutrino Observatory

Contributions to ICRC 2015 Part II: Atmospheric and Astrophysical Diffuse Neutrino Searches of All Flavors

The IceCube Collaboration

Contents

1. Atmospheric muon and electron neutrino energy spectra from IceCube — PoS(ICRC2015)1063 5
2. A search for extremely high energy neutrinos in 6 years (2008-2014) of IceCube data — PoS(ICRC2015)1064 13
3. Combined Analysis of the High-Energy Cosmic Neutrino Flux at the IceCube Detector — PoS(ICRC2015)1066 21
4. A Search for Astrophysical Tau Neutrinos in Three Years of IceCube Data — PoS(ICRC2015)1071 29
5. A measurement of the diffuse astrophysical muon neutrino flux using multiple years of IceCube data — PoS(ICRC2015)1079 37
6. Observation of Astrophysical Neutrinos in Four Years of IceCube Data — PoS(ICRC2015)1081 45
7. Unfolding measurement of the Atmospheric Muon Neutrino Spectrum using IceCube-79/86 — PoS(ICRC2015)1098 53
8. High Energy Astrophysical Neutrino Flux Characteristics for Neutrino-induced Cascades Using IC79 and IC86-String IceCube Configurations — PoS(ICRC2015)1109 59

*The 34th International Cosmic Ray Conference,
30 July- 6 August, 2015
The Hague, The Netherlands*

IceCube Collaboration Member List

M. G. Aartsen², K. Abraham³², M. Ackermann⁴⁸, J. Adams¹⁵, J. A. Aguilar¹², M. Ahlers²⁹, M. Ahrens³⁹, D. Altmann²³, T. Anderson⁴⁵, I. Anseau¹², M. Archinger³⁰, C. Argüelles²⁹, T. C. Arlen⁴⁵, J. Auffenberg¹, X. Bai³⁷, S. W. Barwick²⁶, V. Baum³⁰, R. Bay⁷, J. J. Beatty^{17,18}, J. Becker Tjus¹⁰, K.-H. Becker⁴⁷, E. Beiser²⁹, S. BenZvi²⁹, P. Berghaus⁴⁸, D. Berley¹⁶, E. Bernardini⁴⁸, A. Bernhard³², D. Z. Besson²⁷, G. Binder^{8,7}, D. Bindig⁴⁷, M. Bissok¹, E. Blaufuss¹⁶, J. Blumenthal¹, D. J. Boersma⁴⁶, C. Boehm³⁹, M. Börner²⁰, F. Bos¹⁰, D. Bose⁴¹, S. Böser³⁰, O. Botner⁴⁶, J. Braun²⁹, L. Brayeux¹³, H.-P. Bretz⁴⁸, N. Buzinsky²², J. Casey⁵, M. Casier¹³, E. Cheung¹⁶, D. Chirkin²⁹, A. Christov²⁴, K. Clark⁴², L. Classen²³, S. Coenders³², D. F. Cowen^{45,44}, A. H. Cruz Silva⁴⁸, J. Daughhetee⁵, J. C. Davis¹⁷, M. Day²⁹, J. P. A. M. de André²¹, C. De Clercq¹³, E. del Pino Rosendo³⁰, H. Dembinski³³, S. De Ridder²⁵, P. Desiati²⁹, K. D. de Vries¹³, G. de Wasseige¹³, M. de With⁹, T. DeYoung²¹, J. C. Díaz-Vélez²⁹, V. di Lorenzo³⁰, J. P. Dumm³⁹, M. Dunkman⁴⁵, R. Eagan⁴⁵, B. Eberhardt³⁰, T. Ehrhardt³⁰, B. Eichmann¹⁰, S. Euler⁴⁶, P. A. Evenson³³, O. Fadiran²⁹, S. Fahey²⁹, A. R. Fazely⁶, A. Fedynitch¹⁰, J. Feintzeig²⁹, J. Felde¹⁶, K. Filimonov⁷, C. Finley³⁹, T. Fischer-Wasels⁴⁷, S. Flis³⁹, C.-C. Fösig³⁰, T. Fuchs²⁰, T. K. Gaisser³³, R. Gaior¹⁴, J. Gallagher²⁸, L. Gerhardt^{8,7}, K. Ghorbani²⁹, D. Gier¹, L. Gladstone²⁹, M. Glagla¹, T. Glüschenkamp⁴⁸, A. Goldschmidt⁸, G. Golup¹³, J. G. Gonzalez³³, D. Góra⁴⁸, D. Grant²², J. C. Groh⁴⁵, A. Groß³², C. Ha^{8,7}, C. Haack¹, A. Haj Ismail²⁵, A. Hallgren⁴⁶, F. Halzen²⁹, B. Hansmann¹, K. Hanson²⁹, D. Hebecker⁹, D. Heereman¹², K. Helbing⁴⁷, R. Hellauer¹⁶, D. Hellwig¹, S. Hickford⁴⁷, J. Hignight²¹, G. C. Hill², K. D. Hoffman¹⁶, R. Hoffmann⁴⁷, K. Holzappel³², A. Homeier¹¹, K. Hoshina^{29,a}, F. Huang⁴⁵, M. Huber³², W. Huelsnitz¹⁶, P. O. Hulth³⁹, K. Hultqvist³⁹, S. In⁴¹, A. Ishihara¹⁴, E. Jacobi⁴⁸, G. S. Japaridze⁴, K. Jero²⁹, M. Jurkovic³², B. Kaminsky⁴⁸, A. Kappes²³, T. Karg⁴⁸, A. Karle²⁹, M. Kauer^{29,34}, A. Keivani⁴⁵, J. L. Kelley²⁹, J. Kemp¹, A. Kheirandish²⁹, J. Kiryluk⁴⁰, J. Kläs⁴⁷, S. R. Klein^{8,7}, G. Kohnen³¹, R. Koirala³³, H. Kolanoski⁹, R. Konietz¹, A. Koob¹, L. Köpke³⁰, C. Kopper²², S. Kopper⁴⁷, D. J. Koskinen¹⁹, M. Kowalski^{9,48}, K. Krings³², G. Kroll³⁰, M. Kroll¹⁰, J. Kunnen¹³, N. Kurahashi³⁶, T. Kuwabara¹⁴, M. Labare²⁵, J. L. Lanfranchi⁴⁵, M. J. Larson¹⁹, M. Lesiak-Bzdak⁴⁰, M. Leuermann¹, J. Leuner¹, L. Lu¹⁴, J. Lünemann¹³, J. Madsen³⁸, G. Maggi¹³, K. B. M. Mahn²¹, R. Maruyama³⁴, K. Mase¹⁴, H. S. Matis⁸, R. Maunu¹⁶, F. McNally²⁹, K. Meagher¹², M. Medici¹⁹, A. Meli²⁵, T. Menne²⁰, G. Merino²⁹, T. Meures¹², S. Miarecki^{8,7}, E. Middell⁴⁸, E. Middlemas²⁹, L. Mohrmann⁴⁸, T. Montaruli²⁴, R. Morse²⁹, R. Nahnauer⁴⁸, U. Naumann⁴⁷, G. Neer²¹, H. Niederhausen⁴⁰, S. C. Nowicki²², D. R. Nygren⁸, A. Obertacke⁴⁷, A. Olivás¹⁶, A. Omairat⁴⁷, A. O'Murchadha¹², T. Palczewski⁴³, H. Pandya³³, L. Paul¹, J. A. Pepper⁴³, C. Pérez de los Heros⁴⁶, C. Pfendner¹⁷, D. Pieloth²⁰, E. Pinat¹², J. Posselt⁴⁷, P. B. Price⁷, G. T. Przybylski⁸, J. Pütz¹, M. Quinlan⁴⁵, C. Raab¹², L. Rädcl¹, M. Rameez²⁴, K. Rawlins³, R. Reimann¹, M. Relich¹⁴, E. Resconi³², W. Rhode²⁰, M. Richman³⁶, S. Richter²⁹, B. Riedel²², S. Robertson², M. Rongen¹, C. Rott⁴¹, T. Ruhe²⁰, D. Ryckbosch²⁵, S. M. Saba¹⁰, L. Sabbatini²⁹, H.-G. Sander³⁰, A. Sandrock²⁰, J. Sandroos³⁰, S. Sarkar^{19,35}, K. Schatto³⁰, F. Scheriau²⁰, M. Schimp¹, T. Schmidt¹⁶, M. Schmitz²⁰, S. Schoenen¹, S. Schöneberg¹⁰, A. Schönwald⁴⁸, L. Schulte¹¹, D. Seckel³³, S. Seunarine³⁸, R. Shanidze⁴⁸, M. W. E. Smith⁴⁵, D. Soldin⁴⁷, M. Song¹⁶, G. M. Spiczak³⁸, C. Spiering⁴⁸, M. Stahlberg¹, M. Stamatikos^{17,b}, T. Stanev³³, N. A. Stanisha⁴⁵, A. Stasik⁴⁸, T. Stezelberger⁸, R. G. Stokstad⁸, A. Stöbl⁴⁸, R. Ström⁴⁶, N. L. Strotjohann⁴⁸, G. W. Sullivan¹⁶, M. Sutherland¹⁷, H. Taavola⁴⁶, I. Taboada⁵, S. Ter-Antonyan⁶, A. Terliuk⁴⁸, G. Tešić⁴⁵, S. Tilav³³, P. A. Toale⁴³, M. N. Tobin²⁹, S. Toscano¹³, D. Tosi²⁹, M. Tselengidou²³, A. Turcati³², E. Unger⁴⁶, M. Usner⁴⁸, S. Vallecorsa²⁴, J. Vandenbroucke²⁹, N. van Eijndhoven¹³,

S. Vanheule²⁵, J. van Santen²⁹, J. Veenkamp³², M. Vehring¹, M. Voge¹¹, M. Vraeghe²⁵, C. Walck³⁹, A. Wallace², M. Wallraff¹, N. Wandkowsky²⁹, Ch. Weaver²², C. Wendt²⁹, S. Westerhoff²⁹, B. J. Whelan², N. Whitehorn²⁹, C. Wichary¹, K. Wiebe³⁰, C. H. Wiebusch¹, L. Wille²⁹, D. R. Williams⁴³, H. Wissing¹⁶, M. Wolf³⁹, T. R. Wood²², K. Woschnagg⁷, D. L. Xu⁴³, X. W. Xu⁶, Y. Xu⁴⁰, J. P. Yanez⁴⁸, G. Yodh²⁶, S. Yoshida¹⁴, M. Zoll³⁹

¹III. Physikalisches Institut, RWTH Aachen University, D-52056 Aachen, Germany

²Department of Physics, University of Adelaide, Adelaide, 5005, Australia

³Dept. of Physics and Astronomy, University of Alaska Anchorage, 3211 Providence Dr., Anchorage, AK 99508, USA

⁴CTSPS, Clark-Atlanta University, Atlanta, GA 30314, USA

⁵School of Physics and Center for Relativistic Astrophysics, Georgia Institute of Technology, Atlanta, GA 30332, USA

⁶Dept. of Physics, Southern University, Baton Rouge, LA 70813, USA

⁷Dept. of Physics, University of California, Berkeley, CA 94720, USA

⁸Lawrence Berkeley National Laboratory, Berkeley, CA 94720, USA

⁹Institut für Physik, Humboldt-Universität zu Berlin, D-12489 Berlin, Germany

¹⁰Fakultät für Physik & Astronomie, Ruhr-Universität Bochum, D-44780 Bochum, Germany

¹¹Physikalisches Institut, Universität Bonn, Nussallee 12, D-53115 Bonn, Germany

¹²Université Libre de Bruxelles, Science Faculty CP230, B-1050 Brussels, Belgium

¹³Vrije Universiteit Brussel, Dienst ELEM, B-1050 Brussels, Belgium

¹⁴Dept. of Physics, Chiba University, Chiba 263-8522, Japan

¹⁵Dept. of Physics and Astronomy, University of Canterbury, Private Bag 4800, Christchurch, New Zealand

¹⁶Dept. of Physics, University of Maryland, College Park, MD 20742, USA

¹⁷Dept. of Physics and Center for Cosmology and Astro-Particle Physics, Ohio State University, Columbus, OH 43210, USA

¹⁸Dept. of Astronomy, Ohio State University, Columbus, OH 43210, USA

¹⁹Niels Bohr Institute, University of Copenhagen, DK-2100 Copenhagen, Denmark

²⁰Dept. of Physics, TU Dortmund University, D-44221 Dortmund, Germany

²¹Dept. of Physics and Astronomy, Michigan State University, East Lansing, MI 48824, USA

²²Dept. of Physics, University of Alberta, Edmonton, Alberta, Canada T6G 2E1

²³Erlangen Centre for Astroparticle Physics, Friedrich-Alexander-Universität Erlangen-Nürnberg, D-91058 Erlangen, Germany

²⁴Département de physique nucléaire et corpusculaire, Université de Genève, CH-1211 Genève, Switzerland

²⁵Dept. of Physics and Astronomy, University of Gent, B-9000 Gent, Belgium

²⁶Dept. of Physics and Astronomy, University of California, Irvine, CA 92697, USA

²⁷Dept. of Physics and Astronomy, University of Kansas, Lawrence, KS 66045, USA

²⁸Dept. of Astronomy, University of Wisconsin, Madison, WI 53706, USA

²⁹Dept. of Physics and Wisconsin IceCube Particle Astrophysics Center, University of Wisconsin, Madison, WI 53706, USA

³⁰Institute of Physics, University of Mainz, Staudinger Weg 7, D-55099 Mainz, Germany

- ³¹Université de Mons, 7000 Mons, Belgium
- ³²Technische Universität München, D-85748 Garching, Germany
- ³³Bartol Research Institute and Dept. of Physics and Astronomy, University of Delaware, Newark, DE 19716, USA
- ³⁴Dept. of Physics, Yale University, New Haven, CT 06520, USA
- ³⁵Dept. of Physics, University of Oxford, 1 Keble Road, Oxford OX1 3NP, UK
- ³⁶Dept. of Physics, Drexel University, 3141 Chestnut Street, Philadelphia, PA 19104, USA
- ³⁷Physics Department, South Dakota School of Mines and Technology, Rapid City, SD 57701, USA
- ³⁸Dept. of Physics, University of Wisconsin, River Falls, WI 54022, USA
- ³⁹Oskar Klein Centre and Dept. of Physics, Stockholm University, SE-10691 Stockholm, Sweden
- ⁴⁰Dept. of Physics and Astronomy, Stony Brook University, Stony Brook, NY 11794-3800, USA
- ⁴¹Dept. of Physics, Sungkyunkwan University, Suwon 440-746, Korea
- ⁴²Dept. of Physics, University of Toronto, Toronto, Ontario, Canada, M5S 1A7
- ⁴³Dept. of Physics and Astronomy, University of Alabama, Tuscaloosa, AL 35487, USA
- ⁴⁴Dept. of Astronomy and Astrophysics, Pennsylvania State University, University Park, PA 16802, USA
- ⁴⁵Dept. of Physics, Pennsylvania State University, University Park, PA 16802, USA
- ⁴⁶Dept. of Physics and Astronomy, Uppsala University, Box 516, S-75120 Uppsala, Sweden
- ⁴⁷Dept. of Physics, University of Wuppertal, D-42119 Wuppertal, Germany
- ⁴⁸DESY, D-15735 Zeuthen, Germany
- ^aEarthquake Research Institute, University of Tokyo, Bunkyo, Tokyo 113-0032, Japan
- ^bNASA Goddard Space Flight Center, Greenbelt, MD 20771, USA

Acknowledgment: We acknowledge the support from the following agencies: U.S. National Science Foundation-Office of Polar Programs, U.S. National Science Foundation-Physics Division, University of Wisconsin Alumni Research Foundation, the Grid Laboratory Of Wisconsin (GLOW) grid infrastructure at the University of Wisconsin - Madison, the Open Science Grid (OSG) grid infrastructure; U.S. Department of Energy, and National Energy Research Scientific Computing Center, the Louisiana Optical Network Initiative (LONI) grid computing resources; Natural Sciences and Engineering Research Council of Canada, WestGrid and Compute/Calcul Canada; Swedish Research Council, Swedish Polar Research Secretariat, Swedish National Infrastructure for Computing (SNIC), and Knut and Alice Wallenberg Foundation, Sweden; German Ministry for Education and Research (BMBF), Deutsche Forschungsgemeinschaft (DFG), Helmholtz Alliance for Astroparticle Physics (HAP), Research Department of Plasmas with Complex Interactions (Bochum), Germany; Fund for Scientific Research (FNRS-FWO), FWO Odysseus programme, Flanders Institute to encourage scientific and technological research in industry (IWT), Belgian Federal Science Policy Office (Belspo); University of Oxford, United Kingdom; Marsden Fund, New Zealand; Australian Research Council; Japan Society for Promotion of Science (JSPS); the Swiss National Science Foundation (SNSF), Switzerland; National Research Foundation of Korea (NRF); Danish National Research Foundation, Denmark (DNRF)

Atmospheric muon and electron neutrino energy spectra from IceCube

The IceCube Collaboration¹,

¹ http://icecube.wisc.edu/collaboration/authors/icrc15_icecube

E-mail: takao@hepburn.s.chiba-u.ac.jp

A framework for a unified analysis of high-energy atmospheric neutrinos with the full IceCube is presented in which both muon and electron flavors are included in a single analysis. Combining the IceCube measurements at high energy with measurements from smaller detectors at lower energy will, in the future, determine the atmospheric neutrino flux from <100 MeV to >100 TeV. Precise knowledge of the spectrum will lead to reduced uncertainty for any kind of signal analysis.

Corresponding author: T. Kuwabara^{1*},

¹ *Department of Physics, Faculty of Science, Chiba University, Yayoi-cho 1-33, Inage-ku, Chiba 263-8522, Japan*

*The 34th International Cosmic Ray Conference,
30 July- 6 August, 2015
The Hague, The Netherlands*

*Speaker.

1. Introduction

Atmospheric neutrinos produced through interactions of cosmic rays with nuclei in the Earth's atmosphere constitute an important background in the search for astrophysical neutrinos. They also probe properties of the primary spectrum and of hadronic interactions, such as the kaon to pion ratio. Muon and electron neutrinos from decay of pions and kaons are referred to as “conventional” atmospheric neutrinos. Most conventional atmospheric neutrinos are muon neutrinos from two-body decays of pions and kaons. Conventional atmospheric electron neutrinos are primarily from subsequent muon decay at low energies (< 1 TeV), while three-body decays of charged and neutral kaons give the main contribution to electron neutrinos at higher energy above 1 TeV. The spectrum of conventional neutrinos becomes asymptotically one power of energy steeper than the primary spectrum at high energy. Prompt neutrinos from the decay of mesons containing charmed quarks are a distinct component of the atmospheric neutrino flux. Because of the short lifetime of charmed hadrons, prompt neutrinos have a spectrum similar to the primary cosmic-ray spectrum. Fluxes of prompt electron neutrinos and prompt muon neutrinos are nearly identical to each other, and they become the dominant source at sufficiently high energy, ≥ 100 TeV for electron neutrino, and ≥ 1 PeV for muon neutrino.

The IceCube neutrino observatory, located at the South Pole, detects Cherenkov photons produced by charged particles propagating through the Antarctic ice [1]. When neutrinos interact in the ice, they produce two types of Cherenkov signatures, 'Tracks' and 'Cascades'. 'Track'-like events are produced by muons from the charged current (CC) interaction of muon neutrinos. 'Cascade'-like events are produced by electromagnetic and hadronic showers from the CC interactions of electron neutrinos, or hadronic showers from neutral current (NC) interactions from any kind of neutrino flavors.

IceCube has measured the spectrum of atmospheric muon neutrinos [2] and electron neutrinos [3] in separate analyses. Some uncertainty remains, especially in the electron neutrino flux, because the cascade sample is small, and it contains multiple components. In this paper we describe a unified approach to measure the muon and electron spectrum in a single analysis by combining the track and cascade samples. Due to the large amount of events and purity of flavor, it is possible to determine the muon neutrino flux with high precision from the track sample. In this way, uncertainties in parameters common to both flavors (primary spectrum, kaon/pion ratio, etc.) can be reduced in the cascade analysis. In this paper, the event selection criteria for both track and cascade samples are introduced. The feasibility of the unified analysis has been tested by applying the event selection to simulated data. The statistical sensitivity from one year of IC86 full data sample and additional systematic effects are estimated and discussed.

2. Event Selection

Track and cascade type samples for this analysis are selected from the first year of IceCube 86 full string data, which was obtained between May 2011 and May 2012. Event selection criteria for both samples are established by using simulation and 10% sample of the data. The remaining 90% of data is blinded to avoid experimenter's bias at this stage.

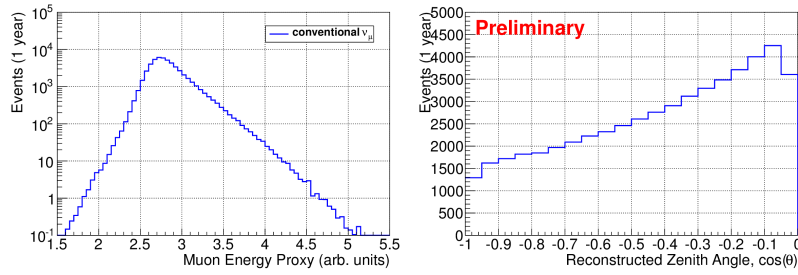


Figure 1: Event distribution of track sample from a simulation of the conventional muon neutrino flux, for reconstructed muon energy (left) and reconstructed zenith angle (right).

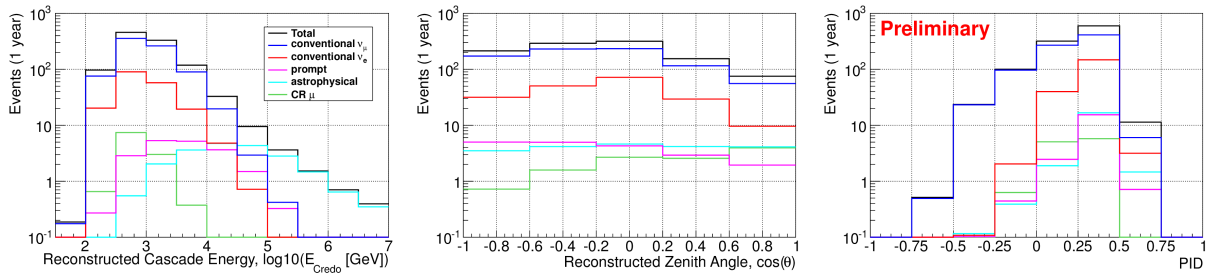


Figure 2: Event distribution of cascade sample for reconstructed energy (left) reconstructed zenith angle (center), and particle identification (right). Simulation of conventional muon neutrinos (blue), electron neutrinos (red), the sum of muon and electron prompt neutrinos (magenta), astrophysical neutrinos (cyan), cosmic ray muon background (green), and total flux (black) are shown.

IceCube has a ~ 2.2 kHz typical trigger rate of events with more than eight sensors recorded in a $5 \mu\text{sec}$ time window, and each triggering sensor is required to have local coincidence with a nearby sensor within $\pm 1 \mu\text{sec}$. Most of the triggers are from cosmic ray muons produced in air showers, and are the background for this analysis. To eliminate this background, simulation data sets are generated for both signal and background, then different cuts are applied to select the two types of signals. Signals of muon and electron neutrinos are simulated with our own module which is based on the ANIS package [4]. The background of atmospheric muons is simulated with CORSIKA [5].

Track Sample: Muons from CC interactions of muon neutrinos are detected as track events in IceCube. However at trigger level most of the track events are from background cosmic ray muons, and are detected as down-going tracks. After the track reconstruction, down-going events are rejected, yet many background events remain due to a misreconstruction of the zenith angle. Further quality cuts are applied to select a pure sample of neutrino induced muons [6]. From first year of IceCube 86, 5526 remained after all cuts are applied to a 10% sample of the data. The remaining background contamination is at the 1% level.

Cascade Sample: Cascade type events are created by electromagnetic and hadronic showers. Since it is not possible at present to distinguish between hadron and electromagnetic showers, the cascade sample includes muon neutrino events from NC interaction, and electron neutrino events from both CC and NC interaction. Charged current interactions of muon neutrinos that start inside the detector

can sometimes be classified as cascades if most of the energy goes into the initial hadronic cascade vertex. This analysis uses cascade samples which had been selected for the electron neutrino measurement [3], in which the selection has been optimized by a Boosted Decision Tree (BDT). In total 86 events remained with 10% sample of the data. The breakdown of the cascade signal is 69% events from conventional muon neutrino flux (60% CC, 40% NC), 17% from conventional electron neutrino flux (92% CC, 8% NC), 11% from cosmic ray muon background, and the remaining 3% from prompt and astrophysical neutrinos.

Event Distribution: Figure 1 and 2 are simulated event distributions of track and cascade events corresponding to the first year of the IceCube 86 string. The colored curves are baseline distributions of expected neutrino flux, simulated separately for each component using the same primary spectrum with separate spectrum models of conventional, prompt and astrophysical neutrinos, as explained in the next section. Distributions are binned into reconstructed muon/cascade energy and zenith angle, for this analysis. We see in the cascade sample that each component has a different characteristic distribution, and these can be distinguished in the fit. The cascade sample analysis also uses additionally the particle identification (PID) number, ranging from -1 (track like events) to +1 (cascade like events), determined from the BDT score, to distinguish CC muon neutrino event from cascades. Additionally, the expected primary neutrino energy distributions of conventional muon neutrinos in the track sample, and conventional muon and electron neutrinos in the cascade sample are shown in Figure 3.

3. Analysis Method

The conventional atmospheric neutrino spectrum is determined with a maximum log-likelihood fitting method. A baseline model of conventional muon and neutrino spectrum is defined, then physics parameters are implemented to modify the baseline model during fitting procedure.

3.1 Model Spectrum

For the conventional atmospheric neutrino spectrum, the Honda2006+GaisserH3a Knee model is chosen. The low energy flux from Honda et al.[7] valid to 10 TeV is extrapolated to higher energy. Then the cosmic ray knee effect [8] is implemented by folding the neutrino yield per primary cosmic ray with the assumed primary spectrum and composition. Other components of the neutrino flux, prompt and astrophysical neutrinos, are included as the background of cascade sample. For the prompt flux, the Enberg model [9] is assumed with the cosmic-ray knee effect. For astrophysical neutrino flux, $10^{-8} \cdot E^{-2} [\text{GeV}^{-1} \text{cm}^{-2} \text{s}^{-1} \text{str}^{-1}]$ per flavor spectrum is assumed, which is consistent with the recent IceCube result $0.95 \times 10^{-8} \cdot E^{-2} [\text{GeV}^{-1} \text{cm}^{-2} \text{s}^{-1} \text{str}^{-1}]$ [10]. Figure 4 is the summary of the baseline spectrum.

3.2 Fit Parameters

The following physics parameters are allowed to vary and modify the baseline model assumptions of this analysis

Normalization, C_{ν_μ} , C_{ν_e} : Normalization parameters C_{ν_μ} and C_{ν_e} scale up/down conventional atmospheric neutrino spectrum, implemented for muon neutrino and electron neutrino. In addition, another normalization parameter, C_{CR} , is implemented for the cosmic-ray muon background in the

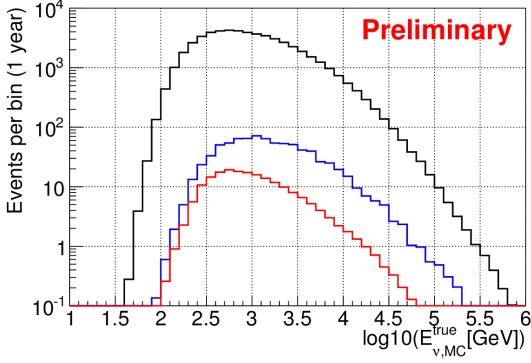


Figure 3: Primary neutrino energy distribution of muon neutrino in track sample (black), muon neutrino in cascade sample (blue), electron neutrino in cascade sample (red) from simulation after event selection.

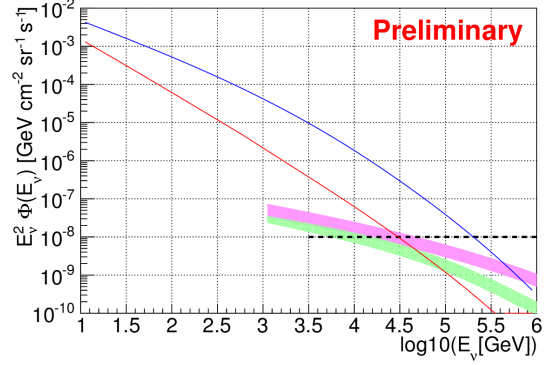


Figure 4: Honda2006+GaisserH3a Knee model of conventional muon neutrino (blue) and electron neutrino (red), prompt neutrinos from Enberg (magenta) and BERSS (light green), astrophysical neutrino (black dashed).

cascade sample.

Spectrum Index, $\Delta\gamma$: This parameter shifts the spectral index of the conventional atmospheric neutrinos. The same value is used for muon neutrino and electron neutrinos to reflect the common uncertainty in the primary cosmic-ray spectrum.

Kaon to Pion ratio, $R_{K/\pi}$: The kaon/pion ratio in extensive air showers affects the shape of the atmospheric neutrino spectrum. To implement this parameter, we use the following analytic approximation [11] for the sum of muon neutrinos and anti-neutrinos,

$$\begin{aligned}\phi_{\nu_\mu}(E_\nu) &= \phi_{\pi \rightarrow \nu_\mu} + \phi_{K \rightarrow \nu_\mu} \\ &= \phi_N(E_\nu) \times \left\{ \frac{Z_{N\pi} A_{\pi\nu}}{1 + B_{\pi\nu} \cos \theta^* E_\nu / \varepsilon_\pi} + \frac{Z_{NK} A_{K\nu}}{1 + B_{K\nu} \cos \theta^* E_\nu / \varepsilon_K} \right\}\end{aligned}\quad (3.1)$$

where the $A_{\pi,K\nu}$ and $B_{\pi,K\nu}$ are decay kinematic factors, described as combination of branching ratio, mass ratio and attenuation length of pion and kaon. $\cos \theta^*$ is the zenith angle where the neutrinos are produced, the critical energies are $\varepsilon_\pi = 115$ GeV and $\varepsilon_K = 850$ GeV. Z-factors ($Z_{N\pi}$ and Z_{NK}) are spectral-weighted moments of the inclusive cross section for a nucleon to produce secondary pions and kaons. At low energy the flux of conventional $\nu_e + \bar{\nu}_e$ is mostly dominated by the decay of muons from pions, however at high energy ($E_{\nu_e} > 100$ GeV) it is dominated by kaon contributions which is expressed as sum of the contributions from charged K, K-long and K-short [13],

$$\begin{aligned}\phi_{\nu_e}(E_\nu) &= \phi_{K \rightarrow \nu_e} + \phi_{K_L \rightarrow \nu_e} + \phi_{K_s \rightarrow \nu_e} \\ &= \phi_N(E_\nu) \times \left\{ \frac{Z_{NK} A_{Ke3\nu}}{1 + B_{Ke3\nu} \cos \theta^* E_\nu / \varepsilon_K} \right. \\ &\quad \left. + \frac{Z_{NK_L} A_{K_L e3\nu}}{1 + B_{K_L e3\nu} \cos \theta^* E_\nu / \varepsilon_{K_L}} + \frac{Z_{NK_s} A_{K_s e3\nu}}{1 + B_{K_s e3\nu} \cos \theta^* E_\nu / \varepsilon_{K_s}} \right\}\end{aligned}\quad (3.2)$$

where the parameters contain the branching ratios, attenuation lengths and Z-factors of K_{e3} decay. Critical energies of neutral kaons are $\varepsilon_{K_L} = 210$ GeV and $\varepsilon_{K_s} = 120,000$ GeV.

In the analysis, contributions of charged pion and charged kaon are modified by changing the ratio of Z-factors, $R_{K/\pi} = Z_{NK}/Z_{N\pi}$. The nominal value of K/pi ratio is taken to be $R_{K/\pi} = \frac{Z_{NK}}{Z_{N\pi}} = \frac{0.0118}{0.079} = 0.149 \pm 0.060$ which is based on laboratory measurements below 100 GeV center of mass energy [11]. The 40% uncertainty corresponds to that in the current cosmic ray interaction models [12]. In the fitting procedure, $R_{K/\pi}$ is floated with a constraint to keep the sum $Z_{N\pi} + Z_{NK}$ constant at its nominal value 0.0908. Change of expected neutrino flux from K/pi ratio is introduced as a weighting factor as $W_{K/\pi} = \frac{\Phi_{\nu}(R_{K/\pi})}{\Phi_{\nu}^0(R_{K/\pi}=1)}$

DOM Efficiency: In addition to the physics parameters, detector related systematic uncertainties are taken as a nuisance parameter. Currently one of the important detector systematics, optical efficiency of a Digital Optical Module (DOM) is implemented. Five different simulation data sets with different DOM efficiencies, ranging from -10% to +10%, are calculated. Final event rates in each bin are parameterized with these efficiencies. Another possible systematic uncertainty, optical properties of the surrounding ice, has not been taken into account, which will be included.

Fitted Model: With the physics parameters $C_{\nu_{\mu,e}}, \Delta\gamma, R_{K/\pi}$, the predicted neutrino flux is described as $\Phi_{\nu_{\mu,e}} = C_{\nu_{\mu,e}} \left(\frac{E_{\nu}}{E_{\nu}^{med}}\right)^{\Delta\gamma} W_{K/\pi}(R_{K/\pi}) \Phi_{\nu_{\mu,e}}^{h3a}$ where E_{ν}^{med} is the median energy of the analyzed event sample.

4. Loglikelihood Fitting

The likelihood \mathcal{L} is calculated as the sum of the likelihood of the track sample and the cascade sample, with nuisance parameters constrained by an additional Gaussian term. Then the best fit parameters are obtained by minimizing the negative loglikelihood as

$$\begin{aligned}
-2\ln\mathcal{L} = & 2\sum_i \sum_j \left[\mu_{i,j}^{track} - n_{i,j}^{track} \ln \mu_{i,j}^{track} + \ln n_{i,j}^{track}! \right] \\
& + 2\sum_i \sum_j \sum_k \left[\mu_{i,j,k}^{cascade} - n_{i,j,k}^{cascade} \ln \mu_{i,j,k}^{cascade} + \ln n_{i,j,k}^{cascade}! \right] \\
& + \frac{(DOM_{eff}^0 - DOM_{eff}^0)^2}{\sigma_{DOM_{eff}}^2}
\end{aligned} \tag{4.1}$$

where $n_{i,j(k)}$ is the number of measured events, $\mu_{i,j(k)}$ is predicted events, at energy (i), zenith angle (j), and PID (k) bin. The first and second terms are respectively the loglikelihood of the track sample and the cascade sample. Predicted events are from conventional muon neutrino for the track sample, while all relevant components contribute to the cascade sample. In the last term from the nuisance parameter, DOM_{eff}^0 is a central value, while $\sigma_{DOM_{eff}}^2$ is the prior uncertainty $\pm 10\%$.

5. Statistical Sensitivity

Statistical sensitivity to each fitted parameter is checked by analyzing artificial test data. Test data is generated from a simulation data set which corresponds to 100% full sample statistics of IC86 one year. Poisson random fluctuations are added to the test data in each bin. Then, maximum loglikelihood fitting is applied. In total, 1000 test data sets are generated. Then the distributions of determined fit parameters are evaluated. Figure 5 shows the histograms of fitted parameters from

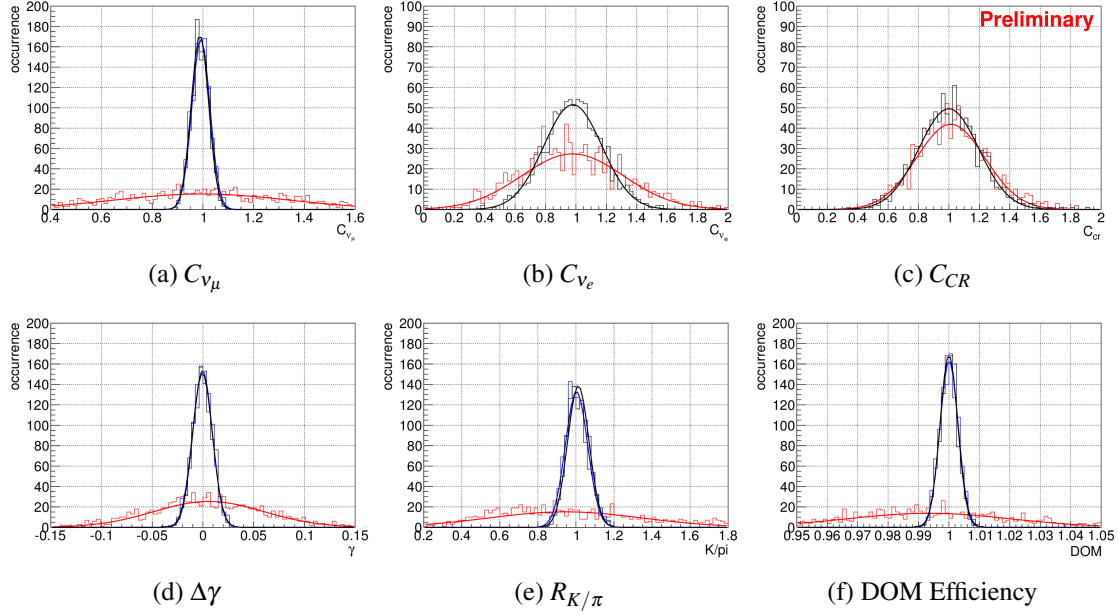


Figure 5: Histogram of fitted parameters from 1000 trial of test data analysis from track + cascade sample (black), track sample only (blue), and cascade sample only (red).

1000 sets of trial test data. The black histograms are from the track + cascade combined analysis, while blue is from track sample only analysis, red is from cascade sample only analysis. Parameters C_{V_e} and C_{Cr} do not apply in the track sample only analysis. One sigma statistical uncertainties of each parameter are listed in the Table 1, for each case of track + cascade combined analysis, track only, and cascade only analysis. Since the track sample has many more events than the cascade sample, most of the parameters determined by the combined analysis are fixed by the track sample (e.g. $C_{V\mu}$, $\Delta\gamma$ and $R_{K/\pi}$). Since parameters are correlated each other, this reduces uncertainties of other parameters, that have previously been determined for the cascade only fit (e.g. C_{V_e}).

6. Systematic Effect

Simultaneously, systematic uncertainties are checked by using simulated test data. Since in this analysis, fluxes of prompt and astrophysical neutrinos are fixed at baseline, we examine how different assumptions for those fluxes could change the results. Recently a new prompt flux called BERSS model [14] has been published, which has a lower flux than the Enberg flux previously used. A test analysis is applied by replacing the fitted model flux with BERSS, while test data is kept produced at Enberg flux. We got +6% higher C_{V_e} , however no significant changes are confirmed in other parameters. The effect from astrophysical flux is also examined in the same way. The value in [10] has $\sim \pm 30\%$ uncertainty, so in extreme case twice of flux is assumed in fitted model flux. Then we got 3% lower C_{V_e} , however no significant changes are seen in other parameters. Additional systematic uncertainties will be evaluated. The neutrino to antineutrino ratio is an uncertainty [12] and also an interest of this analysis, since it also affects the shape of atmospheric neutrino spectrum.

Table 1: Statistic and Systematic error of best fit. One sigma statistical uncertainties expected from test data analysis (Fig. 5) as well as systematic uncertainties are listed.

Fit Parameter	C_{ν_μ}	C_{ν_e}	C_{CR}	$\Delta\gamma$	$R_{K/\pi}$
	statistical				
Combined	$\pm 3\%$	$\pm 19\%$	$\pm 20\%$	± 0.01	$\pm 6\%$
Track	$\pm 4\%$	-	-	± 0.01	$\pm 6\%$
Cascade	$\pm 35\%$	$\pm 33\%$	$\pm 23\%$	± 0.05	$\pm 40\%$
	systematic				
BERSS prompt model	-	+6%	-	-	-
2 \times astrophysical	-	-3%	-	-	-

7. Summary

Conventional atmospheric muon and electron neutrinos will be measured from a combined data sample of track and cascade type events detected by IceCube. An event selection and analysis method has been established. Statistical sensitivity from first year of IceCube 86 string data is performed by test data produced by simulation, which is $\pm 3\%$ for conventional muon neutrino normalization, $\pm 19\%$ for conventional electron neutrino normalization, and ± 0.01 for spectrum index. Statistical uncertainty in electron neutrino normalization will be reduced 43% by combining the track sample and the cascade sample. The statistical sensitivity of the kaon to pion ratio is $\pm 6\%$, sensitive enough to compare with other experimental results [15]. Systematic effects are confirmed in electron neutrino flux, which have prompt and astrophysical neutrino flux model dependencies. Further investigation of model dependent effects will be done by assuming different neutrino fluxes.

References

- [1] IceCube Collaboration, Nucl.Instrum.Meth. **A601** (2009) 294.
- [2] IceCube Collaboration, Eur.Phys.J. **C75** (2015) 116.
- [3] IceCube Collaboration, Phys. Rev. D **91** (2015) 122004.
- [4] A. Gazizov, M. Kowalski, Comput. Phys. Commun. **172** (2005) 203.
- [5] D. Heck, J. Knapp, J. N. Capdevielle, G. Schatz, and T. Thouw, FZKA **6019** (1998) 14.
- [6] IceCube Collaboration, Phys. Rev. D **89** (2014) 062007.
- [7] M. Honda, T. Kajita, K. Kasahara, S. Midorikawa, and T. Sanuki, Phys. Rev. D **75** (2007) 043006.
- [8] T. K. Gaisser, Astroparticle Physics **35** (2012) 801-808.
- [9] R. Enberg, M. H. Reno, and I. Sarcevic, Phys. Rev. D **78** (2008) 043005.
- [10] IceCube Collaboration, Phys. Rev. Lett. **113** (2014) 101101.
- [11] T. K. Gaisser, Cambridge University Press (1991).
- [12] G. D. Barr, S. Robbins, T. K. Gaisser, and T. Stanev, Phys. Rev. D **74** (2006) 094009.
- [13] T. K. Gaisser, S. R. Klein, Astroparticle Physics **64** (2015) 13-17.
- [14] A. Bhattacharya, R. Enberg, M. H. Reno, I. Sarcevic and A. Stasto. (2015)
<http://arxiv.org/abs/1502.01076>
- [15] IceCube Collaboration, Proc. of 32nd ICRC (2011) Beijing, China, arXiv:1111.2735

A search for extremely high energy neutrinos in 6 years (2008-2014) of IceCube data

The IceCube Collaboration¹

¹ http://icecube.wisc.edu/collaboration/authors/icrc15_icecube

E-mail: aya@hepburn.s.chiba-u.ac.jp

Observations of extremely high energy neutrinos ($\gtrsim 10^{16}$ eV) are expected to probe the origin of the highest energy cosmic rays with energies above 10^{20} eV. Cosmogenic neutrinos are produced in the interactions of those most energetic cosmic rays with cosmic microwave background photons (GZK effect) and considered a guaranteed astrophysical neutrino signal. The cosmogenic neutrinos have been searched using the partially and fully completed IceCube detector. We present the updated analysis of the extremely high energy neutrinos above $\sim 10^6$ GeV in the total of 6 years of IceCube sample with 3 years of partially completed IceCube data taken in 2008-2011 and 3 years of completed IceCube data in 2011-2014. The sensitivity for a diffuse flux of cosmic neutrinos with an E^{-2} spectrum in the central 90% energy range 300 TeV to 2 EeV is expected to be at a level of $E^2\phi \leq 3 \times 10^{-9} \text{GeVcm}^{-2}\text{sec}^{-1}\text{sr}^{-1}$ and the improvement corresponds to more than a factor of 2.5 from the previous study with two year data from the nearly completed IceCube detector. The current analysis leads to further constrain or prove the highest energy cosmic-ray origin with the IceCube neutrino observatory.

Corresponding author: Aya Ishihara^{2*}

² *Department of Physics, Graduate School of Science, Chiba University, Chiba 263-8522, Japan*

*The 34th International Cosmic Ray Conference,
30 July- 6 August, 2015
The Hague, The Netherlands*

*Speaker.

1. Introduction

Astrophysical neutrinos are expected to be produced by interactions of ultra-high-energy cosmic-rays (UHECRs) with the surrounding photons and/or matter. These neutrinos, which are undeflected in the Galactic and extra-galactic magnetic field and unattenuated in the photon filled Universe, play an important role as information carriers of hard to identify cosmic accelerators. Moreover, cosmogenic neutrinos [1], also known as GZK neutrinos, that are induced by the highest energy cosmic-ray interactions with background photons in the Universe [2] are expected in the energy region above ~ 10 PeV. These cosmogenic neutrinos are one of the most promising messengers from the high-energy, distant universe beyond PeV energies. They may provide us with direct evidence of the highest energy cosmic-ray sources. However, since the expected flux level of GZK neutrinos is so low, it requires a very large scale neutrino detector. IceCube is a cubic kilometer scale deep underground Cerenkov neutrino detector at the South Pole. The IceCube detector construction was completed in December 2010. The IceCube array comprises 5160 optical sensors on 86 cables, called strings, over a 1 km^3 instrumented volume of ice at a depth of 1450 m to 2450 m. Additional optical sensors frozen into tanks located at the surface near the top of each hole constitute an air shower array called IceTop. In 2008-2009, 2009-2010 and 2010-2011, 40, 59 or 79 out of 86 cables were deployed and taking data with an approximate fiducial volume of 0.5, 0.7 and 0.9 km^3 , respectively. Then in 2011-2014, IceCube accumulated data with the fully completed array. The previous search for cosmogenic neutrinos was carried out with 2 years of data, in which first year data was obtained with 79 strings and second year data was taken with the full array. While two PeV events were discovered by the search [3], no cosmogenic neutrinos were observed [4] and stringent limits were placed on cosmogenic neutrino model fluxes. It was shown that astrophysical objects with populations following a strong cosmological evolution, such as Fanaroff-Riley type II radio galaxies, are unlikely the highest energy cosmic-ray sources. In this proceedings, we present the expected sensitivity of the analysis in search for neutrinos above a PeV with the 6 years of IceCube data taken between April 2008 and May 2014 with an effective livetime of 2050 days.

2. Cosmogenic neutrino events in IceCube

Cosmogenic neutrino fluxes are, to the first order approximation, characterized by broken power-laws above a few PeV. A hard power-law spectrum with spectral index of ~ -0.7 is expected in the energy region below 100 PeV as illustrated in Fig.1. This feature is robust against different highest energy cosmic-ray source models, as this corresponds to the energy threshold of photopion production of the highest energy cosmic-ray proton with the well measured cosmic microwave background photon field. Additionally, the neutrons created in the photopion interactions decay into electron anti-neutrinos with energies around a few PeV. Some models predict an additional contribution in the lower energy region around one PeV [5]. This contribution is highly dependent on higher energy (infrared, optical, and ultraviolet) background photons, as well as the transition energy between Galactic and extragalactic cosmic-rays. Above $\sim 1 \text{ EeV}$ ($=10^9 \text{ GeV}$), the spectrum is expected to soften to $\sim E^{-2.0}$ until $\sim 100 \text{ EeV}$ where the spectrum becomes even steeper depending on the assumed maximal energies of cosmic-ray spectra at the production site.

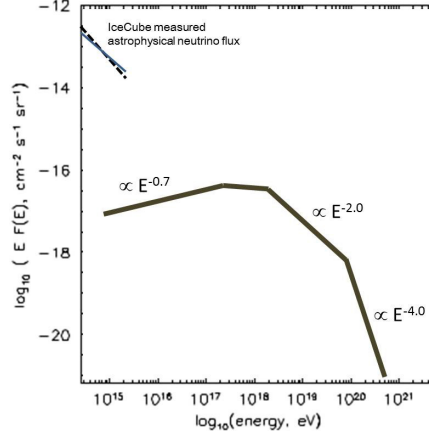


Figure 1: Expected cosmogenic neutrino spectrum and astrophysical neutrino spectrum measured by IceCube

As we see in the next sections, the effective detection area, or the exposure of the current analysis, scales approximately linearly with energy below EeV. The cosmogenic neutrino events observable by IceCube are expected to dominate in the energy range below a few EeV, above which a much more soft spectrum is expected.

When UHECRs interact with the photon field, only ν_e and ν_μ are produced. Due to flavor oscillation, it is expected to become approximately $\nu_e : \nu_\mu : \nu_\tau = 1:1:1$ at Earth. IceCube is sensitive to these three flavors of neutrinos. The largest contribution in the detection of high energy neutrino induced events above a PeV is from the “through-going muon” channel in which muons are created by ν_μ charged current (CC) interactions outside the IceCube fiducial volume and then propagate through the detector emitting Cherenkov light from stochastic energy losses. Since average muons propagate more than 10 km above ~ 1 PeV, this makes the sensitivity of IceCube extend to neutrino interactions far outside the IceCube detector volume. Similarly the contribution from “through-going tau” tracks from ν_τ CC interactions is important in the energy range where the GZK neutrinos are expected, since the tau decay length becomes more than a few km for $\geq 10^8$ GeV whereas it is a few tens of meters for PeV τ s. In addition, particle showers produced at the neutrino interaction vertex position are observed as “cascade” events. Cascade events are induced by neutral current (NC) interactions by all three flavors of neutrinos as well as ν_e CC interactions. While the cascade channel is limited to the interactions occurring inside or near the IceCube detector, their energy deposits in the detector are typically larger than that of muons or taus with equal energy. There is also an interesting contribution from the Glashow resonance [6] at 6.3 PeV, which results when an anti-electron neutrino interacts with an electron in the Earth. This interaction will result in an electron, tau, or hadron induced particle shower, or a muon track.

At energies above ~ 1 PeV, the Earth is not transparent to neutrinos as the neutrino-nucleon cross section increases with energy. Thus, extremely high energy (EHE) neutrinos above the PeV-scale, and their charged secondaries, are able to reach IceCube only from above and slightly below the horizon. Furthermore, the topological features of neutrino induced events change with energy even in each detection channel. For instance, neutrino induced muons exhibit more and more stochastic in energy losses at high energies. In addition, neutrino induced tau events drastically

change from spherical to track-like shapes with increasing energy and above a few PeV electron induced particle showers become elongated due to the LPM effect [7].

3. Signal selections

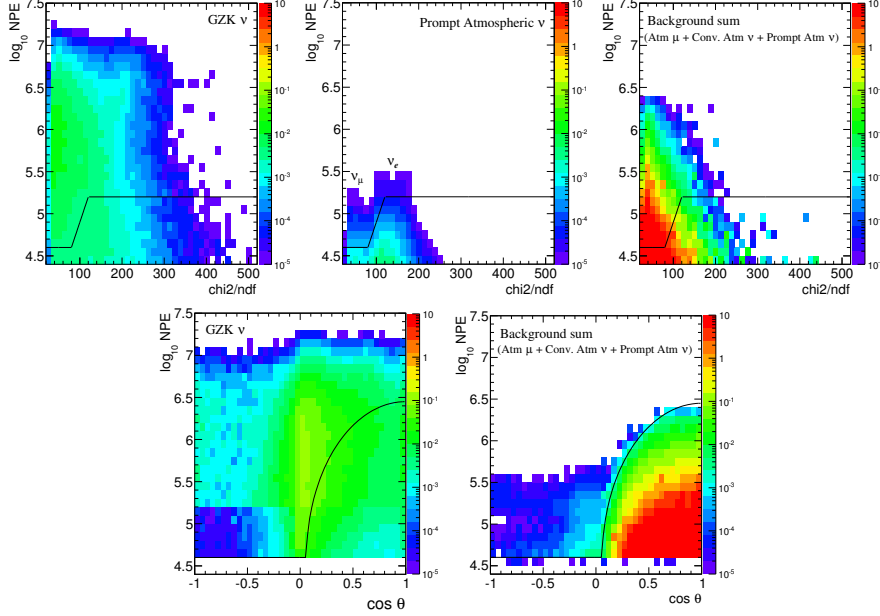


Figure 2: Event number distributions before Level-3 cut (upper panels) and Level-4 cut (lower panels) of the sample corresponding to 2050 days of livetime. The signal distributions in the left panels are from [13] adding all three flavors of neutrinos. The solid lines in each panel indicate the selection criteria in which only the events above the lines are kept. Event distributions from different detector configurations are added. The selection criteria are constant for the samples taken in different data taking periods. Atmospheric muons in the total background shown in the right panels are simulated with pure iron primary cosmic rays. In the case of pure proton primary, the background events are estimated to be a factor of 8 reduced. The upper middle plot shows the prompt atmospheric neutrino distribution to be removed by the Level-3 cut for reference.

The primary background in this analysis is downward-going muon bundles made up of large numbers of muons produced by high energy cosmic-ray interactions in the atmosphere. The secondary background is atmospheric neutrinos. Atmospheric neutrinos are induced by decays of charged mesons produced in cosmic ray interactions with the atmosphere. In particular in the energy region under study, prompt atmospheric neutrinos from decays of short lived heavy mesons are considered to dominate over conventional atmospheric neutrinos from pion and kaon decay. Unlike conventional atmospheric neutrinos, which are dominated by ν_μ , prompt neutrinos are composed of approximately equal fluxes of ν_μ and ν_e . While there must be non-zero prompt atmospheric neutrinos, no experimental observation of a prompt neutrino flux has been made, thus still relatively large theoretical uncertainty remains. In the current study, the model from [8] is considered as the default model. In this analysis, atmospheric muons were simulated with the CORSIKA air-shower simulation package version 6.720 [9] with the SIBYLL 2.1 [10] hadronic interaction model assuming pure proton and iron primary compositions in the energy region between 10^5 and 10^{11} GeV. EHE

neutrino signal events with energy between 10^5 and 10^{11} GeV were simulated using the JULIET package [11].

In the current analysis, signal candidate events are extracted by applying four consecutive background rejection criteria. A large amount of low energy atmospheric muon induced events, typically less than a few TeV, are discriminated by requiring the total number of photo-electrons (NPE) to be greater than 30,000 photo-electrons (p.e.) in the “Level-2” sample. This Level-2 data is subject to the “Level-3” cut which aims to remove atmospheric neutrinos, in particular the prompt neutrinos with a large theoretical uncertainty and atmospheric muons whose direction is not reliably reconstructed. The “Level-4” criterion is optimized to remove well reconstructed atmospheric muons of downward-going directions. Then the final “Level-5” criteria assure that there are no IceTop hits from cosmic-ray air-showers associated with the near final level events.

Figure 2 shows the event distributions as function of χ^2/ndf value and the total number of photo-electrons (NPE) as well as a function of $\cos \theta$ and NPE. The Level-3 and Level-4 NPE threshold as function of reduced χ^2 and cosine of zenith angle are shown as solid lines in Fig. 2. In the Level-4 cut, the NPE threshold for the vertically downward going region is set to a high value ($\sim 2 \times 10^6$) to reject energetic high multiplicity muon bundle events induced by ultra-high-energy cosmic rays. The NPE threshold is gradually reduced towards the horizontal direction because the number and energy of penetrating background atmospheric muons is significantly reduced for the inclined events. An NPE threshold value of $\sim 4 \times 10^4$ is assigned for the events near and below the horizon such that signal EHE cosmogenic neutrino induced events near the horizon can be selected efficiently while rejecting the high energy muon events dominant in the downward-going region and atmospheric neutrinos down to the level of 0.069 events per approximately 6 years of livetime. The Level-4 background events include 0.017 events of atmospheric muons, 0.019 events of conventional atmospheric neutrinos, and 0.033 events of prompt atmospheric neutrinos. To find correlated IceTop hits in the final level cut, downward-going reconstructed event tracks in the ice are extrapolated to the ice surface. Then the time t_{CA} , when the extrapolated tracks are at the closest approach to IceTop tanks, is calculated. The number of the correlated IceTop hits is defined by the number of IceTop hits in the time interval of $-1\mu\text{sec} \leq t_{CA} \leq 1.5\mu\text{sec}$. The final level selection requires the number of the correlated IceTop hits of the event to be less than two. A similar, but more detailed, analysis using the IceTop hits can be found in these proceedings [12].

4. Expected performance

The quasi-differential, model-independent sensitivity of the IceCube detector at 90% CL per energy decade on neutrino fluxes above 10^{15} eV (1 PeV) is shown in Fig. 3 assuming full standard neutrino flavor mixing. The corresponding sensitivity for a diffuse flux of cosmic neutrinos with an E^{-2} spectrum in the central 90% energy range from 300 TeV to 2 EeV is calculated to be $E^2\phi \leq 3 \times 10^{-9} \text{ GeVcm}^{-2} \text{ sec}^{-1} \text{ sr}^{-1}$ with the 6 years of observation. The sensitivity improved by a factor of 2.5 from the previous analysis with approximately two years of IceCube data [4]. Table 1 gives the event rates for several model fluxes for cosmogenic neutrinos assuming the highest energy cosmic-rays above 5×10^{19} eV are protons only. In the present study, at most ~ 5 cosmogenic neutrino events from the models which have not been excluded are expected. This reflects the fact

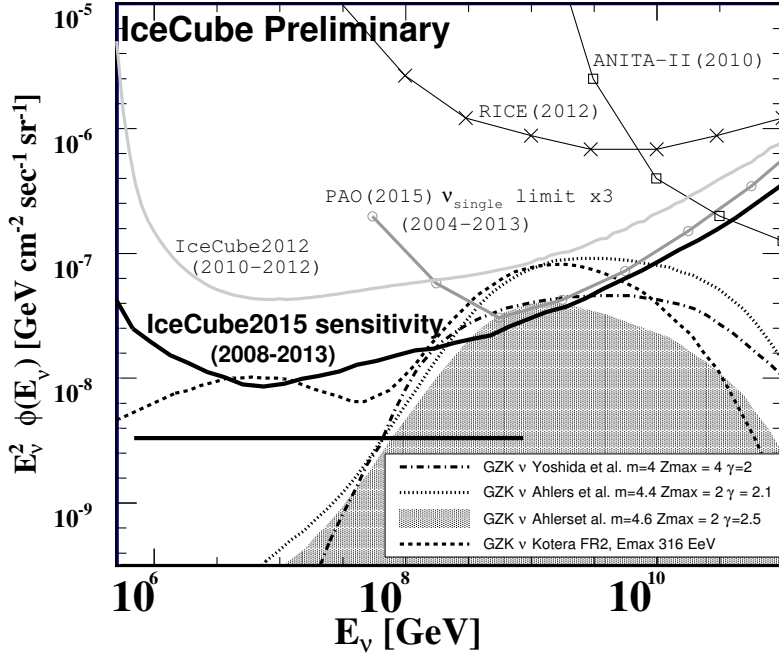


Figure 3: All flavor neutrino flux differential sensitivities of the IceCube detector. Several model predictions (assuming primary protons) are shown for comparison: Ahlers-*max* (the maximal fit), Ahlers-*best* (the best fit, incorporating the Fermi-LAT bound) [13], and Kotera-*SFR* [5] Yoshida-(4,4) ((m , Z_{\max}) = (4,4)) [14]. Model fluxes are summed over all neutrino flavors, assuming standard neutrino oscillations. The model independent differential upper limits by other experiments are also shown for Auger (PAO) [15], RICE [16], ANITA-II [17] Limits from other experiments are converted to the all flavor limit assuming standard neutrino oscillation and a 90% quasi-differential limit per one energy decade when necessary. Errors not included.

that the number of expected signal events is increased by a factor of ~ 2 from the previous study, while a similar background event rate of 0.069 is expected in the total livetime.

The corresponding neutrino effective area averaged over 4π solid angle is shown in the upper plots in Fig. 4. The neutrino effective area represents the surface area of an equivalent detector if it were 100% efficient, and it is proportional to the exposure. The lower panels in Fig. 4 show the Level-4 signal event distributions of each neutrino flavor as a function of neutrino energy at the Earth's surface. It can be seen that the present analysis is sensitive to all three neutrino flavors while the contribution of ν_e is larger near the threshold and decreases with energy.

5. Summary

The selection criteria for the 6 years of IceCube with different detector configurations and the associated analysis sensitivity is presented. The improvement in sensitivity from the previous two-year analysis is approximately a factor of 2.5. IceCube has proven to be the most powerful detector for extraterrestrial neutrinos between several TeV and several PeV. The performance of IceCube in the highest energy region is also expected to be sufficient for the first detection of cosmological neutrinos if the highest energy cosmic-rays have a proton composition. The anticipation for this first detection is thus eagerly awaited.

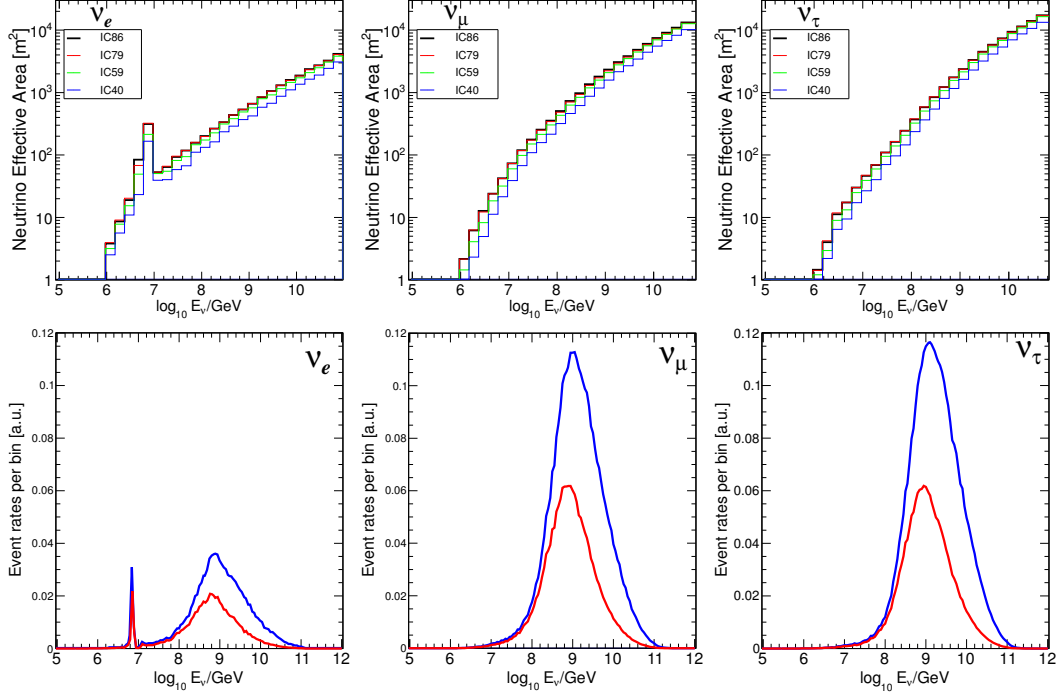


Figure 4: Upper panels show 4π solid angle averaged neutrino effective area for each neutrino flavor and IceCube detector configuration. Each line represented by IC40, IC59, IC79 and IC86 corresponds to effective area for 40, 59, 79 and 86 (full) arrays, respectively. The lower panels present the expected event distribution as function of neutrino energy which passes the Level-4 criteria assuming Ahlers-*Max* (blue line) and Ahlers-*Best* (red line) model from [13].

Models	model parameters				Event rates in 2050 days
	m	Z_{max}	γ	E_{max}	IceCube 2008-2014
Ahlers- <i>Max</i> [13]	4.4	2	2.1	10^{21} eV	7.81 ± 0.03
Ahlers- <i>Best</i> [13]	4.6	2	2.5	10^{21} eV	3.87 ± 0.02
Yoshida-(4,4) [14]	4	4	2.0	10^{22} eV	5.08 ± 0.02
Yoshida-(2,4) [14]	2	4	2.0	10^{22} eV	0.76 ± 0.01
Kotera- <i>GRB</i> [5]	GRB	GRB	2.0	3×10^{20} eV	2.02 ± 0.04
Kotera- <i>SFR</i> [5]	SFR	SFR	2.0	3×10^{20} eV	2.60 ± 0.07

Table 1: Expected number of events detected by IceCube in 6 years from several cosmogenic neutrino models assuming the cosmic-ray primaries to be protons. The spectral indices γ , cutoff energies E_{max} at sources as well as cosmological evolution indices m and extensions in redshift Z_{max} for the cosmic-ray sources are also listed for reference. The corresponding expected number of background events in one year is 0.069 ± 0.003 . Errors are statistical only.

References

- [1] V. S. Berezinsky and G. T. Zatsepin, Phys. Lett. **28B**, 423 (1969).
- [2] K. Greisen, Phys. Rev. Lett. **16**, 748 (1966); G. T. Zatsepin and V. A. Kuzmin, Pisma Zh. Eksp. Teor. Fiz. **4**, 114 (1966) [JETP. Lett. **4**, 78 (1966)].
- [3] M. G. Aartsen *et al.* (IceCube Collaboration), Phys. Rev. Lett. **111**, 021103 (2013).
- [4] M. G. Aartsen *et al.* (IceCube Collaboration), Phys. Rev. D **88**, 112008 (2013).
- [5] K. Kotera, D. Allard, and A. Olinto, J. Cosmol. Astropart. Phys. **10**, 013 (2010).
- [6] S.L. Glashow, Physical Review **118**, 316 (1960).
- [7] For a review, see: S. Klein, Review of Mod. Phys. **71**, 1501 (1999).
- [8] R. Enberg, M.H. Reno, and I. Sarcevic., Phys. Rev. D **78**, 043005 (2008).
- [9] D. Heck *et al.*, Report FZKA **6019**, (Forschungszentrum Karlsruhe 1998).
- [10] E. J. Ahn, R. Engel, T. K. Gaisser, P. Lipari, and T. Stanev, Phys. Rev. D **80**, 094003 (2009).
- [11] S. Yoshida *et al.*, Phys. Rev. D **69**, 103004 (2004).
- [12] D. Tosi and K. Jero for the IceCube Collaboration, PoS(ICRC2015)1086, these proceedings.
- [13] M. Ahlers and F. Halzen, Phys. Rev. D **86**, 083010 (2012).
- [14] S. Yoshida and M. Teshima, Prog. Theor. Phys. **89**, 833 (1993).
- [15] A. Aab *et al.* (Pierre Auger Collaboration), Phys. Rev. D **91**, 092008 (2015).
- [16] I. Kravchenko *et al.* (RICE collaboration), Phys. Rev. D **85**, 062004 (2012).
- [17] P. W. Gorham *et al.* (ANITA Collaboration), Phys. Rev. D **82**, 022004 (2010); P. W. Gorham *et al.* (ANITA Collaboration), Phys. Rev. D **85**, 049901 (2012).

Combined Analysis of the High-Energy Cosmic Neutrino Flux at the IceCube Detector

The IceCube Collaboration

http://icecube.wisc.edu/collaboration/authors/icrc15_icecube

E-mail: lars.mohrmann@desy.de

With the discovery of a high-energy cosmic neutrino flux, the IceCube Neutrino Observatory, located at the geographical South Pole, has opened the field of neutrino astronomy. While evidence for extraterrestrial neutrinos has been found in multiple searches, it was not yet possible to identify their sources; they appear as an isotropic excess. Nevertheless, it is possible to constrain the properties of the sources by measuring the energy spectrum and the flavor composition of the flux, which has been done in several analyses. Typically, these analyses concentrate on specific event classes, such as events with interaction vertices inside the instrumented volume or throughgoing, ν_μ -induced tracks from the Northern hemisphere. Here, we present the latest results from a global analysis, combining the event samples of multiple individual searches, thus covering all detection channels. We derive the energy spectrum and flavor composition of the cosmic neutrino flux in the TeV–PeV energy range. In addition, we show projected sensitivities to the cosmic neutrino flux that can be obtained with further data in the future.

Corresponding author: L. Mohrmann

DESY, Platanenallee 6, D-15738 Zeuthen, Germany

*The 34th International Cosmic Ray Conference,
30 July – 6 August, 2015
The Hague, The Netherlands*

1. Introduction

The discovery of a cosmic neutrino flux in the TeV–PeV energy range at the IceCube Neutrino Observatory [1] has triggered a number of follow-up investigations [2, 3, 4, 5]. Each of these studies was focused on a particular aspect of the flux. Recently, a combined analysis has obtained the most accurate general characterization of the flux so far [6], based on three of the mentioned studies [2, 3, 4] and on previous searches performed with data taken during the construction phase of the IceCube detector [7, 8, 9]. Here, we present the latest results from this analysis, taking into account new data [10, 11, 12]. In addition, we show projected constraints on the properties of the cosmic neutrino flux that can be obtained with more data in the future.

2. Motivation & Expectations

Cosmic neutrinos are produced in interactions of high-energy cosmic rays with matter or radiation [13]. It is expected that such interactions frequently occur within, or close to, the as yet unknown acceleration sites of the cosmic rays [14]. Because neutrinos are neutral and weakly interacting, they can travel unhindered to the Earth, carrying with them unique information about the environments they originate from. Candidate sites for high-energy neutrino emission include active galactic nuclei, gamma-ray bursts, and starburst galaxies, but also objects within our Galaxy, such as supernova remnants or pulsar wind nebulae [15].

Ultimately, the aim of neutrino astronomy is to resolve, and thus identify, individual sources of high-energy neutrinos. However, this was not yet possible for the observed cosmic neutrino flux; the arrival directions of the neutrinos are consistent with an isotropic flux [2, 10]. Nevertheless, it is possible to constrain the properties of the sources by measuring general characteristics of the flux, such as its energy spectrum and its composition of neutrino flavors [16, 17].

The expected energy spectrum of the cosmic neutrino flux depends on the energy spectrum of the primary cosmic rays as well as on the type of interactions and the environments of the source. If the Fermi shock acceleration mechanism is responsible for the acceleration of the cosmic rays, a power law energy spectrum with spectral index close to -2 is expected [18]. If, in addition, the neutrinos are created in interactions of cosmic rays with ambient matter (i.e. pp-interactions), the energy spectrum of the secondary neutrinos approximately follows that of the primary cosmic rays. The energy spectrum of neutrinos created in interactions of cosmic rays with photons (i.e. p γ -interactions) will depend on the target photon field [16]. A power law spectrum with index -2 has served as a popular benchmark scenario in the past.

The majority of cosmic neutrinos are expected to be created in the decay of charged pions ($\pi \rightarrow \mu + \nu_\mu$) and the subsequent decay of the muons ($\mu \rightarrow e + \nu_e + \nu_\mu$). In this scenario, the initial composition of neutrino flavors is $\nu_e : \nu_\mu : \nu_\tau = 1 : 2 : 0$. During propagation, the composition is transformed due to neutrino oscillations, leading to an expected composition of approximately $1 : 1 : 1$ at the Earth [17]. In environments with a large magnetic field, the flux of neutrinos from muon decay is suppressed; in the limiting case the flavor composition becomes $0 : 1 : 0$ (approximately $1 : 1.8 : 1.8$ at Earth) in this scenario [17]. In another scenario, the cosmic neutrinos originate from the decay of neutrons rather than pions, resulting in a flavor composition of $1 : 0 : 0$ (approximately $2.5 : 1 : 1$ at Earth) [17].

Deviations from these idealized scenarios for the energy spectrum and flavor composition are likely to occur, in particular in environments with large matter or radiation densities, or large magnetic fields, see e.g. [19, 20].

3. Detecting Neutrinos with IceCube

The IceCube Neutrino Observatory [21] is a neutrino telescope located at the geographical South Pole in Antarctica. It consists of more than 5,000 optical sensors, installed on 86 vertical strings, buried in a cubic-kilometer of glacial ice between depths of 1,450 m and 2,450 m. Neutrino interactions are recorded by detecting the Cherenkov emission of secondary particles created in the interactions. Based on the arrival time and the amount of light registered in the sensors, the energy and incoming direction of the neutrino can be inferred.

The signatures that neutrinos leave in the IceCube detector can be classified in two categories. On the one hand, *tracks* arise from charged-current ν_μ interactions. The muons created in such interactions can travel for several kilometers, thus leaving an elongated, track-like signature. Depending on whether the interaction occurs inside or outside the instrumented volume of the detector, we distinguish *starting tracks* and *throughgoing tracks*.

On the other hand, charged-current interactions of ν_e and ν_τ and neutral-current interactions of all neutrinos lead to *showers*. The dimensions of the electromagnetic and hadronic particle showers created in these interactions are much smaller than the sensor spacing, resulting in a spherical signature. In the past, only *contained showers* were studied, i.e. those that start well inside the detection volume. In another contribution to this conference [12], *uncontained showers* that start near the edge of the detection volume are analyzed for the first time.

Charged-current interactions of ν_τ can be identified at very high energies, $\gtrsim 1$ PeV. While no ν_τ were identified yet, a new upper limit on the cosmic ν_τ flux is presented in [11]. The limit is derived from a search for events that exhibit *double pulse waveforms*, i.e. a double-peak structure in the time-resolved signal recorded by the sensors. Such a signature is expected for charged-current ν_τ interactions, where the first pulse is due to the interaction of the neutrino and the second pulse results from the decay of the tau.

4. Analysis

The analysis presented here is a continuation of the analysis presented in [6]. The method is summarized in the following; the reader is referred to the reference for more details.

The event samples analyzed here are listed in Table 1. Where data taking periods overlap, the event samples were separated with additional criteria, thus ensuring statistical independence of all samples. Each sample provides simulated probability density functions (PDFs) as well as experimental distributions for the observables listed in the third column of the table. PDFs are available both for background components and for the expected cosmic neutrino flux.

Background contributions to the event samples are entirely of atmospheric origin, i.e. muons and neutrinos created in air showers initiated by cosmic rays impinging on the Earth's atmosphere. The contribution of atmospheric muons is estimated by simulating air showers with the CORSIKA

ID	Signatures	Observables	Period	References
T1	throughgoing tracks	energy, zenith	2009–2010	[7]
T2	throughgoing tracks	energy, zenith	2010–2012	[4]
S1	cont. showers	energy	2008–2009	[8]
S2	cont. showers	energy	2009–2010	[9]
H1*	cont. showers, starting tracks	energy, zenith	2010–2014	[1, 2, 10]
H2	cont. showers, starting tracks	energy, zenith, signature	2010–2012	[3]
DP*	double pulse waveform	signature	2011–2014	[11]
US*	uncont. showers	energy	2010–2012	[12]

Table 1: Event selections used in this analysis. Listed are the selected signatures, observables used in the analysis, and the data taking period. Event selections marked with an asterisk were newly added or extended with respect to the analysis presented in [6]. Note that only the sample of uncontained showers from reference [12], which represents a new signature previously not considered, is used here.

code [22]. Atmospheric neutrinos are divided in two categories: conventional atmospheric neutrinos originate from the decay of pions and kaons and prompt atmospheric neutrinos arise from the decay of mesons containing a charm quark. Because pions and kaons are more likely to re-interact than to decay at the energies relevant here, the energy spectrum of conventional atmospheric neutrinos is steeper than that of prompt atmospheric neutrinos, whose parent particles always decay. We use the models from Honda et al. [23] and Enberg et al. [24] to obtain a prediction of the contribution of conventional and prompt atmospheric neutrinos to the event samples, respectively. Both models were slightly modified (see [7]) to conform with recent measurements of the primary cosmic ray spectrum in the knee region, based on the composition model from [25] (known as H3a model). Furthermore, the normalizations of both components are free parameters in the analysis, denoted by ϕ_{conv} and ϕ_{prompt} , respectively.

We use two different spectral hypotheses to describe the cosmic neutrino flux:

$$\begin{aligned}
 \text{Hypothesis A:} \quad \Phi_{\nu} &= \phi \times \left(\frac{E}{100 \text{ TeV}} \right)^{-\gamma} \\
 \text{Hypothesis B:} \quad \Phi_{\nu} &= \phi \times \left(\frac{E}{100 \text{ TeV}} \right)^{-\gamma} \times \exp(-E/E_{\text{cut}}).
 \end{aligned} \tag{4.1}$$

The first hypothesis is a simple power law, where ϕ denotes the flux at 100 TeV and γ is the spectral index. The second hypothesis allows for an exponential high-energy cut-off in addition, where the cut-off energy is denoted by E_{cut} . To determine the energy spectrum, we assume that the flux is composed of equal flavors at Earth. The flavor composition is then derived by varying the normalizations of all three flavors independently, assuming that their energy spectrum is identical.

Systematic uncertainties, such as the spectral index of the primary cosmic ray spectrum, or the global energy scale, are incorporated in the analysis procedure via several nuisance parameters.

The experimental data are compared to the simulated PDFs by means of a binned Poisson-likelihood analysis. The best-fit parameter values of the models are determined by maximizing the likelihood to obtain the observed distributions of observables in all samples (cf. Table 1) simultaneously.

5. Results

The results of the analysis are summarized in Table 2. When no cut-off is present, the best-fit spectral index is 2.49 ± 0.08 . If an exponential cut-off is allowed, the best-fit spectral index is $2.31^{+0.14}_{-0.15}$, and the best-fit cut-off energy is $(2.7^{+7.7}_{-1.4})$ PeV. These measurements are valid in the energy range 27 TeV – 2 PeV (hypothesis A) and 22 TeV – 5.3 PeV (hypothesis B). The hypothesis with a cut-off is slightly preferred, although with a significance of only 1.2σ ($p = 12\%$). Both models describe the data reasonably well. On the other hand, an unbroken power law spectrum with spectral index $\gamma = 2$ can be excluded with a significance of 4.6σ ($p = 0.00018\%$).

The correlation between the spectral index γ and the cut-off energy E_{cut} is visualized in fig. 1(a). Figure 1(b) shows the best-fit spectrum for both hypotheses together with a differential model that extracts the cosmic neutrino flux in separate energy intervals.

Results on the flavor composition are presented in table 3 and fig. 2. For both spectral hypotheses, the flux consists of ν_e and ν_μ in approximately equal parts at the best fit. However, compositions expected for pion-decay sources (1 : 2 : 0 at source) and muon-damped sources (0 : 1 : 0 at source) are still compatible with our data. On the other hand, a flux composed purely of electron neutrinos at the source is excluded with a significance of 3.7σ ($p = 0.012\%$).

The derived constraints are improved, but largely similar with respect to those of the previous analysis [6]. While the hypothesis with an exponential cut-off is now marginally preferred, no firm conclusion can be drawn at this point.

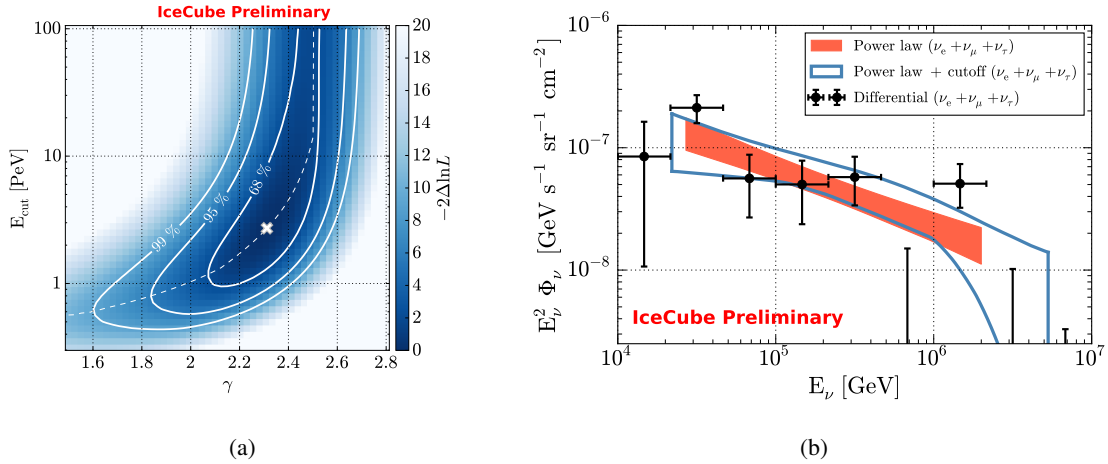


Figure 1: Results on the energy spectrum. (a) Profile likelihood scan of parameters γ and E_{cut} . The best fit is marked with ‘x’. The dashed line shows the conditional best-fit value of E_{cut} for each value of γ . (b) Energy spectrum of the cosmic neutrino flux. Shown are the spectra allowed at 68% C.L. for hypothesis A (power law) and hypothesis B (power law + cutoff). In addition, the strength of the cosmic neutrino flux in separate energy intervals is shown (differential).

Param.	Unit	Hyp. A	Hyp. B
ϕ_{conv}	HKKMS	$1.10^{+0.20}_{-0.15}$	$1.11^{+0.20}_{-0.15}$
ϕ_{prompt}	ERS	$0.0^{+0.7}_{-0.0}$	$0.0^{+0.8}_{-0.0}$
ϕ	$10^{-18} \text{ GeV}^{-1} \text{ s}^{-1} \text{ sr}^{-1} \text{ cm}^{-2}$	$7.0^{+1.0}_{-1.0}$	$8.0^{+1.3}_{-1.2}$
γ	—	$2.49^{+0.08}_{-0.08}$	$2.31^{+0.14}_{-0.15}$
E_{cut}	PeV	—	$2.7^{+7.7}_{-1.4}$
$-2\Delta\ln L$		+1.94	0

Table 2: Best-fit results for the energy spectrum. The quoted uncertainties are at 1σ confidence level.

The impact of the newly added tau search event sample (DP, cf. table 1) is mainly visible in the flavor composition fit, see fig. 2. In contrast, the new event sample of uncontained showers (US) and the extended event sample of analysis H1 mainly affect the energy spectrum and contribute to the slight preference of an exponential cut-off. The samples DP and US represent new event signatures that were previously not considered in the analysis. Almost all of the event selections can be applied to new data that are already recorded. The resulting expected sensitivity to the energy spectrum and flavor composition is investigated in the following section.

6. Projected Sensitivities

In order to derive the future sensitivity of the IceCube detector to the properties of the cosmic neutrino flux, we use a prototype analysis that is based on the event selections of samples T2, H2, DP, and US (cf. Table 1). We weight the simulated cosmic neutrino flux to the current best-fit energy spectrum of hypothesis A or B (cf. previous section) and scale the expected signal up to mimic the collection of additional data. For the conventional and prompt atmospheric neutrino flux, we assume a flux at the level of the predictions by Honda et al. [23] and Enberg et al. [24], respectively. The sensitivity is then derived using the approach described in [26].

The projected sensitivity to the energy spectrum is illustrated in fig. 3(a), where we focus on the sensitivity to the presence of an exponential high-energy cut-off to the spectrum. The two large panels show expected limits on the energy of such an exponential cut-off, where the current best-fit spectrum of hypothesis A and B is assumed to be the true spectrum in the top and bottom panel, respectively. If no cut-off is present, the expected lower limit with 10 years of full detector data is 6.7 PeV at 2σ confidence, i.e. well above the current best-fit value of 2.7 PeV. On the other hand, for a true cut-off energy at the current best fit, the non-existence of an exponential cut-off can be rejected with a significance of $\sim 3\sigma$ with 10 years of data. Note that a single isotropic cosmic neutrino flux is assumed in all cases.

Param.	Unit	Hyp. A	Hyp. B
ϕ_e	$10^{-18} \text{ GeV}^{-1} \text{ s}^{-1} \text{ sr}^{-1} \text{ cm}^{-2}$	$3.2^{+0.7}_{-1.5}$	$3.6^{+0.8}_{-1.7}$
ϕ_μ	$10^{-18} \text{ GeV}^{-1} \text{ s}^{-1} \text{ sr}^{-1} \text{ cm}^{-2}$	$3.3^{+0.7}_{-0.6}$	$3.7^{+0.8}_{-0.7}$
ϕ_τ	$10^{-18} \text{ GeV}^{-1} \text{ s}^{-1} \text{ sr}^{-1} \text{ cm}^{-2}$	$0.0^{+2.4}_{-0.0}$	$0.0^{+2.6}_{-0.0}$
γ	—	$2.53^{+0.08}_{-0.08}$	$2.35^{+0.14}_{-0.15}$
E_{cut}	PeV	—	$2.7^{+7.5}_{-1.4}$
$-2\Delta\ln L$		+1.69	0

Table 3: Best-fit results for the flavor composition fit. The quoted uncertainties are at 1σ confidence level.

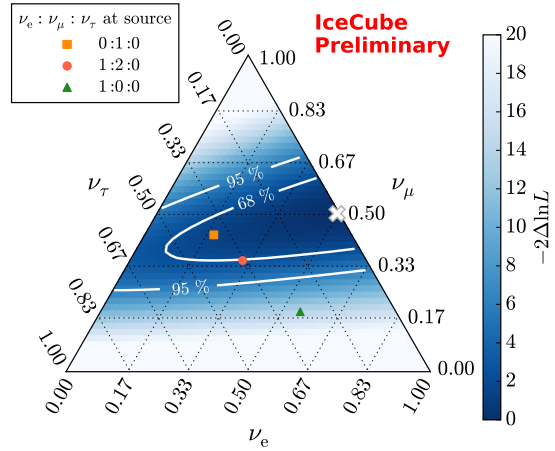


Figure 2: Results on the flavor composition, using hypothesis B for the energy spectrum. Each point on the triangle corresponds to a ratio $\nu_e : \nu_\mu : \nu_\tau$ as measured at Earth. The best fit is marked with ‘x’. Compositions expected for three different source scenarios are indicated.

Finally, to illustrate our future sensitivity to the flavor composition of the cosmic neutrino flux, we show the median expected constraints for 10 years of full detector data in fig. 3(b). Here, we assume an energy spectrum matching the current best fit of hypothesis B and that the cosmic neutrino flux consists of equal flavors. Although we included a search for ν_τ signatures in this analysis for the first time, a degeneracy with respect to the ν_e/ν_τ fraction remains, resulting in the elongated shape of the contours. However, the ability to distinguish between different source scenarios is largely orthogonal to this degeneracy, and thus not affected.

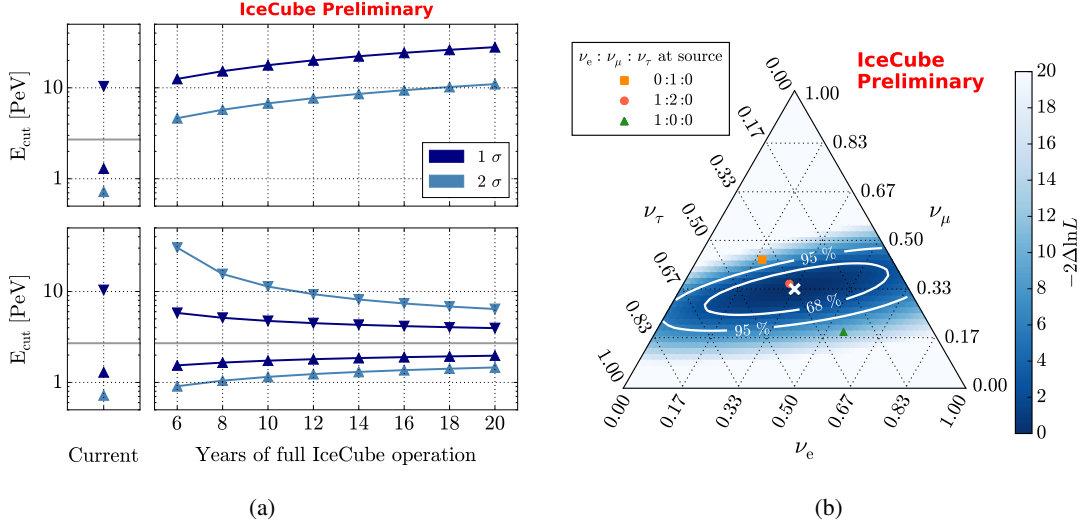


Figure 3: (a) Current (small panels) and projected (large panels) constraints on the energy of an exponential cut-off to the spectrum. The two small panels show the best-fit result of hypothesis B. In the top (bottom) right panel, the best-fit spectrum of hypothesis A (B) is assumed to be true. Dark and light blue points indicate median 1 σ and 2 σ limits, respectively. (b) Projected sensitivity to the flavor composition, for 10 years of full detector data. The white ‘x’ marks the assumed true flavor composition of $\nu_e : \nu_\mu : \nu_\tau = 1 : 1 : 1$.

7. Summary

We have presented a continuation of the combined likelihood analysis of the diffuse cosmic neutrino flux presented in [6]. We find that the energy spectrum of the cosmic neutrino flux is well described by an unbroken power law, with a best-fit spectral index of -2.49 ± 0.08 . This corresponds to a rejection of an unbroken power law with index -2 with 4.6σ significance ($p = 0.00018\%$). While the analysis slightly favors a harder power law ($E^{-2.31 \pm 0.15}$) with an exponential cut-off at $(2.7^{+7.7}_{-1.4})$ PeV over an unbroken power law, the statistical significance of 1.2σ ($p = 12\%$) is too low to draw any conclusion. However, we have shown that the presence of a cut-off can likely be determined with additional data in the foreseeable future. Other, more complex spectral shapes are also possible, although currently not required to describe the data.

The flavor composition of the cosmic neutrino flux is compatible with standard scenarios for the neutrino production at the sources. However, a neutron-decay dominated scenario, in which only electron neutrinos are produced at the sources, can be ruled out with 3.7σ significance ($p = 0.012\%$). A projection of our sensitivity to the flavor composition has shown that while a

degeneracy with respect to the ν_e/ν_τ fraction remains, a distinction between more source scenarios might be possible.

References

- [1] M. G. Aartsen et al. (IceCube Collaboration), *Science* **342** (2013) 1242856. [arXiv:1311.5238].
- [2] M. G. Aartsen et al. (IceCube Collaboration), *Phys. Rev. Lett.* **113** (2014) 101101. [arXiv:1405.5303].
- [3] M. G. Aartsen et al. (IceCube Collaboration), *Phys. Rev. D* **91** (2015) 022001. [arXiv:1410.1749].
- [4] M. G. Aartsen et al. (IceCube Collaboration), *Evidence for Astrophysical Muon Neutrinos from the Northern Sky with IceCube, submitted to Phys. Rev. Lett.* (2015). [arXiv:1507.04005].
- [5] M. G. Aartsen et al. (IceCube Collaboration), *Phys. Rev. Lett.* **114** (2015) 171102. [arXiv:1502.03376].
- [6] M. G. Aartsen et al. (IceCube Collaboration), *A combined maximum-likelihood analysis of the high-energy astrophysical neutrino flux measured with IceCube, accepted by Astrophys. J.* (2015). [arXiv:1507.03991].
- [7] M. G. Aartsen et al. (IceCube Collaboration), *Phys. Rev. D* **89** (2014) 062007. [arXiv:1311.7048].
- [8] M. G. Aartsen et al. (IceCube Collaboration), *Phys. Rev. D* **89** (2014) 102001. [arXiv:1312.0104].
- [9] A. Schönwald et al. for the IceCube Collaboration, *Search for diffuse astrophysical neutrinos with cascade events in the IceCube-59 detector*, in *Proc. 33rd ICRC*, 2013. arXiv:1309.7003.
- [10] M. G. Aartsen et al. (IceCube Collaboration), *PoS(ICRC2015)1081, these proceedings*.
- [11] M. G. Aartsen et al. (IceCube Collaboration), *PoS(ICRC2015)1071, these proceedings*.
- [12] M. G. Aartsen et al. (IceCube Collaboration), *PoS(ICRC2015)1109, these proceedings*.
- [13] T. K. Gaisser, F. Halzen, and T. Stanev, *Phys. Rep.* **258** (1995) 173–236.
- [14] J. G. Learned and K. Mannheim, *Annu. Rev. Nucl. Part. S.* **50** (2000) 679–749.
- [15] J. K. Becker, *Phys. Rep.* **458** (2008) 173–246. [arXiv:0710.1557].
- [16] P. Lipari, M. Lusignoli, and D. Meloni, *Phys. Rev. D* **75** (2007) 123005. [arXiv:0704.0718].
- [17] S. Choubey and W. Rodejohann, *Phys. Rev. D* **80** (2009) 113006. [arXiv:0909.1219].
- [18] T. K. Gaisser, *Cosmic Rays and Particle Physics*. Cambridge University Press, Cambridge, 1990.
- [19] T. Kashti and E. Waxman, *Phys. Rev. Lett.* **95** (2005) 181101. [arXiv:astro-ph/0507599].
- [20] W. Winter, J. Becker Tjus, and S. R. Klein, *Astron. Astrophys.* **569** (2014) A58. [arXiv:1403.0574].
- [21] T. K. Gaisser and F. Halzen, *Annu. Rev. Nucl. Part. S.* **64** (2014) 101–123.
- [22] D. Heck, J. Knapp, J. N. Capdevielle, G. Schatz, and T. Thouw, *CORSIKA: a Monte Carlo code to simulate extensive air showers*, Tech. Rep. FZKA 6019, Forschungszentrum Karlsruhe, 1998.
- [23] M. Honda, T. Kajita, K. Kasahara, S. Midorikawa, and T. Sanuki, *Phys. Rev. D* **75** (2007) 043006. [arXiv:astro-ph/0611418].
- [24] R. Enberg, M. H. Reno, and I. Sarcevic, *Phys. Rev. D* **78** (2008) 043005. [arXiv:0806.0418].
- [25] T. K. Gaisser, *Astropart. Phys.* **35** (2012) 801–806. [arXiv:1111.6675].
- [26] G. Cowan, K. Cranmer, E. Gross, and O. Vitells, *Eur. Phys. J. C* **71** (2011) 1554. [arXiv:1007.1727].

A Search for Astrophysical Tau Neutrinos in Three Years of IceCube Data

The IceCube Collaboration[†],

[†] http://icecube.wisc.edu/collaboration/authors/icrc15_icecube

E-mail: drwilliams3@ua.edu

The IceCube Neutrino Observatory has reported a diffuse flux of TeV-PeV astrophysical neutrinos in three years of data. The observation of tau neutrinos in the astrophysical neutrino signal is of great interest in determining the nature of astrophysical neutrino oscillations. Tau neutrinos become distinguishable from other flavors in IceCube at energies above a few hundred TeV, when the particle shower from the initial charged current interaction can be separated from the cascade from the tau decay: the two cascades are called a "double bang" signature. An analysis is presented which uses the digitized signal from individual IceCube sensors to resolve the two showers, in order to be sensitive to taus at as low an energy as possible. This is the first IceCube search to be more sensitive to tau neutrinos than to any other flavor. No candidate events were observed in three years of completed IceCube data. The resulting limit and prospects for future high energy tau neutrino searches, including a search for higher energy double bangs, will be discussed.

Corresponding authors: D. R. Williams^{1*}, M. Vraeghe²,
D. L. Xu¹

¹ *Dept. of Physics and Astronomy, University of Alabama, Tuscaloosa, AL 35487, USA*

² *Dept. of Physics and Astronomy, University of Gent, B-9000 Gent, Belgium*

*The 34th International Cosmic Ray Conference,
30 July- 6 August, 2015
The Hague, The Netherlands*

*Speaker.

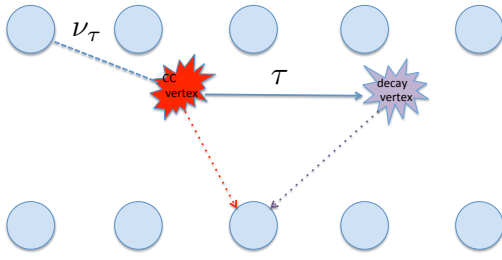


Figure 1: ν_τ double bang event topology

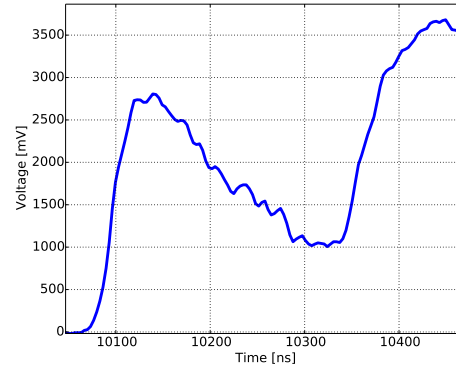


Figure 2: Simulated double pulse waveform from a ν_τ CC interaction.

1. Introduction

The IceCube Neutrino Observatory recently announced a significant detection of diffuse high energy astrophysical neutrinos [1]. The flavor composition of the flux detected by IceCube is consistent with equal fractions of all neutrino flavors [2]. Of particular interest is the identification of tau neutrinos, which are only expected to be produced in negligible amounts in astrophysical accelerators, but should appear in the flux detected by IceCube due to neutrino flavor change. IceCube is a cubic-kilometer neutrino detector installed in the ice at the geographic South Pole between depths of 1450 m and 2450 m [3]. Detector construction started in 2005 and finished in 2010. The reconstruction of neutrino properties relies on the optical detection of Cherenkov radiation emitted by secondary particles produced in neutrino interactions in the surrounding ice or the nearby bedrock. The basic IceCube sensor is the Digital Optical Module (DOM), which contains a photomultiplier tube (PMT) and electronics which digitize the PMT waveform.

Events in IceCube generally have one of two overall topologies: “track” events from ν_μ charged current (CC) interactions, as well as from muons produced in cosmic ray induced air showers; and “cascade” events from ν_e CC interactions and neutral current (NC) interactions of all flavors. At energies below about 1 PeV, ν_τ CC interactions will appear as a single cascade. At energies above about 1 PeV, the tau lepton decay length becomes large enough that IceCube can resolve the first ν_τ CC interaction cascade from the second tau lepton decay cascade. This double cascade signature is called a double bang [4] and is shown in Figure 1. The first tau neutrino search in IceCube used the partially constructed detector (22 strings) and searched for partially contained double bangs [5]. This search was in fact more sensitive to ν_e and ν_μ than to ν_τ . Here we present the result of a search for closely separated ν_τ double bangs in the complete IceCube detector using individual DOM waveforms. This is the first ν_τ search in IceCube to be more sensitive to tau neutrinos than to other neutrino flavors. We also discuss a search for well-separated contained double bangs in IceCube.

2. Double Pulse Event Search

This search for ν_τ in IceCube looks for double bangs which are close enough together that the two cascades are not well resolved, but appear as a double pulse in a single IceCube DOM waveform. A simulated double pulse from a ν_τ CC interaction in IceCube is shown in Figure 2. This search uses 914.1 days of data from the fully constructed IceCube detector between May 13, 2011 and May 6, 2014. The criteria for data selection are that all IceCube strings were collecting data, and no *in situ* calibration light sources were in use. The waveforms used are from the Analog Transient Waveform Digitizer (ATWD) which digitizes at 3.3 ns per sample for 128 samples [7]. Event selection criteria were developed using simulation and 10% of the data; the remaining 90% of data were kept blind until analysis cuts were finalized.

Since resolved double pulses will only be produced in high energy ν_τ interactions, this analysis selects events which pass the IceCube Extremely High Energy (EHE) filter, which requires that the event deposit at least 1000 photoelectrons (PE) in the detector. Further event selection criteria are denoted as Level 4 and higher.

At Level 4, an additional charge cut is applied, requiring events to deposit at least 2000 PE in the detector. Individual DOM waveforms are then examined for double pulse characteristics. An updated implementation of the double pulse algorithm (DPA) previously described in [6] is run on each individual DOM which records a charge of at least 430 PE. This algorithm searches for a rising edge in the waveform followed by a falling edge, which defines the first pulse, followed by another rising edge which defines the second pulse. The falling edge of the second pulse is often outside of the 422 ns ATWD window and is therefore not included in the algorithm. The DPA is optimized to reject small pulses from late light due to scattering. An event is defined as a double pulse event and passes Level 4 if at least one DOM in the event passes the DPA.

The Level 5 event selection is designed to reject track-like events which pass the DPA. Such events result from muons which undergo large stochastic energy losses within a few meters of a DOM. Each event is reconstructed using a maximum likelihood method based on the hypothesis of an infinite track and the hypothesis of a point-like cascade. These reconstructions only make use of the timing information for the earliest photon arriving at the DOMs. The log likelihood ratio between the two hypotheses $\log(L_{\text{cascade}}/L_{\text{track}})$ is required to be negative, indicating the event topology is more cascade-like than track-like. Additionally, the first hit in the event is required to be below the top 40 meters of the instrumented volume.

The final event selection at Level 6 requires events to pass a containment cut in order to eliminate muons interacting near the edge of the detector. An additional reconstruction algorithm is performed on all events which pass the preceding cuts, using full charge and time information, and the reconstructed vertex of the event is required to be within the detector boundary.

The expected number of events in 914 days at the final event selection level are shown in Table 1 for both signal and background. Event rate predictions for astrophysical neutrinos assume a flux of $E^2\Phi_\nu = 1.0 \times 10^{-8} \text{ GeV cm}^{-2} \text{ s}^{-1} \text{ sr}^{-1}$ per flavor [8]. Backgrounds include muons and neutrinos from cosmic ray induced air showers and astrophysical neutrinos of other flavors. The atmospheric neutrino rate prediction takes into account both the π/K decay neutrinos [11] and the charmed meson decay neutrinos [12]. A knee-corrected cosmic ray spectrum is used in predicting the π/K production in the atmosphere [13]. We expect 0.54 signal events and 0.35 background

Table 1: Predicted event rates from all sources at final cut level for the double pulse event search. Errors are statistical only.

Data samples	Events in 914.1 days (final cut)
Astrophysical ν_τ CC	$(5.4 \pm 0.1) \cdot 10^{-1}$
Astrophysical ν_μ CC	$(1.8 \pm 0.1) \cdot 10^{-1}$
Astrophysical ν_e	$(6.0 \pm 1.7) \cdot 10^{-2}$
Atmospheric ν	$(3.2 \pm 1.4) \cdot 10^{-2}$
Atmospheric muons	$(7.5 \pm 5.8) \cdot 10^{-2}$

events in 914 days. The largest background is from astrophysical ν_μ CC interactions, which can produce a high energy muon that loses energy stochastically near a DOM and causes a double pulse waveform.

After unblinding the remaining 90% of the data sample, no events are found in 914 days. The integrated astrophysical ν_τ flux upper limit between 214 TeV and 72 PeV is found to be 5.1×10^{-8} GeV cm⁻² sr⁻¹ s⁻¹, which about 5 times higher than the per-flavor best fit to the IceCube astrophysical flux. A ν_τ flux differential upper limit in the energy region of 214 TeV to 72 PeV is shown in Figure 3. The differential upper limit was extracted following the procedure that was employed in deriving quasi-differential upper limits from previous EHE cosmogenic neutrino searches in IceCube [14, 15, 10]. In this procedure, flux limits were computed for each energy decade with a sliding energy window of 0.1 decade, assuming that the neutrino event spectrum evolves as $1/E$ [16]. Since zero events were found, the 90% C.L. event count limit in each energy decade is 2.4 based on the Feldman-Cousins approach [17]. The energy threshold of this limit is 1000 times lower than previous dedicated tau neutrino searches by cosmic ray air shower detectors [18].

3. Double Bang Event Search

Double bang events have a larger separation between the two cascades than double pulse events, and thus occur at a higher primary neutrino energy. The event selection requires events to pass the EHE filter, denoted Level 3. Figure 4 shows the effective areas after the EHE filter cut for ν_τ obtained by selecting contained double bang events with different minimum separations between the two cascades. It can be seen that the energy threshold for the identification of ν_τ via this signature increases with distance between the two cascades. At Level 4, an additional charge cut is applied, requiring at least 3100 PE total charge deposited in the event. At Level 5, a Boosted Decision Tree (BDT) is used for further background rejection. This BDT is trained using simulated ν_τ CC events (with a minimum separation of 50 m and with the two cascades contained within the detector volume) as signal, and simulated cosmic ray muons as background. Six variables are used in the BDT:

- Total charge
- Duration of the event in the detector
- Average height of the first 5 hit DOMs

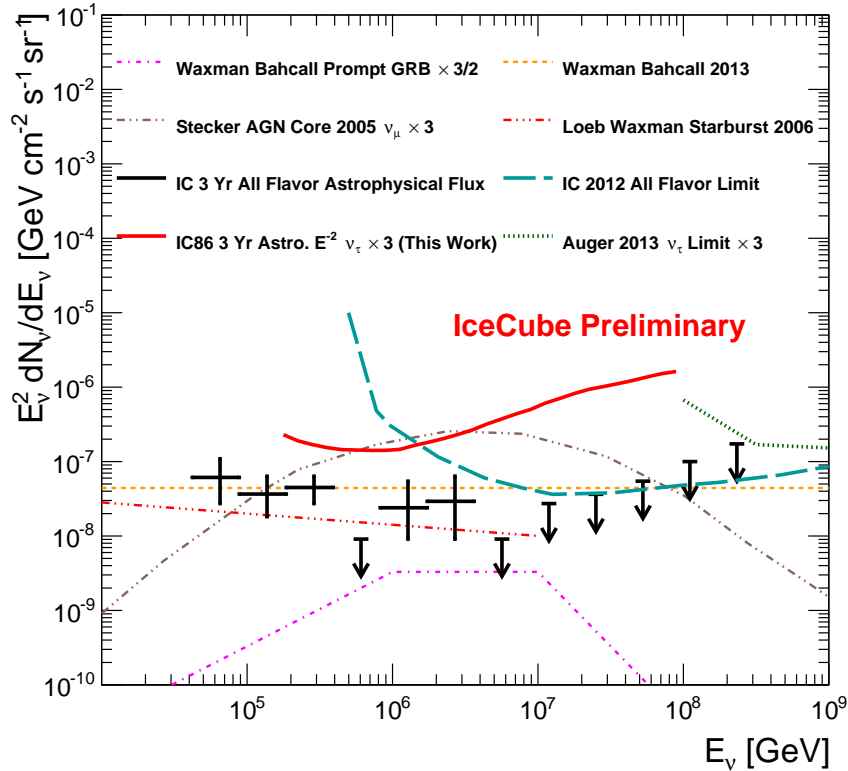


Figure 3: Neutrino flux upper limits and models as a function of the primary neutrino energy. The thick red curve is the ν_τ differential upper limit derived from this analysis. The black crosses depict the all flavor astrophysical neutrino flux observed by IceCube [1]. The thick dashed line is the differential upper limit derived from a search for extremely high energy events which has found the first two PeV cascade events in IceCube [9, 10]. The thick dotted line is the Auger differential upper limit from ν_τ induced air showers [18]. The thin dash line (orange) is the Waxman-Bahcall upper bound which uses the UHECR flux to set a bound on astrophysical neutrino production [19]. The dash-dotted line (magenta) is prompt neutrino flux predicted from GRBs; prompt in this context means in time with the gamma rays [20]. The dash-dot-dot line (grey) is neutrino flux predicted from the cores of active galaxies [21]. The thin dotted line (red) is neutrino flux predicted from starburst galaxies, which are rich in supernovae [22].

- Number of peaks in the distribution of collected charge as a function of time
- Maximum fraction of the total charge collected in a 100 ns timebin
- A variable based on the movement of the center of gravity of the event during the development of the event in the detector

For every event a BDT score is calculated based on these variables ranging from -1 (background-like) to +1 (signal-like) and only events with a sufficiently high score are retained.

At Level 6, a detailed reconstruction of the events is performed assuming a double cascade topology. Several criteria are applied to remove events which are badly reconstructed as double bangs: the maximized likelihoods cannot be too small, causality is required between the two cas-

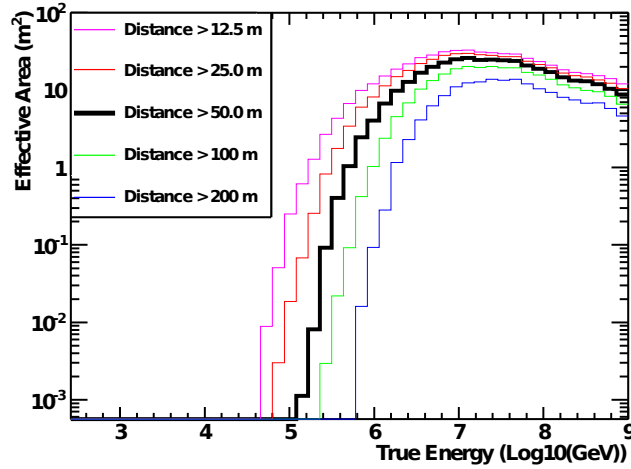


Figure 4: Effective areas after the EHE filter cut for ν_τ obtained by selecting contained double bang events with different minimum separations between the two cascades. No reconstruction errors are included.

Table 2: Preliminary remaining event rates for signal and different backgrounds at Level 6 of the double bang search. The assumed fluxes of the signal and different background are the same as for the double dulse event search. Errors are statistical only.

Data samples	Events in 1 year
Double Bang	$(4.93 \pm 0.04) \cdot 10^{-1}$
Atmospheric muons	(9.5 ± 1.8)
Astrophysical ν_e	$(8.2 \pm 0.3) \cdot 10^{-1}$
Astrophysical ν_μ	$(8.9 \pm 0.2) \cdot 10^{-1}$
Atmospheric ν_e	$(4.4 \pm 0.2) \cdot 10^{-2}$
Atmospheric ν_μ	$(9.3 \pm 0.2) \cdot 10^{-2}$

acades, both cascades need to be reconstructed in or near the detector and not too close together (minimum 20 m apart) and the energy asymmetry ($[E_1 - E_2] / [E_1 + E_2]$, with E_1 and E_2 the energies of the first and second cascade) has to be between -0.999 and 0.9. The median resolution (depending on the energy) of the reconstructed parameters of the remaining signal events at the end of this reconstruction chain is about 3-6% for the distance between the two cascades, 1-4° for the direction and 10-20% for the energy of each cascade.

The remaining event rates of the signal and different backgrounds are shown in Figure 5 and Table 2. The atmospheric neutrino background has been reduced to about an order of magnitude below the signal rate. The astrophysical fluxes of ν_e and ν_μ are of the same order and slightly higher than the signal but the biggest remaining background is still the atmospheric muons. Work is underway to further reduce these backgrounds.

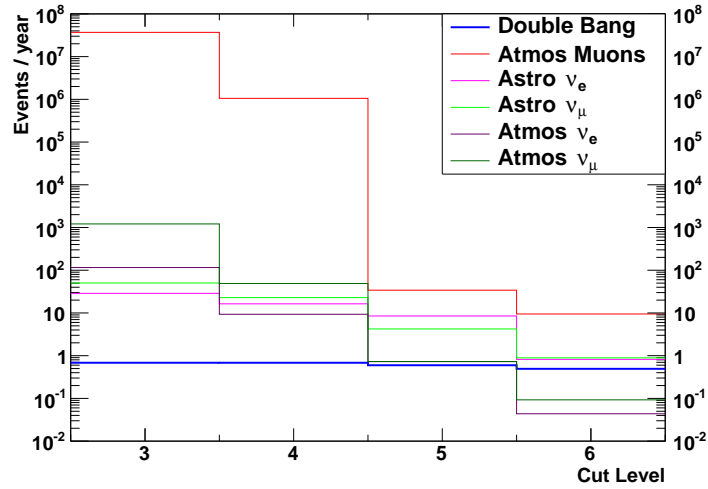


Figure 5: Preliminary remaining event rates for signal and different background at every cut level. The assumed fluxes of the signal and different background are the same as for the Double Pulse event search.

4. Conclusions

The double pulse search for ν_τ in IceCube is more sensitive to tau neutrinos in the $O(100)$ TeV to $O(10)$ PeV energy range than to any other flavor. Given the astrophysical neutrino flux observed by IceCube, fewer than one double pulse tau neutrino event is expected in three years of IceCube data, and none are observed. Searches for well separated double bangs are in progress. Future extensions of IceCube such as the proposed IceCube-Gen2 detector [23] will have a factor of 5 to 10 times more sensitivity to astrophysical tau neutrinos than the current IceCube detector.

References

- [1] M. G. Aartsen *et al.* [IceCube Collaboration], Phys. Rev. Lett. **113**, 101101 (2014).
- [2] M. G. Aartsen *et al.* [IceCube Collaboration], Phys. Rev. Lett. **114**, no. 17, 171102 (2015).
- [3] A. Achterberg *et al.* [IceCube Collaboration], Astropart. Phys. **26**, 155 (2006).
- [4] J. G. Learned and S. Pakvasa, Astropart. Phys. **3**, 267 (1995).
- [5] R. Abbasi *et al.* [IceCube Collaboration], Phys. Rev. D **86**, 022005 (2012).
- [6] M. G. Aartsen *et al.* [IceCube Collaboration], arXiv:1309.7003 [astro-ph.HE].
- [7] R. Abbasi *et al.* [IceCube Collaboration], Nucl. Instrum. Meth. A **601**, 294 (2009).
- [8] M. G. Aartsen *et al.* [IceCube Collaboration], Science **342**, 1242856 (2013).
- [9] M. G. Aartsen *et al.* [IceCube Collaboration], Phys. Rev. Lett. **111**, 021103 (2013).
- [10] M. G. Aartsen *et al.* [IceCube Collaboration], Phys. Rev. D **88**, 112008 (2013).
- [11] M. Honda, T. Kajita, K. Kasahara, S. Midorikawa and T. Sanuki, Phys. Rev. D **75**, 043006 (2007).
- [12] R. Enberg, M. H. Reno and I. Sarcevic, Phys. Rev. D **78**, 043005 (2008).

- [13] T. K. Gaisser, *Astropart. Phys.* **35**, 801 (2012).
- [14] R. Abbasi *et al.* [IceCube Collaboration], *Phys. Rev. D* **82**, 072003 (2010).
- [15] R. Abbasi *et al.* [IceCube Collaboration], *Phys. Rev. D* **83**, 092003 (2011) [*Phys. Rev. D* **84**, 079902 (2011)].
- [16] I. Kravchenko, C. Cooley, S. Hussain, D. Seckel, P. Wahrlich, J. A. Adams, S. Churchwell and P. Harris *et al.*, *Phys. Rev. D* **73**, 082002 (2006).
- [17] G. J. Feldman and R. D. Cousins, *Phys. Rev. D* **57**, 3873 (1998).
- [18] P. Abreu *et al.* [Pierre Auger Collaboration], *Adv. High Energy Phys.* **2013**, 708680 (2013).
- [19] E. Waxman, arXiv:1312.0558 [astro-ph.HE].
- [20] E. Waxman and J. N. Bahcall, *Phys. Rev. Lett.* **78**, 2292 (1997).
- [21] F. W. Stecker, *Phys. Rev. D* **72**, 107301 (2005).
- [22] A. Loeb and E. Waxman, *JCAP* **0605**, 003 (2006).
- [23] M. G. Aartsen *et al.* [IceCube Collaboration], arXiv:1412.5106 [astro-ph.HE].

A measurement of the diffuse astrophysical muon neutrino flux using multiple years of IceCube data

The IceCube Collaboration[†],

[†] http://icecube.wisc.edu/collaboration/authors/icrc15_icecube

E-mail: raedel@physik.rwth-aachen.de,
schoenen@physik.rwth-aachen.de

The IceCube Collaboration has observed a high-energy astrophysical neutrino flux using neutrino candidates with interaction vertices contained within the instrumented volume. A complementary measurement can be done with charged current muon neutrinos where the interaction vertex can be outside the instrumented volume. Due to the large muon range the effective area is significantly larger but the field of view is limited to the Northern Hemisphere. IceCube data from 2009 through 2012 have been analyzed by a likelihood approach with reconstructed muon energy and zenith angle as observables. While the majority of these events are atmospheric neutrinos, the highest energy events are incompatible with that interpretation. Assuming the astrophysical muon neutrino flux to be isotropic the data is well described by an unbroken power law with a normalization of $(0.66^{+0.40}_{-0.30}) \cdot 10^{-18} \text{ GeV}^{-1} \text{ cm}^{-2} \text{ s}^{-1} \text{ sr}^{-1}$ at 100 TeV neutrino energy and a spectral index of $\gamma = 1.91 \pm 0.20$. A purely atmospheric origin of the observed events can be rejected with a significance of 4.3σ . The found spectrum is harder compared to other IceCube measurements of astrophysical neutrinos which are dominantly based on neutrino-induced cascades. These measurements are sensitive to lower neutrino energies. Investigations about the nature of the observed differences are ongoing.

Corresponding authors: Leif Rädels^{*1}, Sebastian Schoenen¹,

¹ *RWTH Aachen University*

*The 34th International Cosmic Ray Conference,
30 July- 6 August, 2015
The Hague, The Netherlands*

^{*}Speaker.

1. Introduction

More than a hundred years after their discovery, the origin of high-energy cosmic rays is still unknown. The dominant fraction of cosmic rays are protons or heavier nuclei. High-energy neutrinos may provide unique information about the nature of sources and acceleration mechanisms of cosmic rays. High-energy neutrinos may be produced in hadronic interactions of cosmic-rays with surrounding matter at the acceleration sites. These neutrinos would reach Earth unaffected by magnetic fields and interactions with the interstellar medium and thus reveal the location of sources. Generic models of the neutrino spectrum [1, 2, 3], based on the acceleration of cosmic rays in strong shock waves predict a power law spectrum with a spectral index $\gamma \approx 2$.

The IceCube Neutrino Observatory is located at the South Pole. The detector instruments a volume of one cubic-kilometer of antarctic ice in a depth between 1450 m and 2450 m with optical sensors [4]. These photosensors measure Cherenkov light caused by charged particles originating from neutrinos interacting in the detector’s vicinity. Neutrino events measured with IceCube can be broadly classified in two basic signatures: tracks and cascades. Long-lived muons from muon-neutrino interactions produce elongated track-like light patterns. Cascade-like spherical patterns are produced by neutral-current (NC) interactions of neutrinos of all flavors, and electrons produced in charged-current (CC) interactions of electron neutrinos¹.

The discovery of astrophysical neutrinos was based on a sample of neutrino events with interaction vertices well-contained within the instrumented volume [6]. Although these events provide a clear signature for an astrophysical neutrino flux, event statistics and directional pointing are only moderate because the effective volume is reduced by requiring containment and the fact that the sample is dominated by cascade-like events. In this analysis a complementary approach is used selecting high-energy muons induced by muon neutrino interactions that can occur outside the instrumented volume. However, this implies using the Earth as shielding to reject the dominant background of atmospheric muons and therefore constrain the field of view to the Northern Hemisphere. Evidence for a flux of astrophysical muon neutrinos has already been shown by previous IceCube analyses. The first hint at the level of 1.8σ was found with one year of IceCube data taken with the partial detector in the 59-string configuration [7]. A second analysis using two years of data from IceCube in its 79- and 86-string configuration excludes the only atmospheric origin of the observed flux with a probability of 3.7σ [8]. We present a combined re-analysis of the two datasets here that is based on a significantly larger sample of neutrino-induced tracks than the earlier analyses. The larger data sample statistics are dominated by conventional atmospheric neutrinos which improve the constraints on the atmospheric flux model uncertainties. With the combination of these datasets a unified approach for a measurement of the astrophysical muon neutrino flux has been prepared. In the next step the same approach will be used to analyze a total of six years of IceCube data recorded between 2009 and 2015.

The main background for such a measurement are atmospheric neutrinos produced in cosmic-ray interactions with the Earth’s atmosphere. Conventional atmospheric neutrinos are produced in the decay of pions and kaons. The expected energy spectrum is about one power in energy softer than the primary cosmic ray spectrum due to the competition between decay and interaction of the

¹CC tau neutrino interactions can produce either signature depending on the decay mode of the tau as well as a “double bang”-signature [5].

mesons. The conventional atmospheric neutrinos flux follows roughly a power law with a spectral index of about -3.7 . Additionally, the interplay between decay and interaction of the mesons leads to a characteristic zenith angle distribution. The flux of conventional atmospheric neutrinos from near the horizon is enhanced because the air shower development occurs higher in the atmosphere and interactions become less likely.

In contrast to conventional ones, “prompt” atmospheric neutrinos are produced in the decay of mesons containing heavy quarks. Though this flux has not been observed to date, several predictions exist [9, 10, 11]. Due to the short lifetime of these heavy mesons the prompt atmospheric neutrino flux will follow the primary cosmic ray spectrum up to very high energies. The expected spectral power law index is about -2.7 and the flux is almost isotropic.

A flux of astrophysical muon neutrinos can be identified by an excess of high-energy events ($\gtrsim 100$ TeV) over the expectations from atmospheric neutrinos of more than about 100 TeV. Since high-energy neutrinos can be absorbed in the Earth an isotropic neutrino flux at the Earth’s surface is shifted towards the horizon. Due to the harder energy spectrum the absorption effect is stronger for an astrophysical flux than for the prompt and conventional atmospheric neutrino flux. Hence, the distribution of arrival directions of neutrinos at the IceCube detector depends on the energy spectrum of the flux. Therefore, the correlation between both quantities contains additional information to distinguish between the different components.

2. Analysis

2.1 Search Strategy

A neutrino sample with a negligible contribution of atmospheric muons is required to measure the flux of astrophysical muon neutrinos based on the distribution of the reconstructed muon energy and zenith angle.

The IceCube detector is triggered by atmospheric muons produced in cosmic-ray air showers at a rate of about 2.5 kHz. The signature of these events are downgoing tracks entering the detector from the outside. In order to reject these events we require reconstructed zenith angles to be larger than 85° which corresponds to more than 12 km of overburden. As a result the remaining background are either mis-reconstructed events or muons produced in interactions of atmospheric neutrinos. The reconstruction of muon arrival directions is done by fitting the hypothesis of a relativistic particle emitting Cherenkov light to the detection times of observed photons which takes into account the propagation effects of photons in the ice. A boosted decision tree trained on parameters that estimate the quality of the directional reconstruction is used to identify and reject mis-reconstructed events. Additionally, cascade-like events are rejected based on the topology of the hit pattern that is different for track-like events. The resulting sample of about 70,000 muon neutrino events per year has a very high purity with a contamination of atmospheric muons below 0.1 %. For all events in the neutrino sample the muon energy at the detector is reconstructed using the truncated mean energy loss reconstruction algorithm described in [12].

The expected zenith angle and muon energy distributions for the conventional, prompt and astrophysical components are computed from Monte Carlo simulations of neutrinos traversing Earth and interacting in the vicinity of the IceCube detector. A generalized weighting scheme is used to

transform a simulated flux of neutrinos to a physical flux. For the astrophysical muon neutrino flux a generic power law model $\Phi(E_\nu) = \Phi_0(E_\nu/100\text{TeV})^{-\gamma}$ is used. Here, the parameters of interest are the flux normalization Φ_0 and the spectral index γ . The conventional atmospheric neutrino prediction is based on the HKKMS07 calculation [13]. The uncertainty on the flux prediction increases with energy to about 25 % at 1 TeV. It was primarily designed for energies up to 10 TeV and has been extrapolated to higher energies according to [7] including the effect of the cosmic-ray knee. As a prediction for the prompt atmospheric neutrino flux we use the ERS model [11] which is based on pQCD calculations.²

2.2 Likelihood Method

In order to compare the experimental data with the expectations which are a function of signal $\vec{\theta}$ and nuisance $\vec{\xi}$ parameters (description below) a binned Poisson likelihood fit is used. Therefore, the experimental and simulated data are binned in reconstructed muon energy and zenith angle. Then, for each bin the measured number of events is compared to the expected number by a Poisson likelihood³

$$\mathcal{L}_{\text{bin}} = \frac{\mu^n(\vec{\theta}, \vec{\xi})}{n!} \times e^{-\mu(\vec{\theta}, \vec{\xi})}, \quad (2.1)$$

where n is the number of measured events in that bin and $\mu = \mu_{\text{conv.}} + \mu_{\text{prompt}} + \mu_{\text{astro.}}$ is the expected number of events as a function of the physics and nuisance parameters. In this analysis, the physics parameters are the astrophysical normalization and spectral index. Additionally, nuisance parameters are introduced to take into account systematic uncertainties which can be divided in two categories: neutrino detection uncertainties and atmospheric flux uncertainties. The former include the optical efficiency of the detector, the neutrino nucleon cross section, the muon energy loss cross section and the optical properties of the antarctic ice. The latter include the flux normalizations, the spectral shape and composition of the cosmic-ray spectrum in the ‘‘knee’’ region, the spectral index of the primary cosmic ray spectrum and the relative production yield of pions and kaons in the atmosphere. The implementation of nuisance parameters in the likelihood function is done similar to [7], with an important improvement for discrete⁴ nuisance parameters. The effect of former discrete parameters on per-bin expectations has been parameterized and it is possible to choose realizations in between discrete points.

The global likelihood is then simply the product of all per-bin-likelihoods $\mathcal{L} = \prod_{\text{bins}} \mathcal{L}_{\text{bin}}$. The significances and parameter uncertainties are derived using the profile likelihood and assuming Wilks’ theorem [16]. The assumption that the test-statistic is χ^2 -distributed and Wilks’ theorem is applicable was tested on pseudo experiments.

Since IceCube’s Monte Carlo simulations improve in quality from year to year, nuisance parameters do not only absorb the systematic effects they are based on but can also absorb differences in the simulated datasets. Thus, for a combined likelihood fit of all years it is necessary to align

²An improved version of the flux prediction [14] will be used in the future which predicts approximately a flux that is half the flux of the ERS calculation.

³An extended version of the Poisson likelihood which takes into account finite statistics of the Monte Carlo simulations is used [15].

⁴A discrete nuisance parameter is a parameter where the fit can only choose between a predefined set of models, e.g. cosmic-ray composition model A or B.

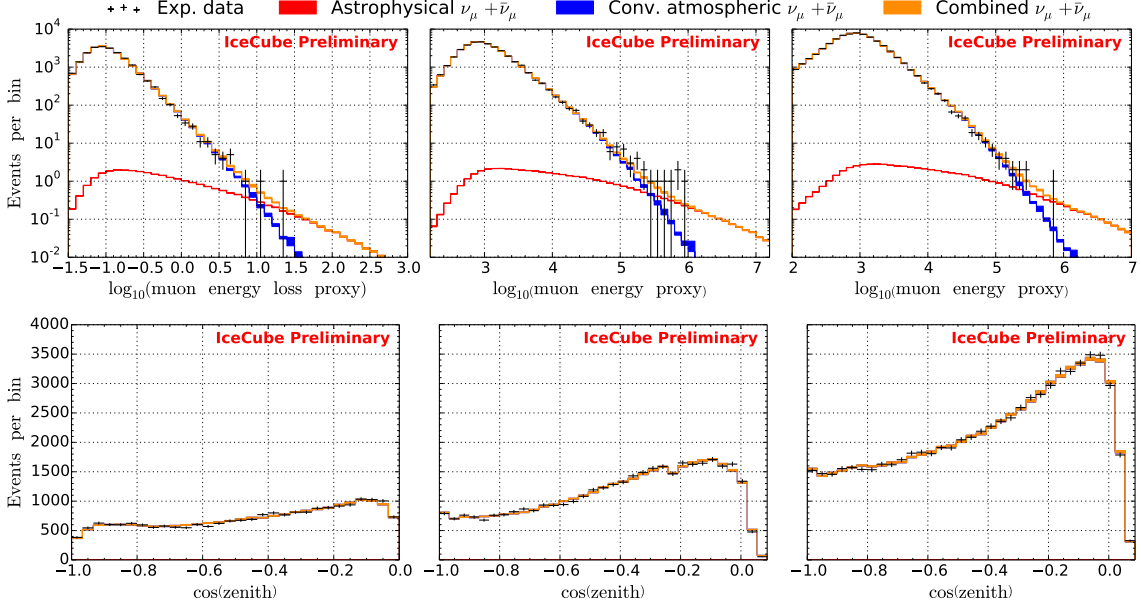


Figure 1: 1d-projections of the fit observables weighted by the best-fit spectrum for each year (left: 59-string, center: 79-string, right: 86-string). The reconstructed muon energy proxy is shown in the top row and the reconstructed zenith angle distribution in the bottom row. Note that [7] used the reconstructed muon energy loss as an observable which is correlated with the muon energy used in the later years. Only statistical errors are shown.

all nuisance parameters to a common baseline ξ_i . This means, that for each year the nuisance parameters are fit individually to adjust them to a common baseline. Then, in the combined fit these baseline values are scaled by a global parameter to give the combined fit the freedom to change the nuisance parameters.

3. Results

The best-fit astrophysical flux is given by

$$\Phi(E_\nu) = (0.66^{+0.40}_{-0.30}) \cdot 10^{-18} \text{ GeV}^{-1} \text{ cm}^{-2} \text{ sr}^{-1} \text{ s}^{-1} (E_\nu/100 \text{ TeV})^{-(1.91 \pm 0.20)} \quad (3.1)$$

in the energy range between 170 TeV and 3.8 PeV.⁵ The quoted errors include both statistical and systematic uncertainties via the profile likelihood using the χ^2 -approximation. The projections in reconstructed zenith angle and muon energy for each year are shown in Figure 1. The excess of events above atmospheric backgrounds becomes visible at high energies (Fig. 1, top center). No contribution from prompt atmospheric neutrinos is preferred for the best fit spectrum.

The significance for rejecting a flux of only atmospheric neutrinos is 4.3σ which is calculated with the profile likelihood assuming Wilks' theorem.

Figure 2 shows the two-dimensional profile likelihood for all combinations of astrophysical normalization, spectral index and prompt normalization. The likelihood ratios of the first column

⁵The energy range has been estimated by the central neutrino energy range which contributes 90% to the total squared significance. Note that this definition is different from [8, 17].

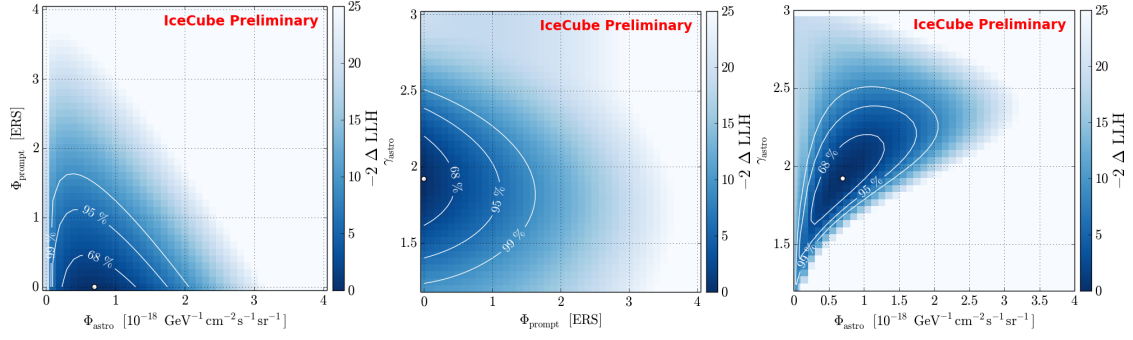


Figure 2: Two dimensional profile likelihood scans of the physics parameters Φ_{astro} , γ_{astro} and the prompt normalization Φ_{prompt} in units of the model in [11]. Additionally, contours at 68%, 90% and 95% CL assuming Wilks' theorem are shown.

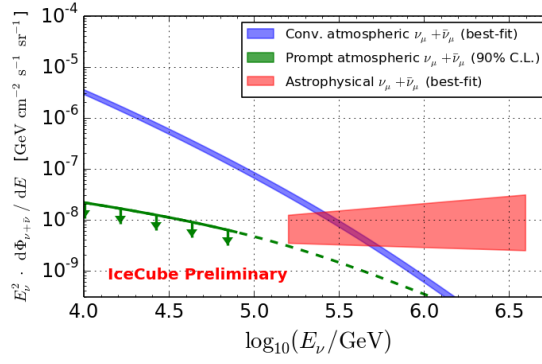


Figure 3: Best-fit muon neutrino spectra for the unbroken power-law model. The line widths (blue, red) represent the one sigma error on the measured spectrum where the green line represents the upper limit at 90% CL for the prompt model [11]. Note that systematic studies about the robustness of the prompt limit are still ongoing. The horizontal width of the red band denotes the energy range of neutrino energies which contribute 90% to the total squared significance.

in the left plot show that even a large prompt flux cannot explain the excess of high-energy neutrinos measured in the three years. The physics parameters are mainly correlated with each other (Figure 2, right) and only a small correlation with the normalization of prompt neutrinos is visible (Figure 2, left and center). The large statistics of conventional atmospheric neutrinos at lower energies strongly constrain the flux uncertainties in the region where the astrophysical component begins to contribute. Therefore, the nuisance parameters for the atmospheric flux uncertainties are strongly constrained and are only weakly correlated with the astrophysical flux parameters. The correlation between astrophysical normalization and spectral index is expected due to the interplay between both quantities. A larger normalization has a similar effect on the reconstructed muon energy spectrum as a softer spectral index. The most likely neutrino energy of the highest energy event assuming the overall best-fit neutrino flux is about 1.4PeV. Figure 3 shows the best-fit muon neutrino spectrum. For prompt atmospheric neutrinos the 90%C.L. upper limit is shown. The vertical width of the bands corresponds to the flux uncertainties at the 1σ -level. Note that the results do not take into account the flux of muons originating from tau decays which themselves are

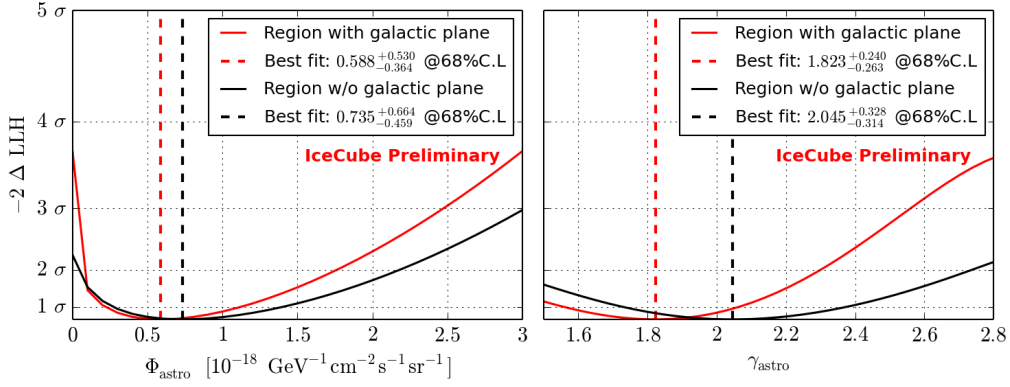


Figure 4: One dimensional profile likelihood scans the astrophysical normalization (left) and spectral index (right) using two different right ascension regions, one containing the Northern Hemisphere part of the Galactic plane (red) and one not (black).

produced by tau neutrino interactions. However, this only affects the astrophysical normalization by about 5 – 10% [7].

In order to test if the measured muon neutrino flux is dominated by a Galactic flux the full sample (limited to the Northern Hemisphere) is split into two parts based on the reconstructed right ascension of the events: the first part contains the region where the Galactic plane intersects the Northern Hemisphere ($0^\circ \leq \alpha < 109^\circ$ and $275^\circ \leq \alpha < 360^\circ$), the second part contains the region where the Galactic plane lies in the Southern Hemisphere ($109^\circ \leq \alpha < 275^\circ$). Because the IceCube detector is located at the South Pole, it rotates daily with the Earth and therefore the systematics for both parts are identical. The likelihood fit has been applied to both parts, resulting in the one-dimensional profile likelihoods shown in Figure 4. Comparing the likelihood profiles, the results of both parts are statistically consistent. Hence, no statistically significant evidence for a Galactic component is found.

Modifying the astrophysical model from an unbroken power law to a power law with an exponential cut-off does not yield a significantly better fit result.

4. Conclusion

Re-analyzing the IceCube data measured between 2009 and 2012 with a significantly larger event sample than in previous analyses [7, 8] yield an excess of events at energies above 100 TeV. The atmospheric-only hypothesis can be rejected at 4.3σ ⁶. Compared to [8] the significance increase is mainly due to the inclusion of the experimental data from [7]. The increased statistics of conventional atmospheric neutrinos and therefore better constrained systematic uncertainties additionally increase the significance. The measured astrophysical muon neutrino flux yields a normalization of $(0.66^{+0.40}_{-0.30}) \cdot 10^{-18} \text{ GeV}^{-1} \text{ cm}^{-2} \text{ s}^{-1} \text{ sr}^{-1}$ at 100 TeV neutrino energy and a hard spectral index of $\gamma = 1.91 \pm 0.20$. So far, no evidence for a cut-off at high energies is found. Additionally, there is no significant evidence for a Galactic component in the measured astrophysical muon neutrino flux.

⁶assuming Wilks' theorem

Comparing the measured spectral index to the measurement of other IceCube analyses [6, 8, 17] the index seems to be somewhat harder. However, due to the large uncertainties the results presented in [6] and [8] are statistically compatible. Investigations about the origin of the moderate tension with the spectral index measured in [17] are ongoing. It could be caused by a statistical fluctuation as well as an underlying more complex spectral shape of the astrophysical neutrino flux. Additionally, systematic studies are still ongoing. Extending this analysis by IceCube data recorded between 2012 and 2015 may show which scenario is more likely.

References

- [1] T. K. Gaisser, F. Halzen, and T. Stanev, *Physics Reports* **258** (1995), no. 3 173 – 236.
- [2] J. Learned and K. Mannheim, *Ann. Rev. Nucl. Part. Sci.* **50** (2000) 679–749.
- [3] J. K. Becker, *Phys. Rept.* **458** (2008) 173–246.
- [4] **IceCube** Collaboration, A. Achterberg et al., *Astropart. Phys.* **26** (2006) 155–173.
- [5] **IceCube** Collaboration, R. Abbasi et al., *Phys. Rev. D* **86** (2012) 022005.
- [6] **IceCube** Collaboration, M. G. Aartsen et al., *Phys. Rev. Lett.* **113** (Sep, 2014) 101101.
- [7] **IceCube** Collaboration, M. Aartsen et al., *Phys. Rev. D* **89** (2014), no. 6 062007.
- [8] **IceCube** Collaboration, M. Aartsen et al., *submitted to Phys. Rev. Lett.* (2015) [[arXiv:1507.04005](https://arxiv.org/abs/1507.04005)].
- [9] A. Martin, M. Ryskin, and A. Stasto, *Acta Phys. Polon. B* **34** (2003) 3273–3304.
- [10] E. Bugaev, V. A. Naumov, S. I. Sinegovsky, and Z. E. S., *Il Nuovo Cimento* **12C** (1989), no. 1.
- [11] R. Enberg, M. H. Reno, and I. Sarcevic, *Phys. Rev. D* **78** (Aug, 2008) 043005.
- [12] **IceCube** Collaboration, R. Abbasi et al., *Nucl. Instrum. Meth. A* **703** (2013) 190–198.
- [13] M. Honda, T. Kajita, K. Kasahara, S. Midorikawa, and T. Sanuki, *Phys. Rev. D* **75** (Feb, 2007) 043006.
- [14] A. Bhattacharya, R. Enberg, M. H. Reno, I. Sarcevic, and A. Stasto, *accepted in JHEP* (2015) [[arXiv:1502.01076](https://arxiv.org/abs/1502.01076)].
- [15] D. Chirkin, *ArXiv e-prints* (Apr., 2013) [[arXiv:1304.0735](https://arxiv.org/abs/1304.0735)].
- [16] S. S. Wilks, *Ann. Math. Statist.* **9** (03, 1938) 60–62.
- [17] **IceCube** Collaboration, M. G. Aartsen et al., *Phys. Rev. D* **91** (Jan, 2015) 022001.

Observation of Astrophysical Neutrinos in Four Years of IceCube Data

The IceCube Collaboration[†]

[†] http://icecube.wisc.edu/collaboration/authors/icrc15_icecube

E-mail: ckopper@icecube.wisc.edu, will.giang@icecube.wisc.edu,
naoko@drexel.edu

The spectrum of cosmic rays includes the most energetic particles ever observed. The mechanism of their acceleration and their sources are, however, still mostly unknown. Observing astrophysical neutrinos can help solve this problem. Because neutrinos are produced in hadronic interactions and are neither absorbed nor deflected, they will point directly back to their source. This contribution will cover continued studies of the high-energy astrophysical neutrino flux observed at the IceCube neutrino observatory, extending them from three to four years of data with a focus on energies above 60 TeV. The spectrum and spatial clustering of the observed neutrinos will be discussed.

Corresponding authors: C. Kopper^{*1}, W. Giang², N. Kurahashi²

¹ *Department of Physics, CCIS 4-181, University of Alberta, Edmonton, Alberta T6G 2E1, Canada*

² *Department of Physics, Drexel University, 3141 Chestnut Street, Philadelphia, PA 19104, USA*

*The 34th International Cosmic Ray Conference,
30 July- 6 August, 2015
The Hague, The Netherlands*

*Speaker.

1. Introduction

Observation of high-energy neutrinos provides insight into the problem of the origin and acceleration mechanism of high-energy cosmic rays. Cosmic ray protons and nuclei interacting with gas and photons present in the environment of sources and in the interstellar space produce neutrinos through decay of charged pions and kaons. These neutrinos have energies proportional to the cosmic rays that produced them and point back to their source since neutrinos are neither affected by magnetic fields nor absorbed by matter opaque to radiation. Large-volume Cherenkov detectors like IceCube [1] observe these neutrinos when they interact by measuring the light produced by secondary leptons and hadronic showers.

Here we present an update to the IceCube high-energy search for events with interaction vertices inside the detector fiducial volume. This search, previously performed on two [2] and three [3] years of detector data, led to the discovery of an astrophysical neutrino flux above atmospheric backgrounds [3]. This update extends the data-taking period by one more year to four years from 2010 to 2014 for a total livetime of 1347 days.

2. Event Selection

Neutrinos in IceCube are detected by observing the Cherenkov light in the glacial ice from secondary particles created by the interaction of high-energy neutrinos. We observe two main event classes: track-like events from charged-current interactions of muon neutrinos (and from a minority of tau neutrino interactions) and shower-like events from all other interactions (neutral-current interactions and charged-current interactions of electron and tau neutrinos). Note that tau neutrino interactions at the highest energies (at the PeV-level) can lead to different event shapes in rare cases, but these are not considered here. We determine the event direction and deposited energy in the detector based on the time sequence and total recorded light. Energy is reconstructed as electromagnetic-equivalent energy. Shower-like events have a typical directional resolution of around 15° , mostly dominated by the uncertainty in the modelling of the glacial ice, whereas track-like events have resolutions of much better than 1° .

In the analysis presented here, signal events are selected by requiring the neutrino interaction vertex to be located inside the IceCube detector volume. We achieve this by means of a simple anti-coincidence veto method [2], requiring that fewer than 3 of the first 250 detected photoelectrons (p.e.) be on the outer detector boundary. In order to ensure a large enough number of photons are detected, we also require at least 6000 p.e. in total charge for each event, corresponding to a soft threshold of about 30 TeV in deposited energy in the detector.

3. Atmospheric Backgrounds

Backgrounds to astrophysical neutrinos are entirely due to cosmic ray air showers. Muons produced in these showers, mainly from π and K decays enter the detector from above. Due to the stochasticity of the muon energy loss, in very rare cases muons can pass through the outer veto layer undetected and appear as starting events, especially close to the charge threshold of 6000 p.e. We use a data-driven method to estimate this background by tagging such muons in one layer of

the detector and then use a second layer, equivalent to our veto to estimate their passing probability. From this, we estimate a total atmospheric muon background of 12.6 ± 5.1 in four years of data.

The same cosmic ray air showers also produce neutrinos from π and K decays. The spectrum of these ν_μ -dominated atmospheric neutrinos is typically one power steeper than the original cosmic ray spectrum. This is due to the increasing lifetime of the parent mesons, making it more and more likely for it to interact before decaying. At energies above around 100 TeV, an analogous flux of muons and neutrinos from charmed mesons is expected to dominate. The shorter lifetime of these particles allows them to avoid interactions before their decay, leading to a harder spectral slope of this component. Until now, this “prompt” component has not yet been observed, but limits from data have been placed by previous IceCube analyses [4, 5]. For purposes of background estimation, we use a limit set by an analysis of incoming muons from muon neutrinos in the 59-string configuration of IceCube [4]. More recent and somewhat more stringent limits are available from IceCube data [5], however we chose to continue to use the same limit as before because it was chosen during the blind definition of this analysis update. The total expected background from atmospheric neutrinos in four years of data including this limit is $9.0^{+8.0}_{-2.2}$.

Note that some of the down-going atmospheric neutrino background will also be vetoed because of accompanying muons from the same air shower. This reduces the background from atmospheric neutrinos in the Southern Sky. This analysis uses the updated description of this reduction described in reference [5].

4. Diffuse Flux Fit

In the full 1347-day sample, we detect 54 events (Fig. 1); 17 of them are observed in the fourth year (see table 1). One of the events observed in the third year (event #32) was produced by a coincident pair of background muons from unrelated cosmic ray air showers and has been excluded from the analysis. We note that none of the events in the fourth year have energies above 1 PeV. We do, however, observe one very high-energy track (event #45) with an almost vertical direction starting in the top part of the detector and depositing more than 400 TeV in the detector before leaving it at the bottom. If this event was a muon produced from a cosmic ray interacting in the atmosphere, the air shower secondaries would likely have been observed by the surface IceTop array (see [6] in these proceedings). Distributions of the events compared to background and best-fit signal expectations as functions of deposited charge, deposited energy and declination can be found in figures 2, 3 and 4, respectively.

In order to describe the data, we perform a likelihood fit of all components (atmospheric muons, atmospheric neutrinos from π /K decay, atmospheric neutrinos from charm decay and an astrophysical flux assuming a 1:1:1 flavor ratio). As in [3], the fit is performed including all events with $60 \text{ TeV} < E_{\text{dep}} < 3 \text{ PeV}$. The only change in fitting procedure from previous analyses is the addition of a prior distribution on the charm background component in line with the limit on this component from the previous IceCube 59-string analysis on incoming muon neutrinos [4]. We fit an unbroken power-law spectrum, both with a fixed index of E^{-2} and with a variable index $E^{-\gamma}$. For the fixed spectral index, we obtain a normalization of $E^2\Phi(E) = 0.84 \pm 0.3 \times 10^{-8} \text{ GeV cm}^{-2} \text{ s}^{-1} \text{ sr}^{-1}$, compatible with previous results. Note, however, that this spectral assumption is not strongly favored by the data, especially with the addition of several new lower-energy events to the sample in

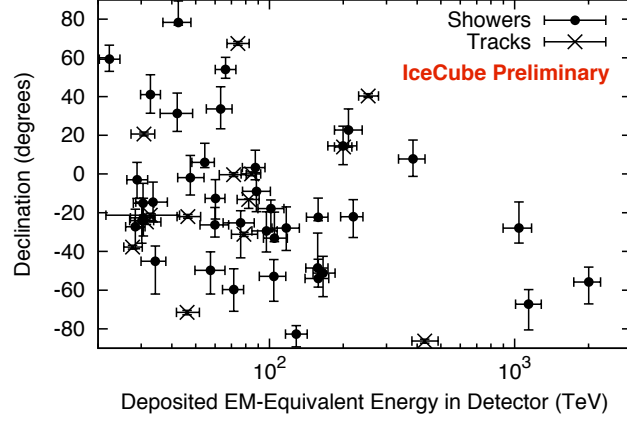


Figure 1: Arrival angles and electromagnetic-equivalent deposited energies of the events. Track-like events are indicated with crosses whereas shower-like events are shown as filled circles. The error bars show 68% confidence intervals including statistical and systematic errors. Deposited energy as shown here is always a lower limit on the primary neutrino energy.

ID	E_{dep} (TeV)	Time (MJD)	Decl. (deg.)	R.A. (deg.)	Ang. Err. (deg.)	Topology
38	$200.5^{+16.4}_{-16.4}$	56470.11038	13.98	93.34	$\lesssim 1.2$	Track
39	$101.3^{+13.3}_{-11.6}$	56480.66179	-17.90	106.17	14.2	Shower
40	$157.3^{+15.9}_{-16.7}$	56501.16410	-48.53	143.92	11.7	Shower
41	$87.6^{+8.4}_{-10.0}$	56603.11169	3.28	66.09	11.1	Shower
42	$76.3^{+10.3}_{-11.6}$	56613.25669	-25.28	42.54	20.7	Shower
43	$46.5^{+5.9}_{-4.5}$	56628.56885	-21.98	206.63	$\lesssim 1.3$	Track
44	$84.6^{+7.4}_{-7.9}$	56671.87788	0.04	336.71	$\lesssim 1.2$	Track
45	$429.9^{+57.4}_{-49.1}$	56679.20447	-86.25	218.96	$\lesssim 1.2$	Track
46	$158.0^{+15.3}_{-16.6}$	56688.07029	-22.35	150.47	7.6	Shower
47	$74.3^{+8.3}_{-7.2}$	56704.60011	67.38	209.36	$\lesssim 1.2$	Track
48	$104.7^{+13.5}_{-10.2}$	56705.94199	-33.15	213.05	8.1	Shower
49	$59.9^{+8.3}_{-7.9}$	56722.40836	-26.28	203.20	21.8	Shower
50	$22.2^{+2.3}_{-2.0}$	56737.20047	59.30	168.61	8.2	Shower
51	$66.2^{+6.7}_{-6.1}$	56759.21596	53.96	88.61	6.5	Shower
52	$158.1^{+16.3}_{-18.4}$	56763.54481	-53.96	252.84	7.8	Shower
53	$27.6^{+2.6}_{-2.2}$	56767.06630	-37.73	239.02	$\lesssim 1.2$	Track
54	$54.5^{+5.1}_{-6.3}$	56769.02960	5.98	170.51	11.6	Shower

Table 1: Properties of the events observed in the fourth year. A list of events #1-#37 can be found in [3]. The E_{dep} column shows the electromagnetic-equivalent deposited energy of each event. “Ang. Err.” shows the median angular error including systematic uncertainties.

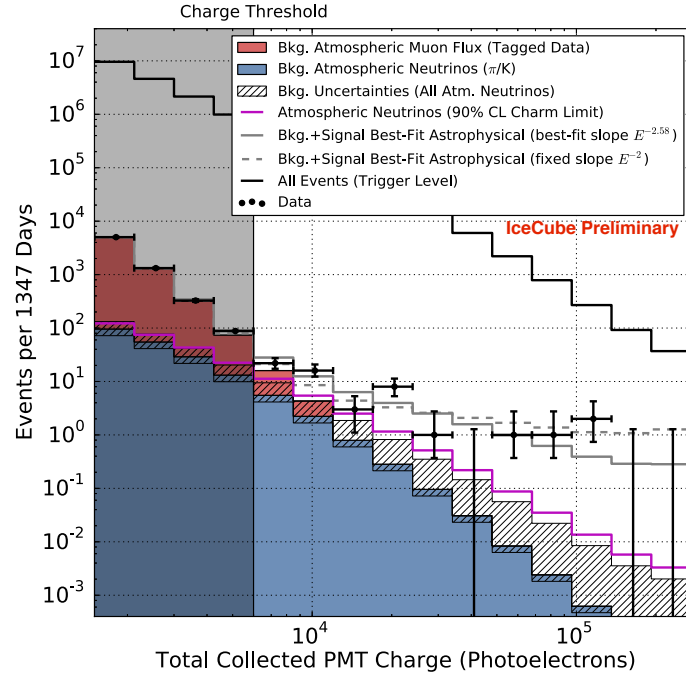


Figure 2: Distribution of deposited PMT charges of the events. Atmospheric muon backgrounds (estimated from data) are shown in red. Due to the incoming track veto, these backgrounds fall much faster than the overall background at trigger level (black line). The data events in the unshaded region at charges greater than 6000 p.e. are the events reported in this work. Atmospheric neutrino backgrounds are shown in blue with 1σ uncertainties on the prediction shown as a hatched band. For scale, the 90% CL upper bound on the charm component of atmospheric neutrinos is shown as a magenta line. The best-fit astrophysical spectra (assuming an unbroken power-law model) are shown in gray. The dashed line shows a fixed-index spectrum of E^{-2} , whereas the solid line shows a spectrum with a best-fit spectral index.

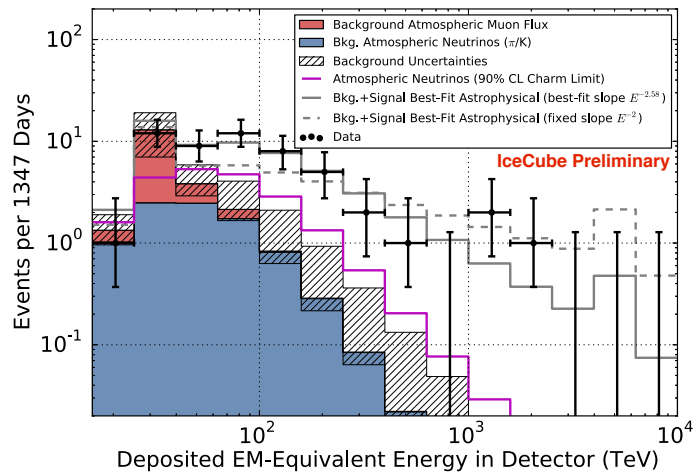


Figure 3: Deposited energies of the observed events with predictions. Colors as in Fig. 2.

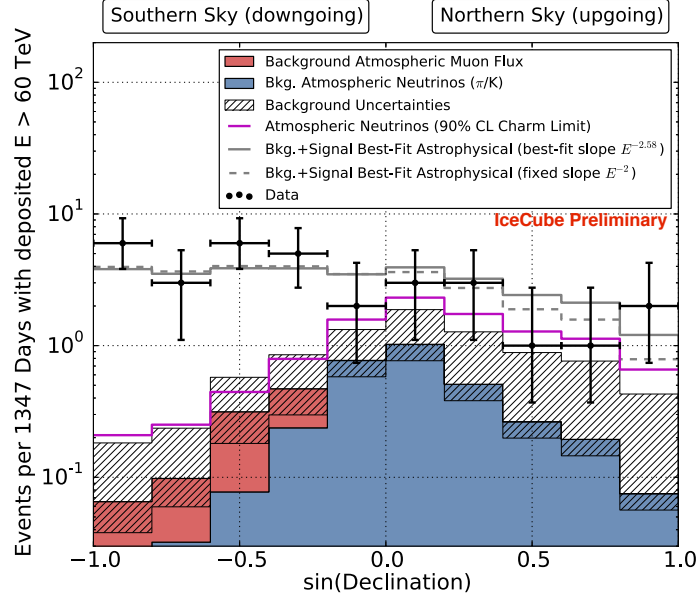


Figure 4: Arrival angles of events with $E_{\text{dep}} > 60 \text{ TeV}$ compared to predictions. Colors as in Fig. 2.

the fourth year of data (see gray dashed line in Fig. 3). The variable spectral index fit results in a best-fit spectral index of -2.58 ± 0.25 , softer than the corresponding best-fit index of -2.3 ± 0.3 obtained with three years of data. The new fit is compatible with the 3-year result within errors (see Fig. 5); however, the lack of PeV-energy events in the fourth year of data in combination with the comparatively high yield of events in that year has resulted in a much steeper spectral fit.

Fig. 6 shows a fit of the spectrum using a more general model, parameterizing the astrophysical flux as a piecewise function of neutrino energy instead of an unbroken single power law. The new dataset presented here is also used in a global fit of several IceCube analyses, presented in these proceedings [7].

5. Spatial Clustering

A maximum-likelihood clustering method [3] was used to look for any neutrino point source in the sample. The test statistic (TS) was defined as the logarithm of the ratio between the maximal likelihood including a point source component and the likelihood for the isotropic null hypothesis. The significance of our observed TS was determined by comparing to maps scrambled in right ascension. As before, the analysis was run twice, once with all events and once with only shower-like events in the sample. We removed events #32 (two coincident muons from unrelated air showers) and #28 (event with sub-threshold hits in the IceTop array) for purposes of all clustering analyses. This test (see Fig. 7) did not yield significant evidence of clustering with p-values of 44% and 58% for the shower-only and the all-events tests, respectively.

We also performed a galactic plane clustering test using a fixed width of 2.5° around the plane (p-value 7%) and using a variable-width scan (p-value 2.5%). All above p-values are corrected for trials.

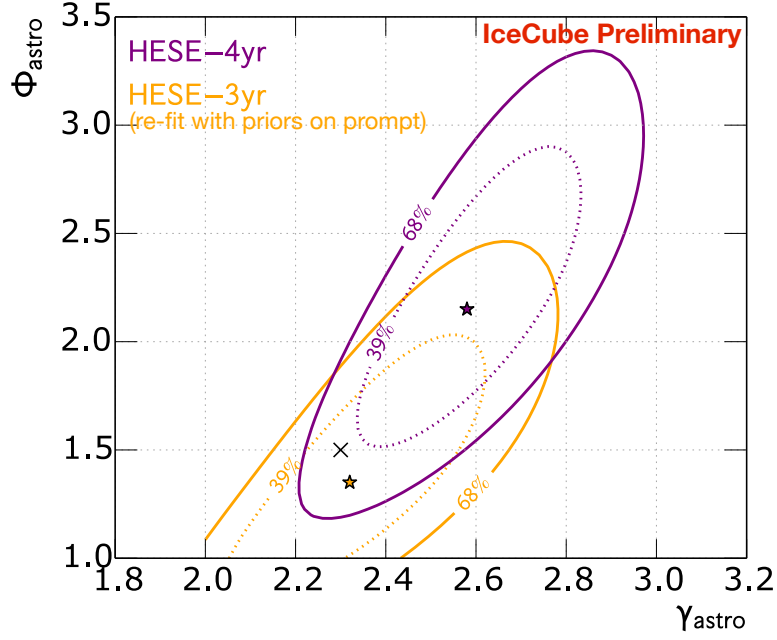


Figure 5: Contour plot of the best-fit astrophysical spectral index γ_{astro} vs. best-fit normalization at 100TeV, Φ_{astro} . Shown are the fit of three years of data, re-fit with a prior on the charm component in yellow (“HESE-3year”). The best-fit point is marked with a yellow star. The previous fit as shown in [3] is marked with a black “x” (this fit used an unconstrained charm component). The fit of all four years of data using the same method is shown in purple (“HESE-4year”) with a best-fit spectral index of $E^{-2.58 \pm 0.25}$, compatible with the 3-year result (although, note that the data used for the 3-year result is a subset of the 4-year result and thus the two are not independent.) The best-fit power law is $E^2\phi(E) = 2.2 \pm 0.7 \times 10^{-8} (E/100\text{TeV})^{-0.58} \text{GeVcm}^{-2}\text{s}^{-1}\text{sr}^{-1}$.

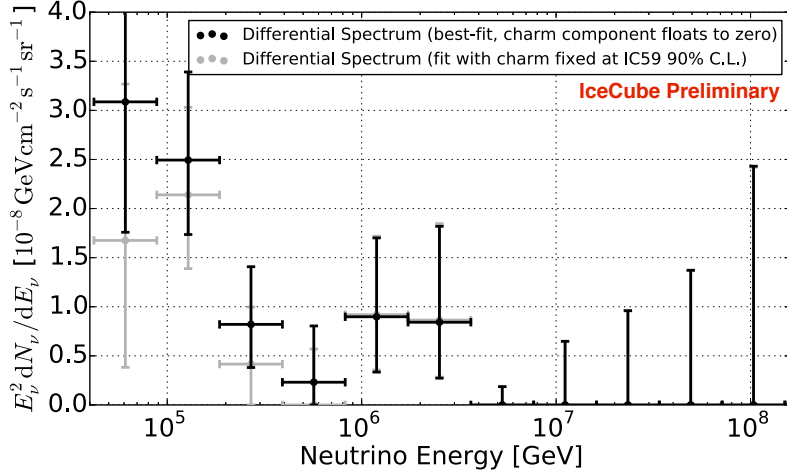


Figure 6: Astrophysical neutrino flux (combined neutrino and anti-neutrino) as a function of energy extracted from a combined likelihood fit of all background components and several pieces of E^{-2} components in neutrino energy. Error bars indicate the $2\Delta\mathcal{L} = \pm 1$ contours of the flux in each energy bin. An increase in the charm atmospheric background to the level of the 90% CL limit from the northern hemisphere ν_{μ} spectrum [4] would reduce the inferred astrophysical flux at low energies to the level shown for comparison in light gray.

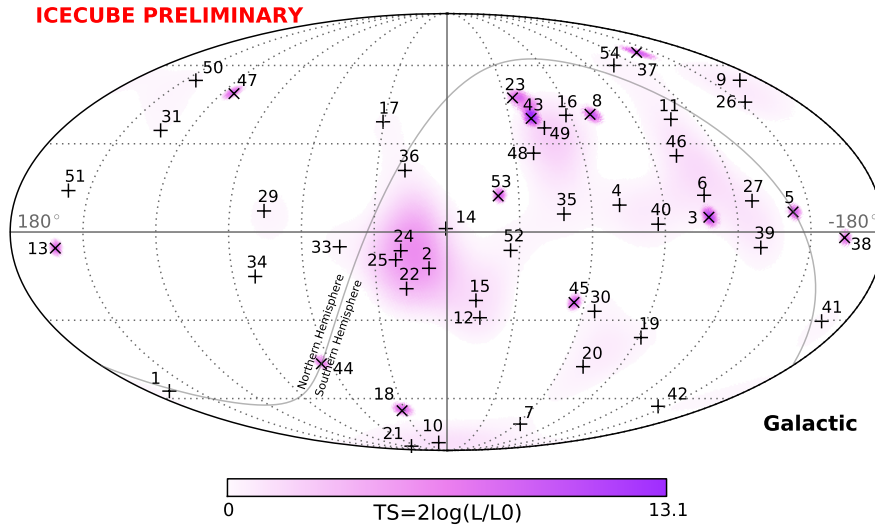


Figure 7: Arrival directions of the events in galactic coordinates. Shower-like events are marked with + and those containing tracks with \times . Colors show the test statistics (TS) for the point-source clustering test at each location. No significant clustering was found.

6. Future Plans

Other searches in IceCube have managed to reduce the energy threshold for a selection of starting events even further in order to be better able to describe the observed flux and its properties [5], but at this time they have only been applied to the first two years of data used for this study. We will continue these lower-threshold searches and will extend them to the full set of data collected by IceCube. Because of its simplicity and its robustness with respect to systematics when compared to more detailed searches, the search presented here is well suited towards triggering and providing input for follow-up observations by other experiments. In the future, we thus plan to continue this analysis in a more automated manner in order to update the current results with more statistics and to produce alerts as an input for multi-messenger efforts.

References

- [1] R. Abbasi et al., Nucl. Instrum. Meth. A601 (2009) 294
- [2] M.G. Aartsen et al., Science 342, 1242856 (2013)
- [3] R. Abbasi et al., PRL 111 (2013) 021103
- [4] M. G. Aartsen et al., PRD89 (2014) 062007
- [5] M. G. Aartsen et al., PRD91 (2015) 022001
- [6] IceCube Coll., PoS(ICRC2015)1086, these proceedings
- [7] IceCube Coll., PoS(ICRC2015)1066, these proceedings

Unfolding measurement of the Atmospheric Muon Neutrino Spectrum using IceCube-79/86

The IceCube Collaboration[†],

[†] http://icecube.wisc.edu/collaboration/authors/icrc15_icecube

E-mail: mathis.boerner@icecube.wisc.edu

IceCube is a cubic kilometer neutrino telescope located at the geographic South Pole. Although primarily designed for the detection of cosmic neutrinos, the detector is well suited for measurements of the atmospheric muon neutrino energy spectrum. We present the measurement of this spectrum obtained in its 79 and its full 86-string configuration. The analysis was carried out using dedicated machine learning algorithms for the selection of neutrino candidates. The spectrum was obtained by applying regularized unfolding as implemented in the unfolding software TRUEE. An additional component due to a diffuse flux of high energy astrophysical neutrinos has been observed in addition to the flux of conventional atmospheric neutrinos.

Corresponding authors: M. Börner^{1*}, T. Ruhe¹, F. Scheriau¹, M. Schmitz¹

¹ *Dept. of Physics, Technical University of Dortmund, 44227 Dortmund, Germany*

*The 34th International Cosmic Ray Conference,
30 July - 6 August, 2015
The Hague, The Netherlands*

*Speaker.

1. Introduction

IceCube is a neutrino observatory with an instrumented volume of one cubic kilometer [1]. The detector consists of 5160 digital optical modules (DOMs). The DOMs are attached to 86 strings. The strings are deployed at depths between 1450m and 2450m in glacial ice at the geographical south pole. The purpose of the DOMs is to measure Cherenkov light emitted by charged particles propagating through the detector. In this analysis muon neutrinos are searched for with through-going muons produced in charged current neutrino interactions.

The unfolded spectra cover an E_ν -range of more than four orders of magnitude from 250 GeV up to 3.2 PeV. Up to TeV energies the muon neutrino spectrum is expected to be dominated by atmospheric neutrinos produced in decays of pions and kaons in cosmic ray air showers. This component is called *conventional*. At higher energies additional neutrinos from the decay of short-lived charmed mesons start to contribute significantly to the spectrum. This component is called *prompt*. Both are purely atmospheric. In 2013 IceCube was the first experiment to prove the existence of a third component, the *astrophysical* component [2]. Those neutrinos are expected to come from active galactic nuclei or gamma ray bursts, but the exact sources are not known yet.

2. Data sample and Analysis

The first year of data analyzed was taken in IceCube's 79-string configuration (IC79) between May 2010 and May 2011. The second year was the first year of IceCube's 86-string configuration (IC86) and data was taken between May 2011 and May 2012. To separate cosmic ray-induced muons from neutrino-induced muons, the earth is used for shielding against atmospheric muons in this analysis. Hence, the datasets only cover the northern hemisphere. For each year separate processes using machine learning algorithms were applied to obtain highly pure neutrino datasets. The core of the separation is a Random Forest [3]. To ensure a good performance for the Random Forest, it is preceded by a maximum relevance minimum redundancy variable selection [4, 5]. The approach is based on the process described in [6]. The separation leads to 66 885 muon neutrino candidates with an estimated purity of $(99.5 \pm 0.3)\%$ for the first year and 92 519 muon neutrino candidates with an estimated purity of $(99.6 \pm 0.2)\%$ for the second year.

The neutrino energy cannot be measured directly. Thus, the spectrum has to be reconstructed from measurable variables correlated to the neutrino energy. One possibility to solve this inverse problem is unfolding. For this analysis both datasets were unfolded separately with a regularized unfolding method implemented in the software TRUEE [7].

3. Energy Spectra for the Northern Hemisphere

The zenith range of the datasets spans from 86° (4° above the horizon) to 180° (north pole). The unfolded spectra in comparison to theoretical predictions are depicted in Fig. 1. While the spectrum of the year before IC79 (IC59) [6] showed no hints of an astrophysical component, both the IC79 and the IC86 spectrum start to exceed an atmospheric only prediction around $E_\nu \approx 50$ TeV. The excess of the IC79 spectrum is significantly higher and not compatible with an atmospheric only prediction within its errors.

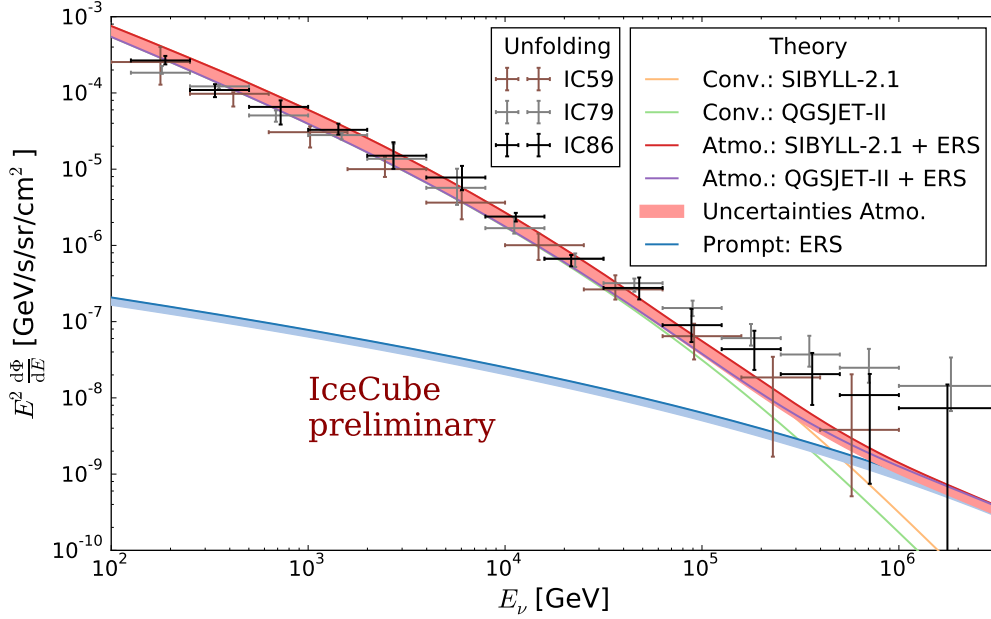


Figure 1: The unfolded spectra for IC79 and IC86 are shown in gray and black. The unfolded spectrum for the year before IC79 (IC59) is shown in brown [6]. For comparison, theoretical predictions for the conventional component QGSJET-II [8] (green) as a lower bound and SYBILL-2.1 [8] (yellow) as an upper bound are shown. Most of the common predictions, like those of Honda et al. [9], are in between those bounds. For the prompt component the prediction by Enberg et al. [10], with the bounds also given in the paper, is shown. In addition the sum of the conventional and the prompt flux is shown for both conventional models. All theoretical predictions are calculated for the primary spectrum by Gaisser [11].

Because the methods and the energy binning for the IC79 and IC86 spectrum are the same, it is reasonable to calculate the weighted average for both spectra to obtain a combined IC79 and IC86 spectrum. This averaged spectrum in comparison to recent IceCube measurements and theoretical prediction for the atmospheric flux is depicted in Fig. 2. The comparison shows that the observed excess is compatible with the recent measurements of the astrophysical component.

4. Zenith Dependent Unfolding

The unfolded spectrum is a measurement of the sum of the conventional, prompt and astrophysical component. It is not possible to disentangle the astrophysical from the atmospheric component without knowing the shape and the normalization of the conventional and prompt flux.

Pions and kaons producing conventional muon neutrinos have a shorter interaction than decay length. Therefore, they interact in the atmosphere resulting in a loss of energy and steepening of the muon neutrino energy spectrum. The length of the path through the atmosphere and therefore the amount of energy lost before the decay depends on the zenith angle. The prompt muon neutrinos on the other hand originate from decays of short-lived mesons decaying directly after production. Therefore, the prompt neutrino flux has no additional zenith dependency. All components have a common zenith dependence due to the increase of the neutrino cross sections for high energies.

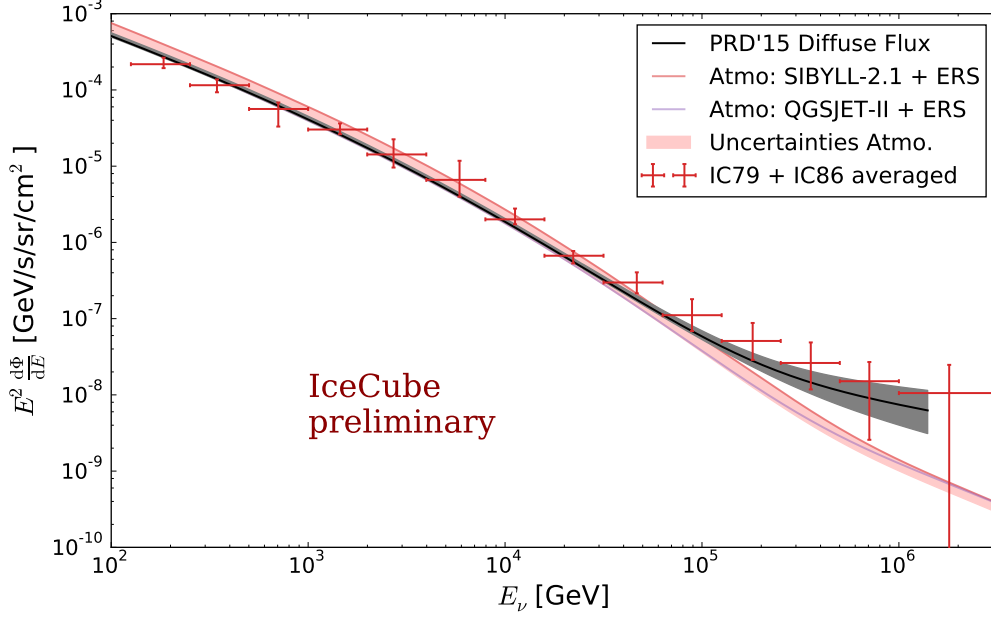


Figure 2: The combined IC79 and IC86 spectrum is shown in red. The spectra were combined with a weighted average. The theoretical predictions for the atmospheric flux are shown as in Fig. 1. The best fit from an IceCube analysis of high-energy neutrinos that interacted inside the detector volume during the same two data taking years [12] is shown in black. The best fit contains $0.97^{+0.10}_{-0.03}$ times the conventional prediction by Honda et al. [9] and $0.00^{+1.57}_{-0.00}$ times the prompt prediction by Enberg et al. [10]. Both fluxes are calculated for the primary spectrum by Gaisser [11]. The additional astrophysical component is described with an unbroken power law $(2.06^{+0.35}_{-0.26}) \cdot 10^{-18} \cdot (E/100\text{TeV})^{-2.46 \pm 0.12} \text{GeV}^{-1} \text{s}^{-1} \text{sr}^{-1} \text{cm}^{-2}$.

This results in an increasing opaqueness of the earth core and a survival probability $< 1\%$ for neutrinos at $E_\nu \approx 1\text{PeV}$ when propagating through the earth core [13].

For the IC86 dataset the statistics are large enough to unfold the dataset in three different zenith bands. The resulting spectra are shown in Fig. 3. Despite IC86 being the largest neutrino dataset unfolded so far, the decreasing statistics in each band especially at the high energies is a big challenge for the zenith dependent unfolding.

The upper energy reach is limited at $E \approx 125\text{TeV}$ for the band looking through the earth and $E_\nu \approx 250\text{TeV}$ for the other two bands. The unfolded spectra are compatible with theoretical predictions within their errors. For more insight in the composition more zenith bands with smaller errors are needed.

5. Conclusion

The unfolding of the muon neutrino energy spectrum for IC79 and IC86 extend the upper energy limit by a factor of ~ 2.5 to 3.2PeV in comparison to previous measurements by IceCube with data from the 59-string configuration [6]. The resulting spectra measure an excess over the atmospheric prediction at the highest energies, showing the transition from a spectrum dominated by the conventional flux to a harder spectrum. The measured excess is compatible with recent

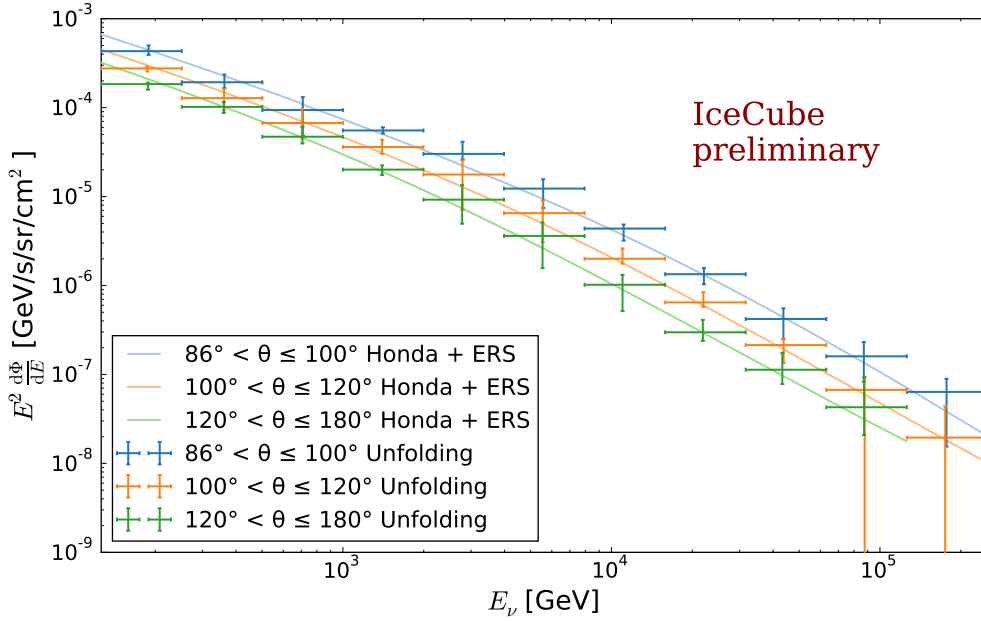


Figure 3: Unfolded energy spectra for different zenith bands for IC86 data. The shown theoretical curves are the sum of conventional flux by Honda et al. [9] and prompt flux by Enberg et al. [10] calculated with the primary spectrum by Gaisser [11].

measurements of the astrophysical neutrino flux in IceCube [12, 14]. Although the unfolding cannot quantify a significance for the existence of an astrophysical component, these measurements strengthen the evidence for an additional, non-atmospheric flux from the northern hemisphere.

The unfolding measures the sum of the atmospheric and the astrophysical flux. To disentangle the astrophysical component, the shape and normalization of the conventional and the prompt flux has to be known precisely. To get deeper insight in the atmospheric flux composition, an unfolding in three zenith bands was performed. The resulting spectra are compatible with the atmospheric prediction by Honda et al. [9] and Enberg et al. [10]. For a better determination of the atmospheric components an unfolding in more zenith bands is needed.

References

- [1] **IceCube** Collaboration, A. Achterberg et al., *Astroparticle Physics* **26** (2006), no. 3 155–173.
- [2] **IceCube** Collaboration, I. Collaboration et al., *Science* **342** (2013), no. 6161 1242856.
- [3] L. Breiman, *Machine learning* **45** (2001), no. 1 5–32.
- [4] H. Peng, F. Long, and C. Ding, *Pattern Analysis and Machine Intelligence, IEEE Transactions on* **27** (2005), no. 8 1226–1238.
- [5] M. A. Hall, *Correlation-based feature selection for machine learning*. PhD thesis, The University of Waikato, 1999.

- [6] **IceCube** Collaboration, M. G. Aartsen et al., *The European Physical Journal C* **75** (2015), no. 3 1–14.
- [7] N. Milke, M. Doert, S. Klepser, D. Mazin, V. Blobel, and W. Rhode, *Nuclear Instruments and Methods in Physics Research Section A: Accelerators, Spectrometers, Detectors and Associated Equipment* **697** (2013) 133–147.
- [8] A. Fedynitch, J. B. Tjus, and P. Desiati, *Physical Review D* **86** (2012), no. 11 114024.
- [9] M. Honda, T. Kajita, K. Kasahara, S. Midorikawa, and T. Sanuki, *Physical Review D* **75** (2007), no. 4 043006.
- [10] R. Enberg, M. H. Reno, and I. Sarcevic, *Physical Review D* **78** (2008), no. 4 043005.
- [11] T. K. Gaisser, *Astroparticle Physics* **35** (2012), no. 12 801–806.
- [12] **IceCube** Collaboration, M. G. Aartsen et al., *Physical Review D* **91** (2015), no. 2 022001.
- [13] I. F. Albuquerque, J. Lamoureux, and G. F. Smoot, *The Astrophysical Journal Supplement Series* **141** (2002), no. 1 195.
- [14] **IceCube** Collaboration, M. G. Aartsen et al., *Physical review letters* **113** (2014), no. 10 101101.

High Energy Astrophysical Neutrino Flux Characteristics for Neutrino-induced Cascades Using IC79 and IC86-String IceCube Configurations

The IceCube Collaboration[†],

[†] http://icecube.wisc.edu/collaboration/authors/icrc15_icecube

E-mail: hans.niederhausen@stonybrook.edu

We have performed a new measurement of the all-sky diffuse flux of high energy, $E > 10\text{TeV}$, extraterrestrial neutrinos by studying neutrino-induced particle showers (cascades) with IceCube data collected during 641 days in 2010–2012. Cascades arise predominantly in electron and tau neutrino interactions and have good energy resolution, and thus are well-suited for the spectral characterization of the extraterrestrial flux. We have improved upon previous analyses by including high-energy cascades with vertices outside, but close to the detector, thereby enlarging the event sample by up to a factor of two for $E > 100\text{TeV}$. A total of 172 cascades with energies ranging from 10TeV to 1PeV have been observed, of which approximately 60% (75% above 100TeV) have not previously been reported by IceCube. The dominant extra-terrestrial component is well described by a smooth and featureless power-law. The preliminary fit result is a soft spectral index of $\gamma = 2.67_{-0.13}^{+0.12}$ and a per-flavor normalization at 100 TeV of $\phi = (2.3_{-0.6}^{+0.7}) \cdot 10^{-18} \text{GeV}^{-1} \text{s}^{-1} \text{sr}^{-1} \text{cm}^{-2}$ in agreement with previous IceCube results. The background-only hypothesis is rejected with a significance of 4.7σ . Finally, we have divided the cascade data according to the neutrino arrival direction into two samples corresponding to the Northern and Southern celestial hemispheres. No spectral difference was found ($\gamma_{\text{north}} = 2.69_{-0.34}^{+0.34}$, $\phi_{\text{north}} = 1.7_{-1.2}^{+1.3} \text{GeV}^{-1} \text{s}^{-1} \text{sr}^{-1} \text{cm}^{-2}$, $\gamma_{\text{south}} = 2.68_{-0.22}^{+0.20}$, $\phi_{\text{south}} = 1.9_{-0.6}^{+0.8} \text{GeV}^{-1} \text{s}^{-1} \text{sr}^{-1} \text{cm}^{-2}$), so that the extraterrestrial neutrino fluxes originating from the Northern and Southern hemispheres are consistent.

Corresponding authors: Hans Niederhausen^{1*}, Mariola Lesiak-Bzdak¹, Achim Stoessl²

¹ Department of Physics and Astronomy, Stony Brook University, Stony Brook, NY 11794-3800

² DESY-Zeuthen, D-15735 Zeuthen, Germany

*The 34th International Cosmic Ray Conference,
30 July- 6 August, 2015
The Hague, The Netherlands*

*Speaker.

Introduction

IceCube is a cubic-kilometer neutrino detector installed in the glacial ice at the geographic South Pole [1] between depths of 1450m and 2450m. IceCube observes neutrinos based on optical measurements of Cherenkov radiation emitted by secondary particles produced in neutrino interactions in the surrounding ice or the nearby bedrock. Those interactions are dominated by deep-inelastic scattering (DIS) of neutrinos off nucleons in the ice. Events are classified according to the topology of their light deposition with tracks and cascades being the main signatures. Tracks arise primarily from through-going muons while cascades may be produced by charged-current interactions of ν_e and ν_τ and by neutral current interactions of any flavor. They are characterized by their point-like light emission. Various hybrid signatures exist, e.g. ν_μ CC events that start inside the detector appear as cascade with an outgoing track. At highest energies ($E_\nu > 1$ PeV) multiple ν_τ -topologies are possible with the “double-bang” being the most prominent [2]. At trigger level the vast majority of events in IceCube are muons that have been produced in cosmic ray induced air showers. Their rate in IceCube exceeds that of neutrinos by orders of magnitude ($\sim 10^6$). Atmospheric neutrinos are produced in the same air showers and form the second largest contribution. At energies relevant to this work, conventional atmospheric neutrinos are dominated by ν_μ ($\nu_\mu : \nu_e \sim 30$ at $E_\nu \sim 10$ TeV) that stem primarily from the decay of charged kaons (K^\pm) and charged pions (π^\pm). Conventional ν_e instead come equally from the decay of charged and neutral kaons ($K^{\pm,0}$). Those light mesons experience energy loss before they decay and thus the conventional neutrino spectrum follows $\sim E^{-3.7}$. ‘Prompt’ atmospheric neutrinos are associated with the decay of heavier mesons involving charm quarks and thus produce an equal admixture of ν_μ and ν_e . Due to the very small lifetime of those mesons the corresponding prompt spectrum mimics that of primary cosmic rays, i.e. $\sim E^{-2.7}$. The cascade channel benefits from the small conventional atmospheric background levels compared to the track channel. In addition fully contained cascades with vertices well within the instrumented volume have superior (deposited) energy resolution of $\sim 15\%$ at relevant energies since for such events the detector acts as a calorimeter. Partially contained cascades that start beyond the detector boundary can be reconstructed with an average energy resolution of $\sim 30\%$.

IceCube recently reported the discovery of an all-sky diffuse flux of high energy neutrinos ($E_\nu > 60$ TeV) [3] from yet unresolved sources with an intensity almost at the level of the Waxman-Bahcall bound [4]. It was found to be well described by a single power-law with spectral index $\gamma = 2.3 \pm 0.3$ [3]. Subsequently an extension of this analysis to lower energies concluded $\gamma = 2.46 \pm 0.12$ ($E_\nu > 1$ TeV) [5]. Astrophysical neutrino production is generally assumed to be associated with the acceleration of cosmic rays at their sources. Detailed predictions of the neutrino flux characteristics are source specific [6] and at present those neutrino sources still escape experimental detection. Based on diffusive shock acceleration and neutrino oscillations over astrophysical relevant distances one expects the astrophysical neutrino flux to exhibit a power-law spectrum [7] with an approximately equal flavor admixture at earth ($\nu_e : \nu_\mu : \nu_\tau \approx 1 : 1 : 1$) [8]. This expectation, especially the flavor ratio, is modified when more complex source environments are considered [9]. Furthermore the flux is expected to be isotropic if many individually weak sources contribute to the flux. The current IceCube measurements focusing on “starting events” (tracks and cascades) of all neutrino flavors and interactions are consistent with these expectations [3, 5, 10]. The astrophysical flux has also been observed using ν_μ -tracks from the northern celestial hemisphere. A spectral index of 2.2 ± 0.2 [11] was found to be in agreement with the earlier

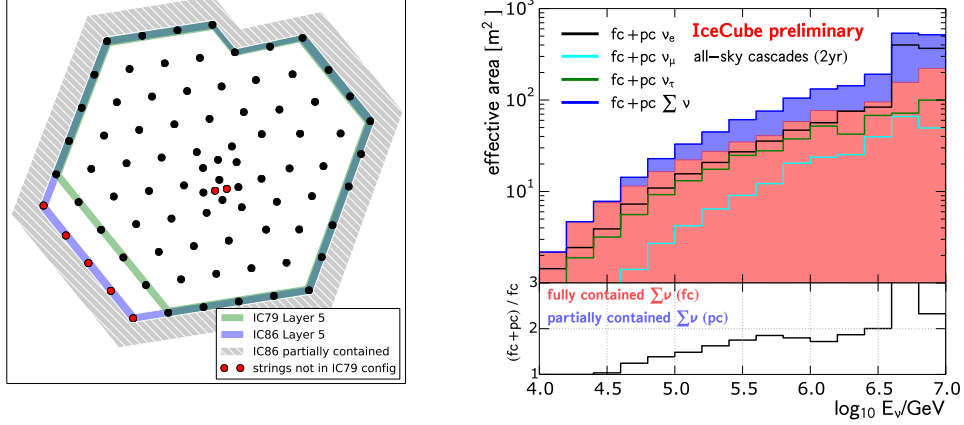


Figure 1: Cross-sectional visualization of the detector in the x, y -plane (left); 2-year effective area of this event selection for combined fully and partially contained cascades (right).

“starting event” results [3, 5, 10].

In this paper we present the first results on the astrophysical neutrino induced cascades flux characteristics using 641 days of IceCube data taken from May 2010 to May 2012. The analysis is based on the event topology selection criteria of ref. [12] to select high energy cascades ($\geq 10\text{TeV}$). We achieved an improved sensitivity to cascades compared to earlier analyses by including cascades which are partially contained in the detector volume (in addition to cascades which are fully contained), thus significantly enhancing this cascade sample in the background free region above 100TeV (see Fig. 1). The final event selection, optimized for maximum signal significance, retained 172 (contained: 152, partially contained: 20) cascades with energies greater than 10TeV . From Monte Carlo simulations we estimated a neutrino purity of 90% (atmospheric and astrophysical ν). The neutrino effective area is shown in Fig. 1 (right). Fig. 2 shows the distribution of the “DelayTime” variable used in the event selection at a level where the data is dominated by atmospheric muon background. It measures the time difference between the time of the first observed photon in the event and the earliest possible time for that photon to stem from the reconstructed cascade (causality). The data is well described by the Monte Carlo simulations. The *CORSIKA* [13] software package was used to generate cosmic ray background according to the composition model of ref. [14]. For the simulation of neutrino propagation and interaction the *neutrino-generator* package is used. The atmospheric neutrino flux has been calculated according to the HKKMS06 [15] (conventional ν) and ERS [16] (prompt ν) models, modified and extrapolated according to the expected dampening of the neutrino flux due to the presence of the knee in the cosmic ray energy spectrum [17]. For contained cascades originating in the IceCube instrumented volume (see Fig. 1 (left)) we further take into account the “self-veto” effect of refs. [18]. The baseline model for astrophysical neutrinos is a single power-law with normalization parameter ϕ at $E_\nu = 100\text{TeV}$ and γ being the spectral index parameter: $\Phi_\nu = \phi \times (E_\nu/100\text{TeV})^{-\gamma}$. The measurement of the astrophysical neutrino spectrum is performed by matching the reconstructed

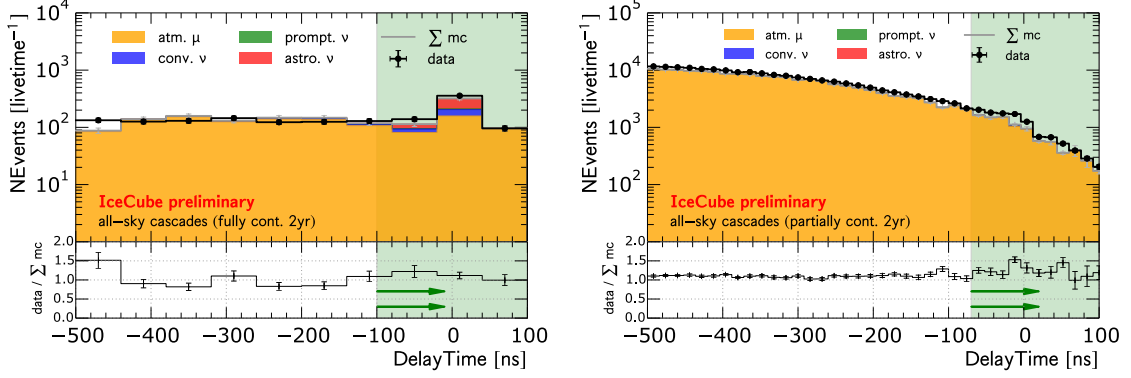


Figure 2: Distribution of the “*DelayTime*” for a μ -background dominated event selection. Left: contained sample; Right: partially contained sample. Signal region shown in green. Neutrino expectations according to fit result to the final event sample.

deposited energy distribution to the simulation prediction using frequentist methods based on maximum likelihood.

Analysis Method

In order to make an inference about the astrophysical flux from the astrophysical component in this cascade sample we employ the method of maximum likelihood, similar to previous IceCube analyses [17, 3, 5, 10]. We separate the contained cascade events according to their reconstructed zenith angle Θ_{reco} into two groups: ‘Northern sky’ ($\cos \Theta_{reco} < 0$) and ‘Southern sky’ ($\cos \Theta_{reco} \geq 0$). We then consider the all-sky partially contained cascade sample as the third group. For each group we obtain a frequency distribution of the reconstructed deposited energy by binning its values into N bins. This allows us to construct the following standard poisson profile likelihood function for a joint fit of the three groups

$$L(\boldsymbol{\theta}_r | \underline{n}) = \underset{\boldsymbol{\theta}_s}{\operatorname{argmax}} L(\boldsymbol{\theta}_r, \boldsymbol{\theta}_s | \underline{n}) = \underset{\boldsymbol{\theta}_s}{\operatorname{argmax}} \prod_{i=1}^3 \prod_{j=1}^N \frac{\mu_{ij}(\boldsymbol{\theta}_r, \boldsymbol{\theta}_s)^{n_{ij}}}{n_{ij}!} e^{-\mu_{ij}(\boldsymbol{\theta}_r, \boldsymbol{\theta}_s)} \quad (1)$$

where n_{ij} is the observed number of events in the ij -th bin, while $\boldsymbol{\theta}_r, \boldsymbol{\theta}_s$ are vectors of physics parameters and nuisance parameters to include systematic uncertainties, respectively. The expected number of events in the ij -th bin, $\mu_{ij}(\boldsymbol{\theta}_r, \boldsymbol{\theta}_s) = \mu_{ij}^{atm.\mu} + \mu_{ij}^{atm.v} + \mu_{ij}^{astro.v}$, is a superposition of the different models described in the previous section. The maximum likelihood estimate $\hat{\boldsymbol{\theta}}_r$ is obtained numerically by minimizing $-2 \log L(\boldsymbol{\theta}_r | \underline{n})$ with respect to $\boldsymbol{\theta}_r$. We construct approximate confidence intervals and regions with asymptotic coverage using Wilk’s theorem [19]. Here we consider ϕ and γ as physics parameters and the flux normalizations of the neutrino backgrounds $\phi_{conv}, \phi_{prompt}$ as well as an energy related scaling parameter ε as nuisance parameters. Those nuisance parameters $\boldsymbol{\theta}_s$ contribute additional additive penalty terms $\log(L_{sys}) = \sum_s (\theta_s - \theta_{s,0})^2 / \sigma_{\theta_s}^2$ to the likelihood function that reflect the associated systematic uncertainties σ_{θ_s} . The fit is performed in the energy range from $\log_{10} E / \text{GeV} = 4.1$ to $\log_{10} E / \text{GeV} = 6.9$. There are two main sources of detector related systematic uncertainties. The in-situ sensitivity of the IceCube Digital Optical Module (DOM), dominated by the absolute efficiency of its PMT, has a relative uncertainty of 10% [21]. Additionally, in order to model the

Detector Syst.	Value	$\hat{\epsilon}$	Par	Prior	Result
DOM	-10%	1.11	γ	-	$2.67_{-0.13}^{+0.12}$
DOM	+10%	0.91	ϕ	-	$2.3_{-0.6}^{+0.7}$ c.u.
Scatt.	+10%	1.11	ϕ_{conv}	1.0 ± 0.3	$0.85_{-0.29}^{+0.28} \cdot \Phi_{HKKMS06}$
Abs.	+10%	1.11	ϕ_{prompt}	1_{-1}^{+3}	$0.5_{-0.5}^{+2.2} \cdot \Phi_{ERS}$
Scatt./Abs.	-7%	0.96	ϵ	1.00 ± 0.15	$0.96_{-0.15}^{+0.14}$
Combined ϵ_{tot}		1.00 ± 0.15	with 1 c.u.	$\equiv 10^{-18} \text{ GeV}^{-1} \text{ s}^{-1}$	$\text{sr}^{-1} \text{ cm}^{-2}$

Table 1: Summary of systematics evaluation (left); summary of fit results (right).

photon propagation in the glacial ice at the South Pole we rely on a measurement of scattering and absorption using IceCube’s LED calibration system. The associated uncertainty is 10% [22]. The influence of those effects on this analysis has been studied using dedicated simulations with different DOM efficiencies (-10%, +10%) and variations of the scattering and absorption of the ice ($\Delta\alpha_{scatt} : +10\%$, $\Delta\alpha_{abs} : +10\%$, both : -7%). In order to account for those uncertainties in the likelihood method, a nuisance parameter ϵ that effectively translates the model predictions to lower ($\epsilon < 1$) or higher ($\epsilon > 1$) reconstructed energies was added. The result of a dedicated simulation study is summarized in Table 1 (left). We find that the DOM efficiency uncertainty and the ice model uncertainty each translate into a 10% uncertainty on ϵ . By adding them in quadrature we conclude that detector related systematics are well accounted for by including $\epsilon = 1.00 \pm 0.15$ into the likelihood function. The average uncertainty of the expected conventional atmospheric neutrino flux at energies relevant for this work is 30% [20]. Uncertainties of the prompt atmospheric neutrino flux are model dependent and no experimental evidence for this flux exists. An upper limit of $\phi_{prompt} < 2.4$ (< 3.8) at 68% C.L. (90% C.L.) has been obtained in ref. [17] based on the ERS model. Accordingly, we assume a systematic uncertainty of 300% on the normalization of the prompt ERS model.

Results

The observed reconstructed energy distributions of all events that pass the cascade selection criteria of this work are shown in Fig. 3 and compared to the expectation according to the best-fit single, unbroken power-law: $\phi = (2.3_{-0.6}^{+0.7}) \cdot 10^{-18} \text{ GeV}^{-1} \text{ s}^{-1} \text{ sr}^{-1} \text{ cm}^{-2}$ and $\gamma = 2.67_{-0.13}^{+0.12}$. A good description of the data is achieved as evidenced by the corresponding goodness-of-fit (g.o.f) p-value of 0.32. This is based on the g.o.f test-statistic described in ref. [23] for which we obtained the sampling distribution from parametric bootstrap (“toy experiments”) assuming the best-fit. The approximate 68% confidence region (red) for the astrophysical parameters is shown in Fig. 4 (right). We find this cascade sample to be dominated by astrophysical neutrinos ($\sim 65\%$) over the entire energy range. The best-fit values for the remaining parameters are shown in Table 1 (right). When the “background-only” hypothesis ($\phi = 0$) is assumed, an unrealistically large prompt atmospheric neutrino component characterized by $\phi_{prompt} = 7 \cdot \Phi_{ERS}$ is required to describe the data. This however is strongly disfavored w.r.t the best-fit by 4.7σ based on the sampling distribution of the likelihood ratio test-statistic $-2 \cdot \log(L_b/L_{s+b})$ that has obtained assuming the background-only result. The rejection is based on the relative suppression of the prompt flux from the Southern hemisphere compared to the flux

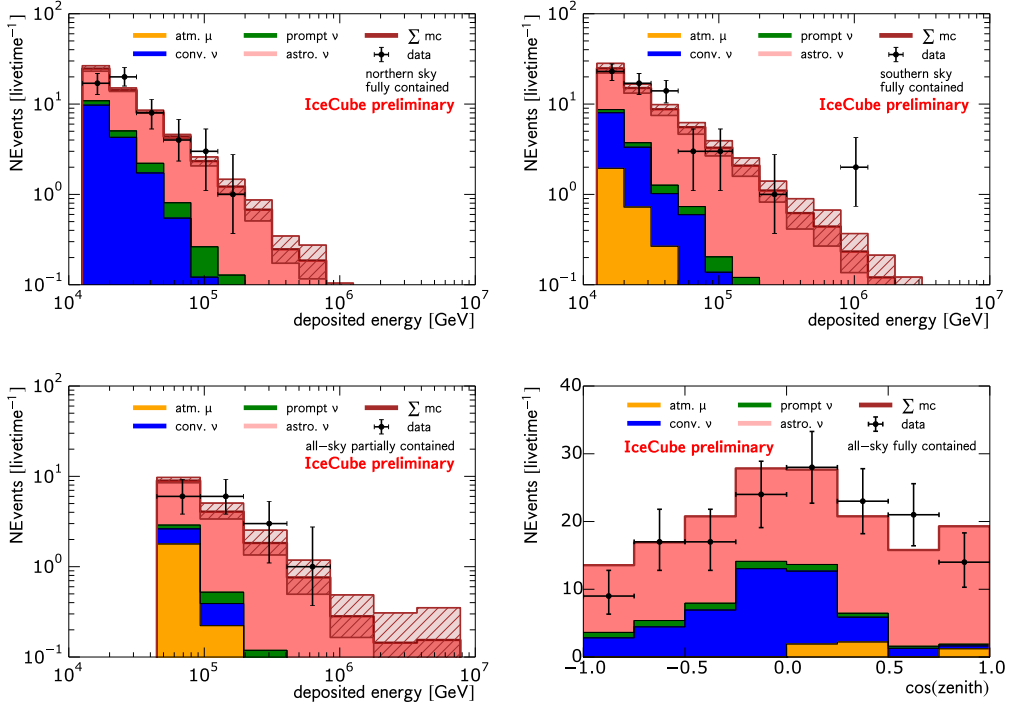


Figure 3: Energy distributions at final selection level: fully contained cascades, Northern sky (top left), Southern sky (top right), all-sky partially contained cascades (bottom left), hatched regions show 1σ uncertainty on sum of m.c.; zenith distribution for fully contained cascades (bottom right)

from the North due to the atmospheric self-veto effect that breaks the spectral degeneracy between the prompt neutrino flux with the soft astrophysical flux we observed. This measurement also disfavors a hard spectral index of $\gamma = -2$. In this case we find a small astrophysical contribution $\phi = 6 \cdot 10^{-19} \text{ GeV}^{-1} \text{ s}^{-1} \text{ sr}^{-1} \text{ cm}^{-2}$ that requires a rather large prompt component of $\phi_{\text{prompt}} = 5 \cdot \Phi_{\text{ERS}}$. Such a combination is rejected at 3.5σ based on the sampling distribution of the corresponding likelihood ratio test-statistic under this ‘ E^{-2} -hypothesis’. The isotropy assumption about the astrophysical flux could be challenged by looking for spectral differences between the fluxes measured from the Northern and Southern skies. Due to their better angular resolution compared to partially contained cascades, we constrain this investigation to contained cascades only. Here we perform the same maximum likelihood estimation for the samples from the Northern and Southern skies separately. For upward oriented showers we find the same parameters as for downward oriented showers $\gamma_{\text{north}} = 2.69^{+0.34}_{-0.34}$, $\gamma_{\text{south}} = 2.68^{+0.20}_{-0.22}$ and $\phi_{\text{north}} = 1.7^{+1.3}_{-1.2} \text{ GeV}^{-1} \text{ s}^{-1} \text{ sr}^{-1} \text{ cm}^{-2}$, $\phi_{\text{south}} = 1.9^{+0.8}_{-0.6} \text{ GeV}^{-1} \text{ s}^{-1} \text{ sr}^{-1} \text{ cm}^{-2}$ within large uncertainties due to the spectral degeneracy with the prompt normalization. This consistency remains when all nuisance parameters are kept fixed at the values obtained by the joint fit. For fixed nuisance parameters we find insignificantly higher astrophysical normalizations in very good agreement with the joint result. Any deviation of the data from the single power-law model may provide valuable insight into the nature of the observed astrophysical flux. Although we found no evidence for inconsistency between data and model, we did perform an alternative fit based on a

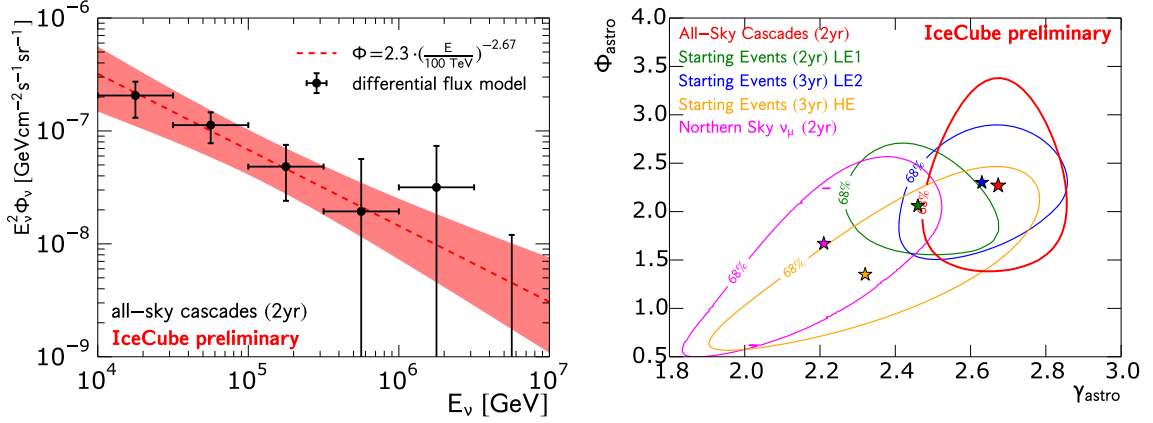


Figure 4: Left: best-fit astrophysical- ν flux (dashed line, red) and 1σ band (red) compared to the “differential model” fit; Right: Comparison of recent ν -flux measurements in IceCube: this analysis (red), ref. [5] (green), ref. [3] (purple), ref. [10] (blue) and ref. [11] (yellow).

“differential model” to measure the energy dependence of the observed flux. Similar to ref. [3] we extract the flux normalization in bins of neutrino energy E_ν . Within each bin a E^{-2} -distribution is assumed. The corresponding expected distributions of the deposited energy serve as a basis to describe the data as linear combination on top of the expected background from atmospheric neutrinos and muons. The result (black) is shown in Fig. 4 (left) and compares very well to the power law model fit (red). The amount of overlap between this cascade-based event selection with the samples from the starting event analyses [3, 5, 10] was found to be smaller than $\sim 25\%$. There is no overlap with the Northern sky ν_μ -sample [11]. The measurement of the astrophysical flux parameters presented here can thus be regarded as approximately independent and is found to agree well with previous IceCube measurements (refs. [3, 5, 10]) as shown in Fig. 4. This was quantified to be better than 1σ by applying Wald’s method [24] in a bivariate normal approximation using the observed information matrices as estimates of the respective covariance matrices. This result seems to be in insignificant ($< 2\sigma$) tension with the ν_μ measurement [11] (Northern sky). Future data will help clarify the situation. We would like to point out that uni-variate comparisons of multi-variate measurements (e.g. “looking at γ only”) can lead to erroneous inference about consistency, as no statement about the other parameters is made.

Summary

We have performed the first high energy ($E > 10\text{ TeV}$) cascade-only measurement of the diffuse astrophysical neutrino flux recently discovered by IceCube using 641 days of IceCube data (2010-2012). For the first time we extend topological cascade selection criteria to also include partially contained cascades with vertices in near proximity to the detector. This analysis found 172 cascade events of which approximately 60% (75% above 100 TeV) have not previously been reported by IceCube. The measured astrophysical component is well described by a smooth and featureless power-law. The preliminary fit result is a soft spectral index of $\gamma = 2.67^{+0.12}_{-0.13}$ and a per-flavor normalization of $\phi = (2.3^{+0.7}_{-0.6}) \cdot 10^{-18} \text{ GeV}^{-1} \text{ s}^{-1} \text{ sr}^{-1} \text{ cm}^{-2}$ at $E = 100\text{ TeV}$ in agreement with the previous IceCube measurements. This sample can not be

explained by atmospheric backgrounds, which would require a prompt neutrino contribution 7 times larger than expected and is rejected with a significance of 4.7σ . Similarly this sample disfavors a harder spectrum with $\gamma = -2$ at 3.5σ . We further measure the same astrophysical fluxes from the Northern ($\gamma_{\text{north}} = 2.69^{+0.34}_{-0.34}$) and Southern skies ($\gamma_{\text{south}} = 2.68^{+0.20}_{-0.22}$). This is consistent with the isotropic expectation for extra-galactic sources.

References

- [1] A. Achterberg et al., *Astropart. Phys.* 26, 155 (2006)
- [2] R. Abbasi et al., *Phys. Rev. D* 86, 022005 (2012)
- [3] M. G. Aartsen et al., *Science* 342, 1242856 (2013)
M. G. Aartsen et al., *Phys. Rev. Lett.* 113, 101101 (2014)
- [4] E. Waxman and J. Bahcall, *Phys. Rev. D* 59, 023002 (1998)
- [5] M. G. Aartsen et al., *Phys. Rev. D* 91, 022001 (2015)
- [6] E. Waxman and J. Bahcall, *Phys. Rev. Lett.* 78, 2292 (1997); K. Murase, S. Inoue, and S. Nagataki, *Astrophys. J* 689, L105 (2008); F. W. Stecker, *Phys. Rev. D* 88, 047301 (2013)
- [7] T. K. Gaisser, F. Halzen, and T. Stanev, *Physics Reports* 258, 173 (1995)
- [8] H. Athar, M. Jezabek and O. Yasuda, *Phys. Rev. D* 62, 103007 (2000)
- [9] T. Kashti and E. Waxman, *Phys. Rev. Lett.* 95, 181101 (2005); P. Lipari, M. Lusignoli and D. Meloni, *Phys. Rev. D* 75, 123005 (2007); S. Choubey and W. Rodejohann, *Phys. Rev. D* 80, 113006 (2009)
- [10] M. G. Aartsen et al., *Phys. Rev. Lett.* 114, 171102 (2015)
- [11] M. G. Aartsen et al., *Evidence for Astrophysical Muon Neutrinos from the Northern Sky with IceCube*, submitted to *Phys. Rev. Lett.* (2015).
- [12] M. Lesiak-Bzdak and A. Stoessl (for the IceCube Collab.), *Proc. of the 33nd ICRC*, paper 0370 (2013)
- [13] D. Heck et al., *CORSIKA*, Tech. Rep. FZKA 6019, Forschungszentrum Karlsruhe (1998)
- [14] T. Gaisser, *Astroparticle Physics*, Vol. 35, 12 (2012)
- [15] M. Honda et al., *Phys. Rev. D* 75, 043006 (2007)
- [16] R. Enberg, M. H. Reno and I. Sarcevic, *Phys. Rev. D* 78, 043005 (2008)
- [17] M. G. Aartsen et al., *Phys. Rev. D* 89, 062007 (2014)
- [18] T. Gaisser, K. Jero, A. Karle, J. van Santen, *Phys. Rev. D* 90, 023009 (2014)
- [19] S. S. Wilks, *Ann. Math. Statist.* Vol. 9, 1 (1938)
- [20] A. Fedynitch, J. Becker Tjus and P. Desiati, *Phys. Rev. D* 86, 114024 (2012)
- [21] R. Abbasi et al., *Nucl. Instr. Meth. Phys. Res. A*, Vol. 618, 1-3 (2010)
- [22] M. G. Aartsen et al., *Nucl. Instr. Meth. Phys. Res. A*, Vol. 711 (2013)
- [23] S. Baker and R. D. Cousins, *Nucl. Instr. Meth. Phys. Res.*, Vol. 221, 2 (1984)
- [24] A. Wald, *Trans. Amer. Math. Soc.* 54 (1943); T. W. F. Stroud, *Ann. Math. Stat.*, Vol. 42, No. 4 (1971)